UNIVERSITÀ DEGLI STUDI DI MILANO
PhD Course in Molecular and Cellular Biology

XXX Cycle

Approaches for improvement of human pluripotent stem cell-derived striatal neuron differentiation protocols and quantitative fluorescence microscopy methods.

Angela Laporta

PhD Thesis

Scientific tutor: Prof. Chiara Zuccato

Academic year: 2016-2017

SSD: BIO/14

Laboratory of Stem Cell Biology and Pharmacology of Neurodegenerative Diseases

Directed By Prof. Elena Cattaneo

Contents

Paper: Andrea Faedo, **Angela Laporta**, Alice Segnali, Maura Galimberti, Dario Besusso, Elisabetta Cesana, Sara Belloli, Rosa Maria Moresco, Marta Tropiano, Elisa Fucà, Stefan Wild, Andreas Bosio, Alessandro E. Vercelli, Gerardo Biella, and Elena Cattaneo "Differentiation of human telencephalic progenitor cells into MSNs by inducible expression of Gsx2 and Ebf1", PNAS, 114(7), 2017.

Abstract

Directed differentiation of human Embryonic Stem cells (hESC) and induced Pluripotent Stem Cells (hiPS) is used to produce *in vitro* models to understand the mechanisms involved in neural development and to study the cellular and molecular processes affected in neurodegenerative diseases. Furthermore, these cells represent a potential source of *in vitro* generated mature neurons that can be used in cell replacement therapies.

The laboratory where I performed my PhD thesis is interested in studying Huntington Disease (HD), a rare inherited disorder caused by an expanded stretch of CAG trinucleotide repeats in the huntingtin (*HTT*) gene, which results in neuronal dysfunction and death. In HD, the medium spiny neurons (MSNs) of the striatum represent the population most severely affected. The study of the different stages of striatal development *in vitro* from human pluripotent stem cells (hPSC) could be instrumental for both the identification of the molecular processes that are affected in HD and the generation of MSNs for cell replacement therapies. For this reason, the main goal of my doctoral degree was to create *in vitro* models that recapitulate human striatal development *in vivo* and ultimately generate authentic MSNs.

In the first part of my thesis, I confirmed previous data from the lab showing that H9 hPSC can efficiently differentiate towards the striatal lineage (Delli Carri et al., 2013). Moreover, I extended this finding by showing that this protocol can be successfully applied to other three hPSC lines. Additionally, to better characterize the progenitor and neuronal subpopulations generated at different stages of the *in vitro* differentiation, I developed an automated microscope image quantification pipeline that enabled a high degree of accuracy in a diverse range of molecular marker measurements. With this new method, I was able to monitor cell identity transitions observed during *in vitro* differentiation and quantify the resulting neuronal subpopulations.

Previous *in vivo* analysis of cell transitions in the human developing striatum allowed to identify two transcription factors (TFs), Gsx2 and Ebf1, involved in neuronal identity progression. Based on this, in the second part of my PhD work, I developed a strategy to improve MSNs generation efficiency from hESC. Following *in vitro* differentiation, I monitored the effects of the exogenous TFs expression by analysing the expression of various cell identity molecular

markers by immunofluorescence. By using this strategy, I was able to improve the differentiation of hPSCs into MSNs *in vitro* from 7% to 38%.

In the future, we are planning to take advantage of the tools and knowledge gathered in the course of my PhD to develop a differentiation protocol in line with the GMP procedures necessary for the cell replacement approach.

State of the Art

State of the Art

1. Huntington's disease
   1.1. The CAG repeats in the etiology of HD
   1.2. HD in the striatum
   1.3 Using hPS to generate MSNs *in vitro*

2. Embryonic development of the brain
   2.1. Neurulation
   2.2. Neural tube regionalization
   2.3. Neural tube patterning

3. Development of the striatum
   3.1. Molecular definition of the telencephalic region
   3.2. Dorsal Telencephalon
   3.3. Ventral Telencephalon
      3.3.1. MGE
      3.3.2. LGE
      3.3.3. CGE
   3.4. Medium-sized striatal projection Neurons

4. Obtaining authentic MSNs *in vitro* from human pluripotent stem cells (hPSC)
   4.1. Overview on published MSN differentiation protocols
   4.2 Focus on Delli Carri et al. protocol, 2013

State of the Art

1. Huntington's disease

1.1. The CAG repeats in the etiology of HD

Huntington's disease (HD) is a rare neurodegenerative disease that leads to movement, behaviour and cognitive defects, and ultimately to death, as there is no effective treatment available at the moment. The disease is inherited in a dominant autosomic fashion and is due to the expansion of a CAG repeat, which encodes for a polyglutamine (polyQ) tract, in the first exon of the *huntingtin* (*HTT*) gene.

The disease has a CAG-related and age-dependent penetrance, in particular the lengths of the CAG tract of 36 or more repeats are associated with nearly full penetrance by age 65 years. In some cases, symptoms start before the age of 20 years (Juvenile Huntington's disease; JHD). Therefore, longer CAG repeats predict earlier onset, accounting for up to 50–70% of variance in age of onset, with the remainder likely to be due to modifying genes and the environment (Ross & Tabrizi, 2011). The prevalence in the Caucasian population is estimated at 1/10,000-1/20,000. Clinical features of HD include progressive motor dysfunction, cognitive decline, and psychiatric disturbance, probably caused by both neuronal dysfunction and neuronal cell death. In particular, mutant huntingtin contains an abnormally long polyQ sequence that corresponds to the CAG genetic expansion; the protein exhibits toxic properties that cause dysfunction and death of neurons. Medium spiny neurons of the striatum are particularly vulnerable to mutant huntingtin induced harm, but HD is increasingly recognized as a disease of the whole brain (Bates et al., 2015). In fact, studies carried out by *in vivo* neuroimaging of brains of HD patients have detected early changes in the volume and shape of the basal ganglia, cerebral cortex, and other regions, and these were evident several years prior to symptomatic onset (Rosas et al., 2005). Within the brain, in fact, there is massive striatal neuronal cell death, with up to 95% loss of GABAergic medium spiny projection neurons, which project to the globus pallidus and the substantia nigra, whereas large interneurons are selectively spared (Ross & Tabrizi, 2011). The damages affecting progressively the whole brain reflect clinical disorders caused by HD.

1.2. HD in the striatum

The striatum, the most affected brain structure in HD, is also one of the core components of the basal ganglia circuitry. The term basal ganglia refers to nuclei embedded deep in the brain hemispheres (striatum or caudate-putamen and globus pallidus), whereas related nuclei consist of structures located in the diencephalon (subthalamic nucleus), mesencephalon (substantia

nigra), and pons (pedunculopontine nucleus) (Nery et al., 2002) (Figure 1).

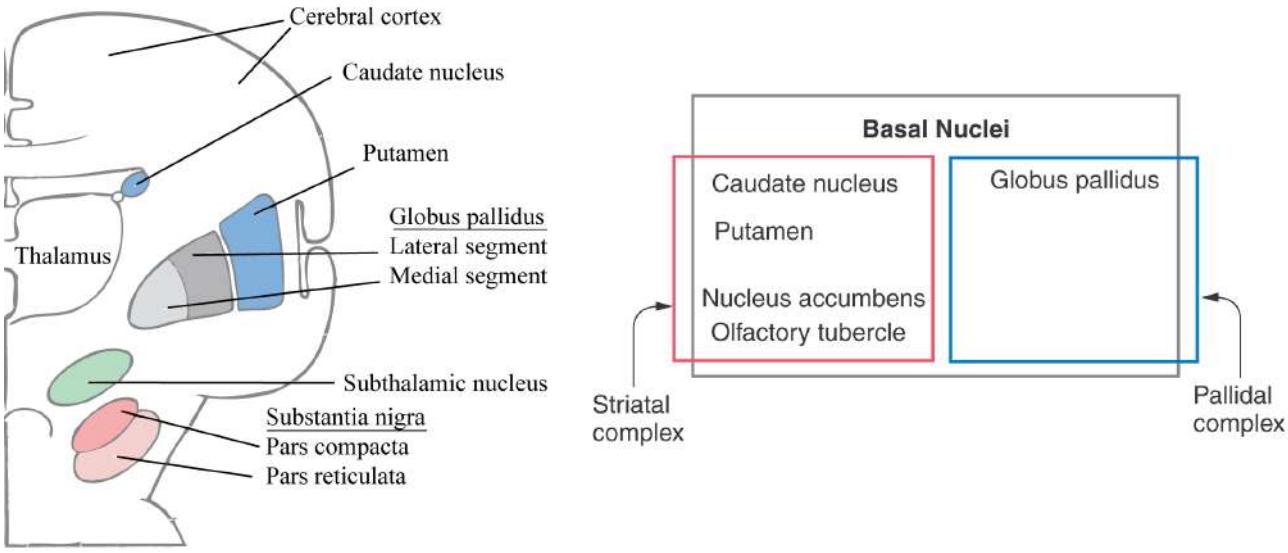

Figure 1: Nuclei in the basal ganglia.

The basal ganglia, therefore, is a heterogeneous structure that receives afferents from several cortical and subcortical structures and projects to other basal ganglia nuclei. In particular, the basal ganglia and related nuclei can be broadly categorized as (1) input nuclei, (2) output nuclei, and (3) intrinsic nuclei. Input nuclei are those structures that receive incoming information from different sources, mainly cortical, thalamic, and nigral in origin. The caudate nucleus (CN), the putamen (Put), and the accumbens nucleus (Acb) are all considered input nuclei. The output nuclei are those structures that send basal ganglia information to the thalamus and consist of the internal segment of the globus pallidus (GPi) and the substantia nigra pars reticulata (SNr). Finally, intrinsic nuclei such as the external segment of the globus pallidus (GPe), the subthalamic nucleus (STN) and the substantia nigra pars compacta (SNc) are located between the input and output nuclei in the relay of information. Cortical and thalamic efferent information enters the striatum (CN, Put, and Acb) to be processed further within the basal ganglia system (Lanciego et al., 2012) (Figure 2).

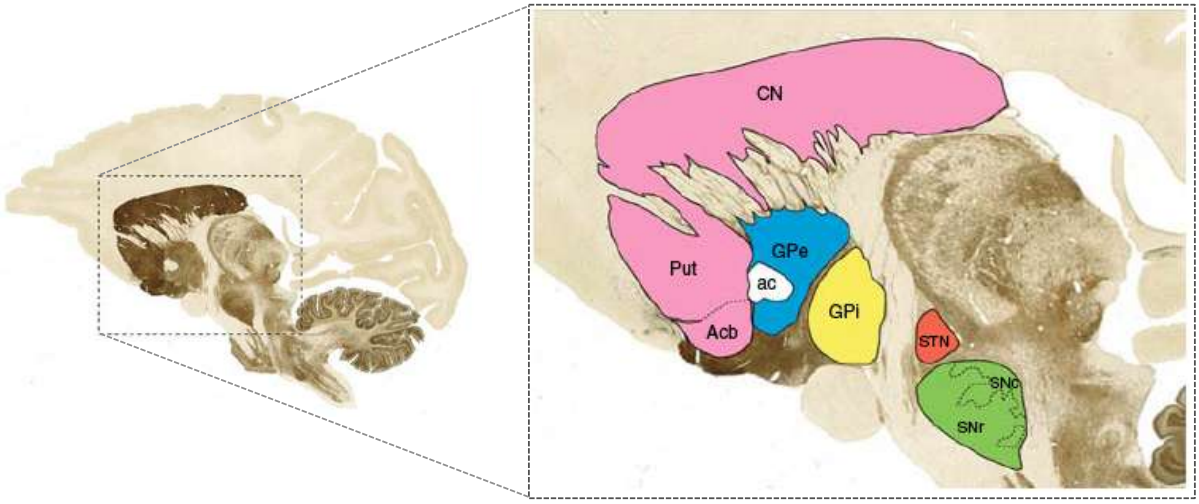

Figure 2: Identification of the areas in the striatum (Lanciego et al., 2012).

The striatum, in fact, receives inputs from different areas of the cerebral cortex, including association cortical areas as well as the sensori-motor cortex, and has connections via the globus pallidus and substantia nigra to the thalamus and thence to premotor and prefrontal cortical areas. Recordings of the activity of neurons in different parts of the striatum show that they have the following properties: (i) neurons in much of the putamen, which receives inputs from the sensori-motor cortex, have activity related to movements; (ii) neurons in the caudate nucleus, which receives from the association cortex, have activity related for example to environmental stimuli which signal preparation for or initiation of behavioural responses; (iii) neurons in the tail of the caudate nucleus, which receives strongly from the inferior temporal visual cortex, respond when a patterned visual stimulus changes; (iv) some neurons in the posterior ventral putamen, which receives from the inferior temporal visual cortex and the prefrontal cortex, respond in a visual short term memory task; (v) some neurons in the ventral striatum, which receives from limbic structures such as the amygdala and hippocampus, respond to stimuli associated with reinforcement or to novel stimuli (Ehrlich, 2012). The disruption of these striatal pathways in HD leads to the development of motor dysfunction including hyperkinetic, hypokinetic, and dyskinetic movements.

Therefore, to understand the disease and its progression is important to study the striatum, the most affected in this pathology.

The striatum encompasses two different types of neurons: projection neurons and interneurons (90% and 10%, respectively). Projection or striatofugal neurons are also called medium-sized spiny neurons (MSNs) because these multipolar neurons have small to medium cellular somata (20 μm in diameter), and their dendritic processes are covered by postsynaptic specializations

called dendritic spines. All striatal MSNs are inhibitory neurons that use γ-amino butyric acid (GABA) as the neurotransmitter. The medium spiny neurons are innervated by excitatory neurons from the cerebral cortex, by thalamic neurons, and by dopaminergic neurons from the SNc, and cholinergic and GABAergic interneurons of the striatum (Figure 3).

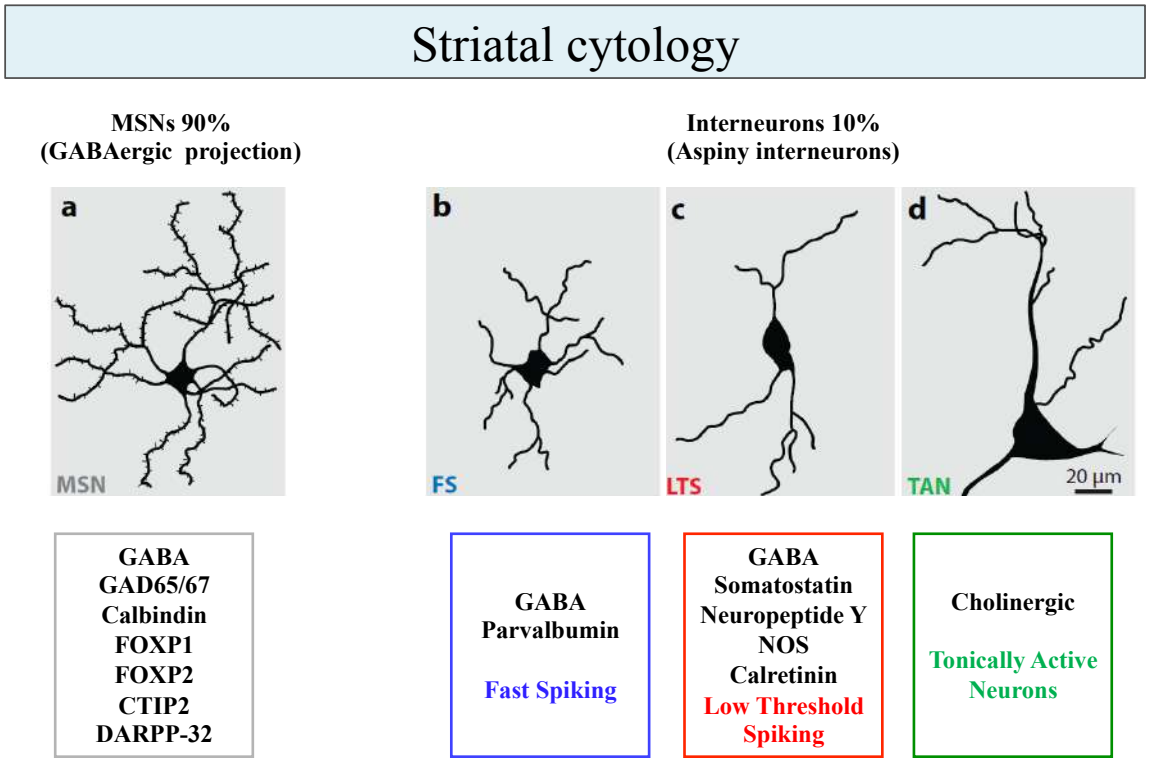

Figure 3: Schematic of type of cells that are present in the striatum (modified from Kreitzer, 2009).

According to their projection targets, the MSNs can be divided further into those innervating the GPe nucleus and those projecting to the output nuclei GPi and SNr. Striatal MSNs innervating the GPe nucleus express the dopamine receptor subtype 2 (D2R), which inhibits intracellular adenyl-cyclase trough G protein signalling, and projects via the indirect pathway (striato-GPe-STN-GPi/SNr). Striatal MSNs that project directly to GPi and SNr contain dopamine receptor subtype 1 receptors (D1R), which activate adenylcyclase signalling (D1-containing neurons), take part in the direct striatopallidal pathway. Direct and indirect MSNs can be further identified by the expression of a few neuropeptides. Indeed, indirect MSNs express enkephalin, whereas substance P and dynorphin are expressed in direct MSNs.

In addition to these spiny projection neurons, the striatum also contains several different classes of local-circuit neurons (interneurons), all of which show smooth dendrites. Interneurons in the striatum are often classified into four groups depending on their neurochemical profiles and morphological characteristics (Kawaguchi et al., 1995) (Figure 4).

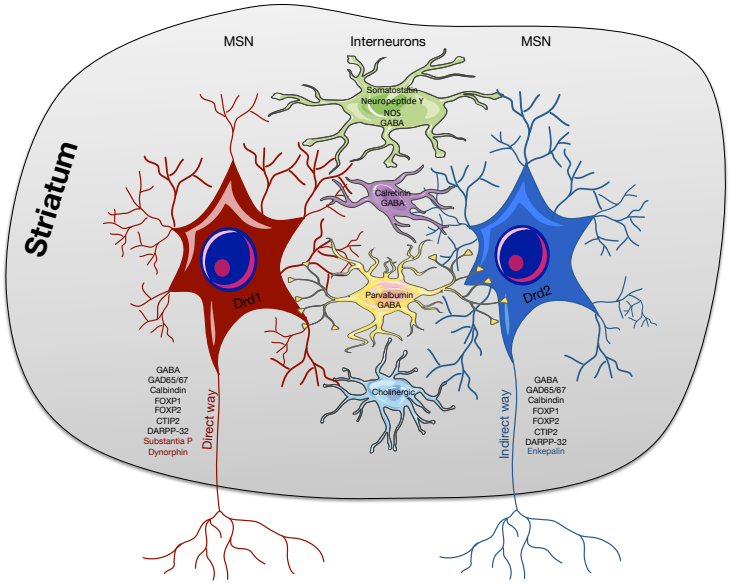

Figure 4: Cell types in the striatum. MSNs Drd1, involved in the direct pathway, are indicated in red, whereas MSNs Drd2, involved in the indirect pathway, are indicated in blue. The four types of interneurons are represented in four different colours: in green the interneurons GABAergic somatostatin positive, in violet the calretinin and GABAergic positive, in yellow the parvalbumin and GABAergic positive, and in blue the cholinergic.

In HD, both enkephalin and substance P MSNs neurons are lost, but indirect MSNs have been shown to be the most vulnerable in the disease process (Deng et al., 2004; Reiner et al., 1988), and degenerate prior to direct MSNs (Deng et al., 2004; Gerfen et al., 1990).

The possible pathogenic mechanisms of HD that affect preferentially MSNs include abnormal aggregation (inclusions) and clearance of polyQ-HTT, bioenergetic deficits, neurotrophin deficiency, transcriptional dysregulation, disorders of axonal transport, and excitotoxicity. The first point is the transcriptional dysregulation induced in MSNs by full length mutant HTT (mHTT) or a fragment thereof (polyQ-HTT) are to some extent exclusive to the MSN, even if the same transcripts are expressed outside the striatum (Sugars & Rubinsztein, 2003); *in vivo*, viral mediated expression of polyQ-HTT exclusively in the striatum results in reversible formation of inclusions, transcriptional dysregulation, and MSN death, while sparing interneurons (Ruiz & Déglon, 2012).

The cortex is the source of 80 to 90% of the BDNF in the striatum, to where it is anterogradely transported (Altar et al., 1997; Canals, 2004; Fusco et al., 2003). Several works have demonstrated the important role for BDNF in the maturation of the MSN, and there is also a requirement for BDNF in the maintenance of adult striatum. In HD, the amount of BDNF reaching the striatum is further reduced secondary to axonal transport deficits (Cattaneo et al., 2001; Crook & Housman, 2011; Gauthier et al., 2004).

Finally, the status of autophagy and the role of ubiquitin-proteasome system and the clearance of aggregated polyQ-HTT are of great interest, and could clarify the toxic effect of mHTT on

MSNs (Ehrlich, 2012).

Albeit less pronounced than in the striatum, differential vulnerability and loss of selected neuronal populations is also readily observed in the cerebral cortex of HD patients. Specifically, large pyramidal projection neurons in cortical layers V, VI and to a lesser extent, layer III, are preferentially lost (Cudkowicz & Kowall, 1990; Hedreen et al., 1991). Long axons emanating from cortical projection neurons in layers V and VI innervate the striatum. In primates, these axons are thin and unbranched with a single target. As in the striatum, there is remarkable preservation of small cortical interneurons (i.e., layer IV granule cells) in HD (Cudkowicz & Kowall, 1990; Han et al., 2010) (Table 1).

Anatomical location	Cell type	Relative vulnerability	Morphology	Afferents	Target	NT receptors	NT	Peptides	Other molecular markers
Striatum	MSN (direct pathway)	+++	projection neurons, long axon	Cortex (Glu), SNc (DA), Thalamus (Glu)	GPi, SNr	D1, NMDA, AMPA	GABA	Substance P/ Dynorphin	DARPP32 GAD
	MSN (indirect pathway)	+++++	projection neurons, long axon	Cortex (Glu), SNc (DA), Thalamus (Glu)	GPe	D2, NMDA, AMPA	GABA	Enkephalin	DARPP32 GAD
	Interneurons	+	extensive dentritic network, axon projects locally	MSNs, other interneurons	MSNs, other interneurons	D2, NMDA, AMPA	Ach.	Neuropetide Y, parvalbumin	iNOS somatostatin
Cerebral Cortex	Pyramidal neurons (layers V/VI)	+++	projection neurons, long axon	Thalamus, brainstem nuclei	Striatum, brainstem, thalamus	Glu, Ach, DA, NE, 5HT	Glu		MAP2 CaMK
	Interneurons	+	extensive dentritic network, axon projects locally	Thalamus	Pyramidal neurons	Glu, GABA	GABA	Neuropetide Y, somatostatin	GAD

Table 1: Summary of striatal and cortical neurons affected in HD and their characteristics (modified from Han et al., 2010).

1.3. Using hPS to generate MSNs *in vitro*

Currently, there is no known cure for HD. However, the specificity of cell loss seen at least in early stages of the disease principally involving loss of the MSN projection neurons has made cell transplantation a viable therapeutic prospect (Reddington et al., 2014). Transplants using primary human fetal striatal tissue have demonstrated “proof-of-principle” that cell replacement is feasible, that the grafts are safe and do not accelerate disease progression (Bachoud-Levi et al., 2000; Bachoud-Lévi et al., 2006; Barker et al., 2013). These studies have been conducted on a very small number of HD subjects and have revealed a significant, although incomplete and temporally limited to a few years after transplantation, functional recovery in at least some patients (Bachoud-Levi et al., 2000; Bachoud-Lévi et al., 2006; Barker et al., 2013). However, due to the ethical issues associated with the use of human fetal cells obtained from elective termination of pregnancies, the logistical issues arising from the amount of fetal tissue required

per patient, and the difficulties in achieving an appropriate level of standardization and quality control for tissues derived from such a recurrent clinical source, better renewable sources of cells for transplantation are under active exploration.

Human pluripotent stem cells (hPSCs) are the leading contender under consideration, by virtue of their capacity for indefinite expansion as well as their potential for differentiation to essentially any mature fate. The principle sources being human embryonic stem cells (hESCs) and/or induced pluripotent stem cells (hiPSCs), followed by directed differentiation *in vitro* towards a specific neural phenotype prior to transplantation as required for each disease target.

Over the last 6 years there has been some considerable success in producing MSN-like neurons from diverse hPSC sources, including from hESCs that have been directed to a neuronal phenotype, and then ventralised using sonic hedgehog (Arber et al., 2015; Aubry et al., 2008; Delli Carri et al., 2013; Ma et al., 2012; Nicoleau et al., 2013). These studies are very important as they may improve our understanding of the mechanisms underlying HD and to study the specific deficits of MSNs and, in the future, to obtain MSNs for the cell replacement approach.

However, although there is some evidence that the transplanted cells corrected motor deficits in a rodent model of striatal neurodegeneration, in no case to date have the cells demonstrated a full repertoire of functional improvements (Arber et al., 2015; Aubry et al., 2008; Delli Carri et al., 2013; Ma et al., 2012; Nicoleau et al., 2013). Thus, this data suggest that the obtained cells are not pure MSN populations and that an improved protocol for *in vitro* differentiation is necessary.

To obtain authentic human MSNs from hPSCs it is important to accurately guide their differentiation and to do so, it is vital to take in account the lessons gained from the study of embryonic development, in particular to reconstruct the passages that *in vivo* lead to striatum formation.

2. Embryonic development of the brain

2.1. Neurulation

Neurulation is the developmental process upon which the neural tube is formed. This complex developmental phenomenon starts around the third week post fertilization in humans and involves numerous cell processes that result in the formation of the central nervous system and the spinal cord.

At the end of the 2nd week (post fertilization), the embryo consists of a bilaminar disc with epiblast cells located at the top, and hypoblast cells located at the bottom layer (Figure 5). Soon, a groove, the primitive streak, appears in the caudal third of the disc, along the midline, signalling the initiation of gastrulation: the formation of a trilaminar disc containing three germ layers, ectoderm, mesoderm, and endoderm (Figure 5).

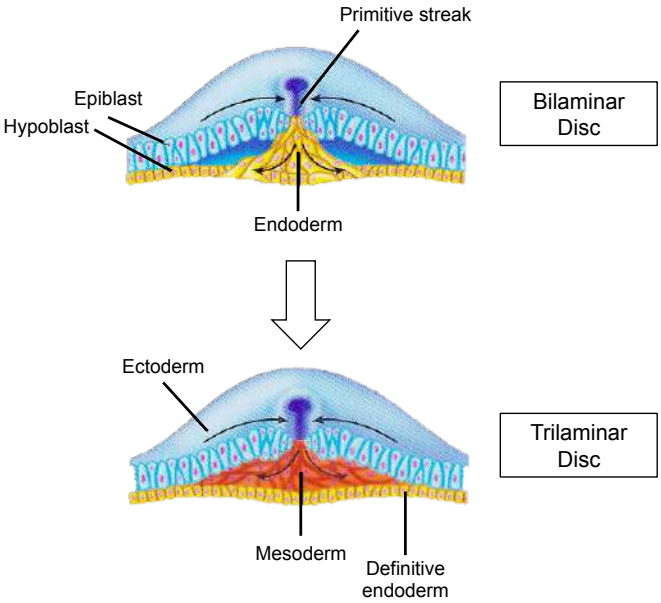

Figure 5: Schematization of the disc with two and three germ layers, ectoderm, mesoderm, and endoderm (modified from Sanes & Harris, 2006). Cross-sectional view of embryo to show movements of epiblast (ectoderm)(blue) through primitive streak to form the prospective endoderm (yellow), and mesoderm (red).

At the cranial end of the streak lies the primitive node, Hensen's node, an important center for the organization of the embryonic axes. During gastrulation, epiblast cells migrate towards and through the streak and the node, detach, and form two new layers ventral to the remaining epiblast. Cells remaining in the epiblast that do not migrate through the streak or node constitute the ectoderm. Cells that migrate cranially through the node will form the prechordal plate and the notochord. These structures initiate the process of neurulation by inducing formation of the neural plate from the overlying ectodermal cells. The remaining ectodermal cells surrounding the neural plate will form the epidermis. Induction of the neural plate originates from the inhibition of epidermis formation by signals emanating from the primitive node. Thus, the default state of the original ectodermal germ layer is neural, not epidermal (Figure 6).

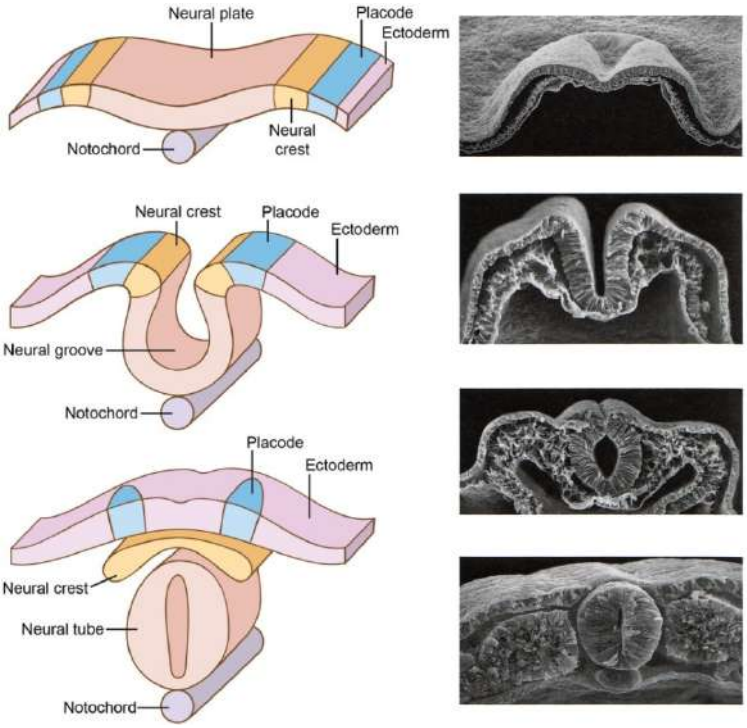

Figure 6: The image represents the primary neurulation process where the neural plate folds to originate the nascent neural tube (modified from Feinberg & Mallatt, 2013).

The neural plate is subsequently converted into the neural tube by a two-stage process, the primary and the secondary neurulation. The primary neurulation gives rise to the neural tube that will develop later into the brain and most of the spinal cord; the secondary neurulation leads to the formation of the neural tube in the caudal sacral and coccygeal regions (Copp et al., 2003; Greene et al., 2009; Schoenwolf & Nichols, 1984; François Guillemot, 2005). In both, the primary and secondary neurulation processes, closure of the tube does not occur synchronously along the anterior-posterior axis, but generally progresses from anterior to posterior axis.

2.2. Neural tube regionalization

At the end of the process of neurulation, the neural tube will differentiate to create patterns of cell types in three axes, antero-posterior, dorso-ventral and medio-lateral, thus forming the brain in the anterior part, and the spinal cord in the posterior end of the neural tube.

Based on gene expression patterns as well as morphological information, a segmental-topological model called “prosomeric model” has been used to interpret neural plate and tube regionalization (Puelles & Rubenstein, 1993; Rubenstein et al., 1994). This model hypothesizes that the embryonic forebrain is a neuromeric structure subdivided into a grid-like pattern of histogenic domains by longitudinal (columnar) and transverse (segmental) boundaries (Puelles

& Rubenstein, 1993; Bulfone et al., 1993; Rubenstein et al., 1994; Shimamura et al., 1995). The longitudinal boundaries segregate columns of cells with similar properties that are specified by dorso-ventral (DV) patterning mechanisms, while the transverse boundaries are specified by antero-posterior (AP) patterning. DV and AP patterning originate from the interplay between different morphogens gradients and transcription factor expression patterns in the neural tube. At the end of these processes, the Central Nervous System (CNS) is highly regionalized along these main axes.

2.3. Neural tube patterning

Along the AP axis, signals divide the neural tube into four major divisions: forebrain, midbrain, hindbrain, and spinal cord, and these differences can be detected soon after the formation of the neural plate. The FGF, WNT, and RA signalling pathways have been implicated in the caudalization of neural tissue. Boundaries of *Hox* gene expression are observed along the AP axis and have been suggested to be involved in establishing different identities in the hindbrain and spinal cord (Altmann & Brivanlou, 2001).

Along the DV axis, cell fate determination involves the action of two opposing signalling pathways: SHH ventrally from the notochord and BMP dorsally from the boundary of neural and non-neural ectoderm and later from the roof plate. In addition, WNT signalling has been shown to act in DV patterning too (Altmann & Brivanlou, 2001) (Figure 7).

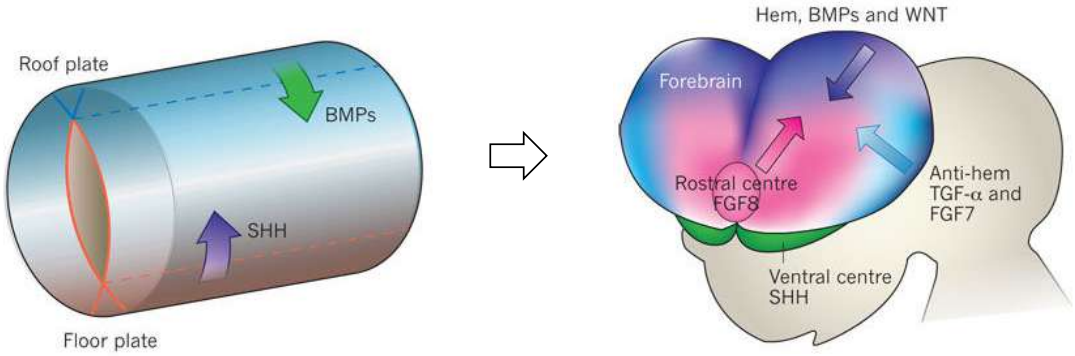

Figure 7: Signalling involved into dorso-ventral pattering (modified from Rowitch & Kriegstein, 2010).

Before the expression of other morphogens, the initial AP pattern is induced by the combined action of *Lim1, Otx2* and *Cerberus* signals, produced by the dorsal mesoderm, that initiate neural development and induces the neuroectoderm, which has an anterior neural fate (forebrain and midbrain) (Doniach, 1993). Candidate transcription factors for neuroectodermal induction are *Lim1* and *Otx2,* while a candidate morphogen is *Cerberus*, a WNT inhibitor. The two homeodomain transcription factors, *Lim1* and *Otx2*, are expressed in the tissues underlying the

anterior neural plate and seem to be essential for the development of anterior CNS structures. Loss-of-function mutants result in mouse embryos lacking forebrain and midbrain structures, suggesting that *Lim1* and *Otx2* have a role in early AP patterning.

Basic FGF and RA, regulating *Hox* gene expression, create a gradient of signals that are able to posteriorize the neural plate, inducing hindbrain and spinal cord development (Lamb & Harland, 1995; Cox & Hemmati-Brivanlou, 1995; Hemmati-Brivanlou & Melton, 1997) .

Fgf8 encodes a signalling molecule that regulates forebrain morphogenesis (Rubenstein et al., 1998) and that is expressed in the rostrodorsal and rostroventral midlines (and surrounding tissues), respectively (Ohkubo et al., 2002; Fukuchi-Shimogori, 2001). Additionally, recent work has shown that FGF signalling has a role also in ventralization of the telencephalon and the eye (Lupo et al., 2006).

The first signalling molecule to be implicated, as a regulator of *Hox* expression, was a derivative of vitamin A, RA. Experiments performed on ES cells have demonstrated that with low concentrations of RA only those *Hox* genes normally expressed in the anterior embryo are expressed, while at progressively higher concentrations of RA, more posteriorly expressed *Hox* genes are expressed in the cells (Simeone et al., 1995). In mammals, this latter gene family comprises closely related genes for homeodomain transcription factors, organized in 4 homologous clusters (Pearson et al., 2005). *Hox* genes are principally involved in specifying segmental identity, but before any molecular marker of morphological segmentation exists. The pattern of expression of the different *Hox* genes determines the morphological identity of the cranial nerves and other pharyngeal arch derivatives that arise from specific rhombomeres (Lumsden & Krumlauf, 1996).

Another morphogen important in AP patterning and implicated also in DV pattering are the WNTs, which belong to the wingless protein family and are a class of ligands that are crucial in embryogenesis. WNTs can signal through three different pathways, one of which is the canonical pathway, which is implicated in DV pattering. In this case, *β*-catenin is indirectly activated by a WNT ligand binding to the cell surface receptor, Frizzled.

Early in vertebrate development, WNT signalling controls AP axis formation (Takahashi & Liu, 2006). In particular, essential to this process is the establishment of a rostral–caudal WNT gradient, as the effects of WNTs are highly dose-dependent. Low levels of anterior WNT activity and high posterior levels are required for proper patterning of neural structures along the AP axis (Takahashi & Liu, 2006).

Bone-morphogenic proteins (BMPs) are members of a very large family of proteins, known as the TGF- β family of factors, which are mainly involved in DV patterning. BMPs are expressed in the prospective neuroectoderm before neural induction, and then in the dorsal neural tube and adjacent non-neural ectoderm, whereas secreted BMP antagonists are expressed in the notochord and the paraxial mesoderm surrounding the ventrolateral neural tube. Diffusion of BMPs and their antagonists is thought to create a dorsal (high) to ventral (low) gradient of BMP activity, which specifies distinct progenitor domains in the dorsal spinal cord. The results of several studies strongly support this model, showing that increasing or decreasing BMP signalling in the dorsal neural tube expands or reduces specification of dorsal cell types.

BMP signals have a role in patterning the dorsal telencephalon, and inhibition of BMP signalling, for example effect of SHH signal, might be necessary for ventral telencephalic specification (Furuta & Hogan, 1998) (Figure 8).

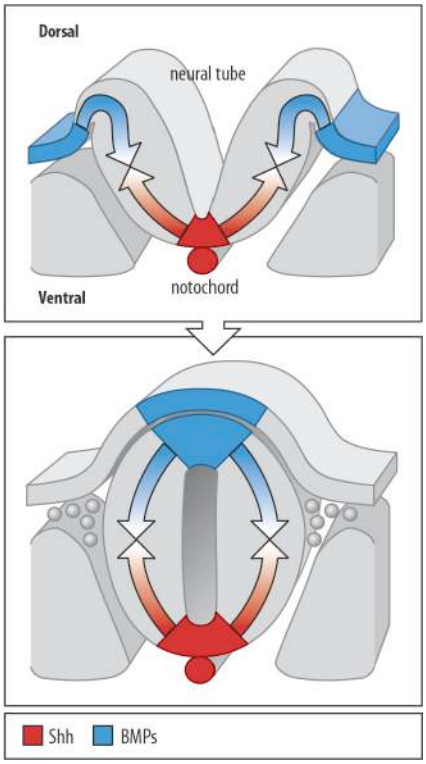

Figure 8: Schematic representation of BMP signal, which promote dorsalizing fate, in opposition to ventralizing effect of SHH signal (from Developmental Biology, 11th edition).

Different concentrations of BMPs differentially regulate the growth of different prosencephalic regions, suggesting that a normal function of these molecules may be necessary to regulate regional growth and patterning of the brain (Crossley et al., 2001).

There are many similarities between the WNT and BMP signalling pathways. In fact, there are several natural inhibitors of these pathways; for the BMP pathway, FOLLISTATIN, NOGGIN, and CHORDIN can interfere with the activation of the pathway by blocking BMP from binding

to the receptor, and for the WNT pathway, CERBERUS, and Dickkopf-related protein 1 (DKK 1) prevent activation, most likely by blocking the WNT.

In particular, NOGGIN binds several BMPs with very high (picomolar) affinities, with a marked preference for BMP2 and BMP4 over BMP7. By binding tightly to BMPs, NOGGIN prevents BMPs from binding their receptors (Zimmerman et al., 1996) (Figure 9).

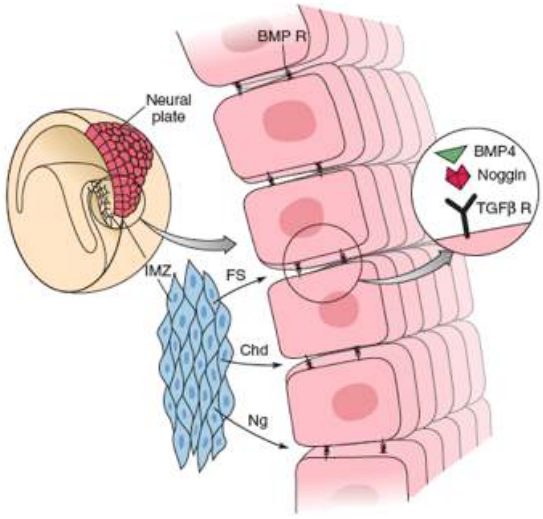

Figure 9: The current model of neural induction in embryos (Development of the Nervous System, 2012). NOGGIN interferes with the activation of the BMP receptor by the BMPs in the ectoderm and thereby blocks the anti-neuralizing effects of BMP4. In other words, NOGGIN "induces" this region of the embryo to develop as neural tissue, ultimately generating the brain, spinal cord, and most of the peripheral nervous system.

Although NOGGIN does not play an essential role in the induction of neural tissue, it is required for subsequent development of the neural tube. In *noggin* mutants, the neural tube fails to close in cranial and lumbar regions: there is a dramatic reduction in the amount of posterior neural tissue, and a precluded ventral development in the posterior neural tube. Mice lacking *dkk1* alone are similar to the double *noggin*/*chordin* knockout mice: they lack head and brain structures anterior to the hindbrain (Schoenwolf & Smith, 1990).

Sonic hedgehog (SHH), which has an opposite effect to BMPs signalling, is a member of the HH family of secreted proteins and is expressed in the floor plate and the underlying notochord. Overexpression and functional inhibition studies have shown that SHH is necessary and sufficient to induce the floor plate and the ventral progenitor domains all along the neural tube (Briscoe & Ericson, 2001; Jessell, 2000; Ruiz I Altaba et al, 2003). Extensive experimental data, based on both gain- and loss-of-function approaches performed in all the main vertebrate model systems (fish, frog, chick and mouse), have shown that SHH signals are crucial in the specification of ventral cell fates throughout the CNS (Briscoe & Ericson, 2001; Chiang et al.,

1996; Wilson & Maden, 2005). *Shh* is expressed, also, along the entire AP extent of the prechordal plate and the notochord. Whereas SHH induces the expression of some genes (e.g. *Shh, HNF3, Nkx2.2*) in all regions of the medial neural plate/ventral neural tube, other genes are induced specifically within particular regions along the AP axis. For instance, SHH induces the expression of *Nkx2.1* in the prosencephalic neural plate, whereas in more posterior locations it induces *Nkx6.1* expression (Hogan et al., 1995) (Figure 10).

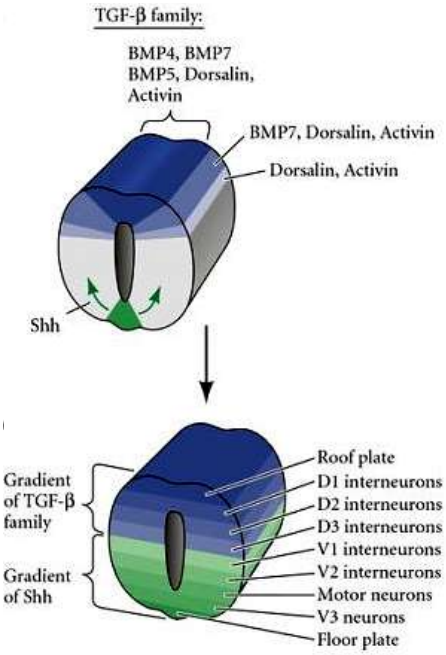

Figure 10: Schematic representation of SHH and TGF-β gradient in the CNS (Development of the Nervous System, 2012)

3. Development of the striatum

Following neural patterning, the most anterior portion of the neural tube shows drastic changes before the posterior portion of the tube is formed. Indeed, in this region the tube balloons into

three primary vesicles: the forebrain (prosencephalon), midbrain (mesencephalon) and hindbrain (rhombencephalon). While the rhombencephalon is subdivided into the metencephalon and myelencephalon, the forebrain is subdivided into the prosencephalon, from which are derived the telencephalon and diencephalon (Figure 11).

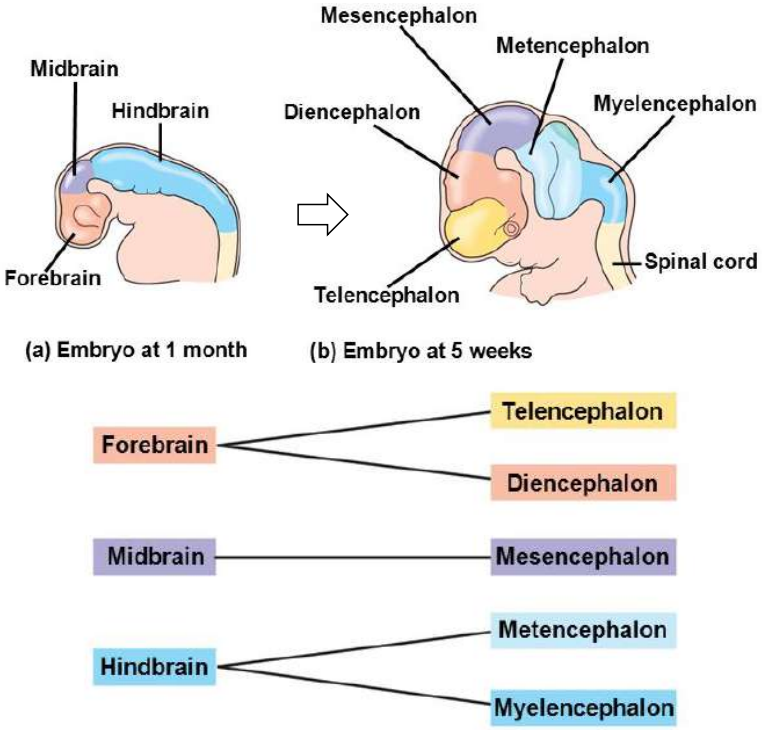

Figure 11: Schematic representation of forebrain (prosencephalon), midbrain (mesencephalon) and hindbrain (rhombencephalon) (modified from Pearson Education, 2011).

In particular, the prosencephalon is subdivided into the anterior secondary prosencephalon (telencephalon and hypothalamus) and the more caudal diencephalon (Pombero & Martinez, 2009) (Figure 12).

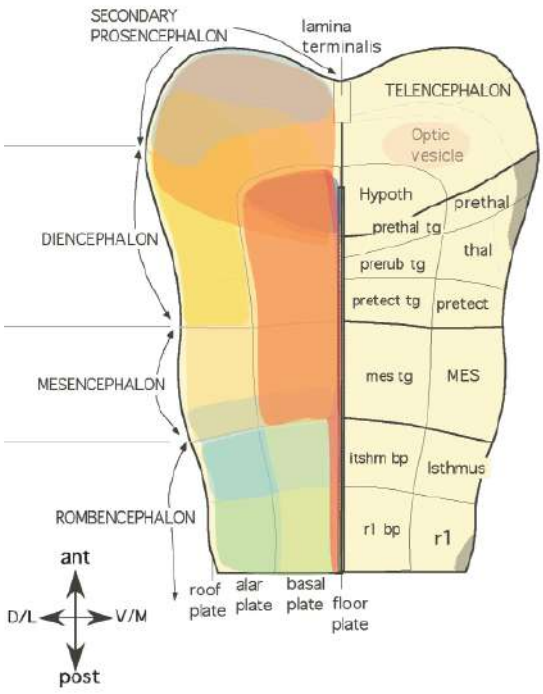

Figure 12: Subdivization of the prosencephalon into the anterior secondary prosencephalon (telencephalon and hypothalamus) and the more caudal diencephalon (Vieira et al., 2010).

The telencephalic primordium is located in the anterolateral neural plate and anterior neural ridge (ANR), and it is the latter structure that is important in regulating the growth of the anterolateral neural plate. For its specification, there is a discrete group of adjacent cells that act as an organizer to induce the formation of the telencephalon. Cells at the rostrolateral end of the neural plate are fated to become the telencephalon (Cobos et al., 2001; Inoue et al., 2000). These cells turn on expression of *Foxg1*, a transcription factor that belongs to the forkhead family of genes. RNA in situ hybridization analysis and lineage tracing using $Foxg1^{Cre}$ mice have shown that *Foxg1* expression in the anterior neuroepithelium specifically marks telencephalic precursor cells and delineates most of the embryonic telencephalon (Hébert & McConnell, 2000; Shimamura et al., 1995, 1997; Tao & Lai, 1992).

Once the anterior neural plate acquires a telencephalic fate and expresses *Foxg1*, it becomes further subdivided into domains distinguishable by the expression of other molecular markers. These include genes encoding transcription factors that are expressed in specific telencephalic subdomains, such as *Nkx2.1*, *Gsx2*, *Pax6*, and *Emx2*, as well as extracellular factors that are expressed in signalling centres at the edges of these subdomains, such as SHH, FGFs, WNTs, and BMPs (Hébert & McConnell, 2000; Shimamura et al., 1995, 1997; Tao & Lai, 1992). The expression and function of these TFs will be described in the following sections.

3.1. Molecular definition of the telencephalic region

The specification of the DV patterning of telencephalic region requires the correct establishment of SHH signalling, and Glioma-associated oncogene homolog 3 (GLI3) activity. The latter is a member of the Gli family of zinc finger TFs, and its expression is regulated in a SHH-dependent manner. Specifically, it is believed that the activity of *Gli3* is negatively regulated by SHH. At the dorsal region of the telencephalon, where the concentration of SHH is limited, the *Gli3* protein is converted from an activator into a repressor form and promotes dorsal patterning (Evans, Kelly, Precious, & Rosser, 2012). SHH signalling also supports the expansion of progenitors of the ventral telencephalon by inducing and maintaining the expression of *Nkx2.1* until at least E14 in the mouse and later into neurogenesis (Evans et al., 2012). Although BMP inhibition is required for neuronal development, BMPs are needed to dorsalize the telencephalon and restrict ventral telencephalic development. BMPs over-expression has shown inhibition of *Foxg1, Nkx2.1*, and *Dlx2* genes, TFs typical of the ventral telencephalon.

Likewise, WNTs are crucial for the generation of the dorsal telencephalon (Houart et al., 2002) and specific concentrations are needed to further refine regional patterning and to induce the expression of *Pax6,* a dorsal telencephalon marker (Kim, Anderson, Rubenstein, Lowenstein, & Pleasure, 2001).

Taken together, these conserved mechanisms provide the core of telencephalon patterning (Lupo et al., 2006) (Figure 13).

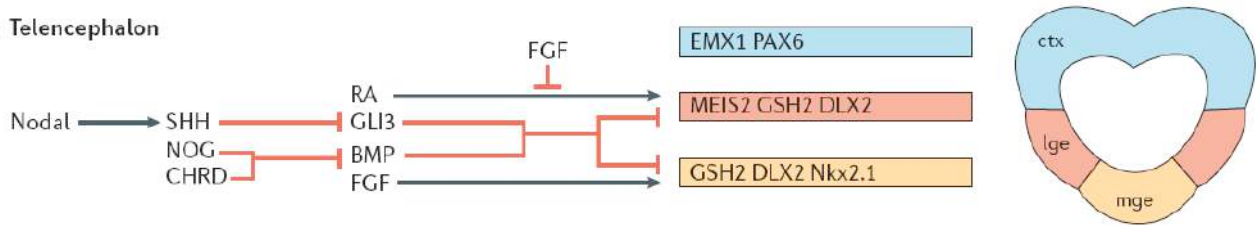

Figure 13: Signalling involved in telencephalon patterning (Lupo et al., 2006).

The primary division within the telencephalon is the pallial-subpallial boundary (PSB), a cell-lineage restricted boundary that divides the telencephalon into the ventral (subpallial) and dorsal (pallial) telencephalon (L Puelles & Rubenstein, 1993; Rink & Wullimann, 2002) (Figure 14).

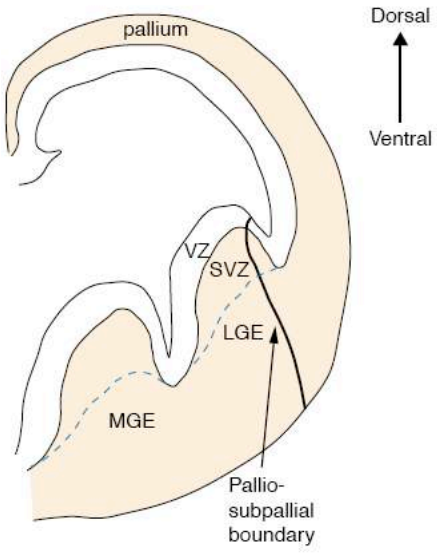

Figure 14: Dorsal-ventral subdivision of the telencephalon (modified from Toresson et al., 2000).

The pallium includes the developing cerebral cortex, while the subpallium the ganglionic eminences which are constituted by the medial (MGE) and lateral (LGE) elevations, whereas at caudal levels there is a single eminence, known as the caudal ganglionic eminence (CGE) (Figure 15).

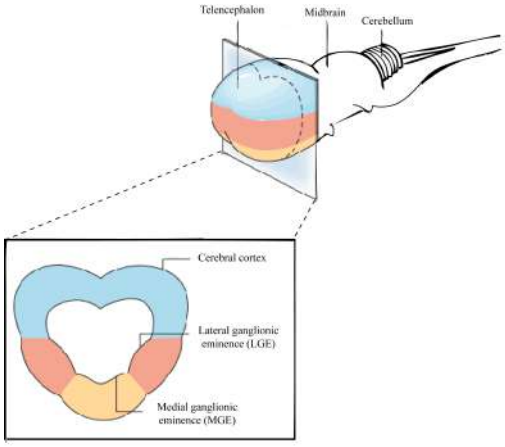

Figure 15: Partition of the telencephalon into cerebral cortex, lateral ganglionic eminence and medial ganglionic eminence (modified from Lupo et al., 2006).

3.2. Dorsal telencephalon

The pallium contains the cortical structures and the pallial nuclei (Nural & Mastick, 2004). Several transcription factors are important for dorsal telencephalic patterning, *Pax6* and *Emx2* are two examples of TFs whose expression is essential for cortex development (Figure 16). *Pax6* in mouse is first detected at embryonic day 8 (E8) in the developing forebrain in a broad domain, encompassing the prospective optic vesicles, telencephalon and diencephalon. During the period of neurogenesis in the telencephalon (E10.5–18.5), *Pax6* is expressed in the

mitotically active ventricular zone of the dorsal telencephalon, and in the stream of cells linking the ventral pallium through the adjacent striatum and parastrial area. *Pax6* is also expressed at low levels in the ventricular zone of the LGE, future striatum, located just ventral to the pallio-subpallial boundary but is absent in the MGE, future pallidum (Manuel & Price, 2005). *Pax6* loss-of-function leads to an expansion of the expression of MGE marker genes *Shh*, *Nkx2.1* and *Lhx6* into the territory of the LGE. This mispatterning alters the regional identity of the LGE, resulting in an enlargement of the MGE territory at mid gestation followed by underdevelopment of the striatum later on (Manuel & Price, 2005) (Figure 16).

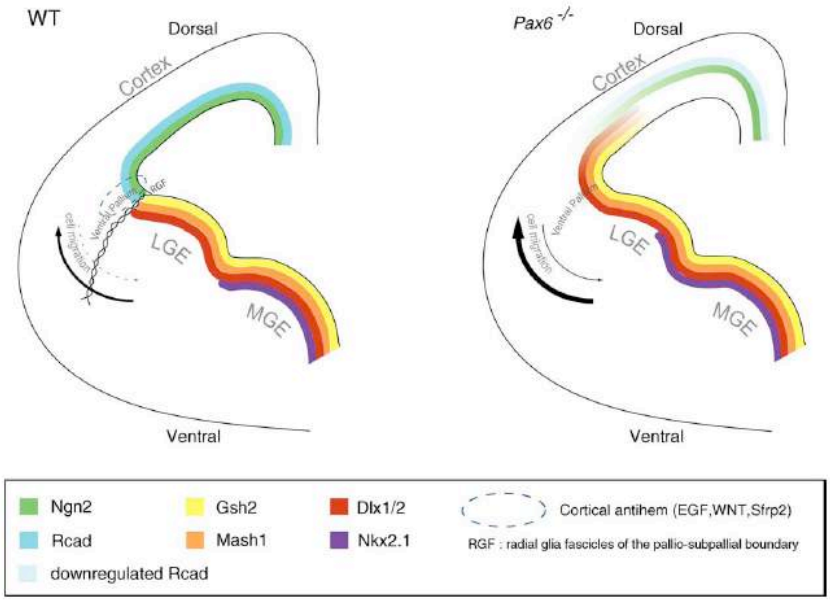

Figure 16: Pallium and subpallium border in WT and *Pax6*$^{-/-}$ embryos (Manuel & Price, 2005).

The bHLH transcription factors *Ngn1*, *Ngn2* and *Ascl1* are implicated in the specification of dorso-ventral fates in the telencephalon. *Ngn1* and *Ngn2* are required to establish pallial properties and to repress subpallial properties including the expression of the ventral specific genes like *Ascl1*. Since there is evidence of a direct regulation of *Ngn2* by *Pax6* in the dorsal telencephalon, it is likely that *Pax6* regulates pallial development in part by activating the expression of *Ngn1* and *Ngn2*, which in turn represses ventral identity (Manuel & Price, 2005).
The homeobox gene *Emx2* is expressed in the ventricular zone of the dorsal telencephalon in a gradient opposite to that of *Pax6*, rostro-lateral^{low} to caudo-medial^{high} (Muzio et al., 2002).
As in *Pax6*$^{-/-}$ mutants, the dorsal telencephalon of *Emx2*$^{-/-}$ embryos is severely affected. Nevertheless, in the absence of either EMX2 or PAX6, the cerebral cortex forms and is morphologically and molecularly distinguishable from adjacent structures such as basal ganglia

and fimbria. In double homozygous *Pax6*$^{-/-}$/*Emx2*$^{-/-}$ mutants the cortex does not form, and ventral progenitor domains expand across the entire dorsal telencephalon (Molyneaux et al., 2007) (Table 2).

Thus, PAX6 and EMX2 define rostral and caudal cortical areas, and in combination are both essential for the formation of the telencephalon.

Gene	Phenotype	References
COUP-TF1(Nr2f1)	Altered cortical area-specific gene expression	Zhou et al., 1999
	Loss of cortical layer IV; Undifferentiated subplate neurons	Zhou et al., 2001
Emx1	Thin cortical plate and white matter; incomplete cortical layers; loss of subplate; small hippocampus	Yoshida et al., 1997
Emx2	Altered cortical area-specific gene expression	Bishop et al., 2000
	Thin cortical plate and white matter	Yoshida et al., 1997
	Expanded cortical hem	Pellegrini et al., 1996
	Deletion of dentate gyrus of the hippocampus	Tole et al., 2000; Mallamaci et al., 2000
LEF1	Complete deletion of the hippocampus	Galceran et al., 2000
Foxg1	Reduction of the dorsal cortex	Hanashima et al., 2002
	Expanded expression of BMPs in the telencephalon	Dou et al., 1999; Xuan et al., 1995
Lhx2	Loss of the medial cortex including the hippocampus	Monuki et al., 2001
	Expanded cortical hem and the choroids plexus	Bulchand et al., 2001
Lhx5	Loss of the cortical hem and the choroid plexus; undifferentiated hippocampus	Zhao et al., 1999
Ngn1	Loss of the preplate neurons; decreased expression of Ngn2	Fode et al., 2000
Ngn2	Neural tube closure defect	Fode et al., 2000
	Ectopic expression of ventral markers in the cortex	Fode et al., 1998
Pax6	Altered cortical area-specific gene expression	Bishop et al., 2000
		Stenman et al., 2003b
	Overgrowth of cortical VZ/SVZ	Warren et al., 1999
	Ventralization of gene expression in coticostriatal boundary	Stoykova et al., 2000
Tlx(Nr2e1)	Abnormal hippocampus and amygdala	Stenman et al., 2003b
	Altered corticostriatal boundary	Monaghan et al., 1997
Wnt3a	Complete deletion of the hippocampus	Lee et al., 2000

Table 2: Neural phenotypes of mutant mice carrying null alleles of genes enriched in the dorsal telencephalon (Takahashi and Liu, 2006).

3.3. Ventral telencephalon (Subpallium)

The subpallium is marked by the expression of *Gsx1* and *Gsx2* and develops into the basal ganglia, which is responsible for coordination and planning of movement and quickly further subdivides into the dorsal pallidum and the ventral olfactory bulbs (Puelles et al., 2000; Sueiro et al., 2004).

Gsx1 and *Gsx2* are homeobox genes that are expressed in subpallial progenitor neuroepithelium regions (Valerius et al., 1995). Their expression patterns largely overlap, which suggests functional redundancy. However, *Gsx2* expression extends beyond the dorsal limit of *Gsx1* in the LGE, implying that *Gsx2* has unique functions in the dorsal LGE. In addition, *Gsx1* mutants do not show an obvious telencephalic phenotype (Li et al., 1996), while *Gsx2* mutants have a hypoplastic LGE (Szucsik et al., 1997).

Different studies have provided evidence that PAX6 and GSX2 have complementary functions in patterning the progenitors that flank the PSB by regulating opposing genetic programs (Yun et al., 2001). In fact, deletion of the murine *Gsx2* gene causes an expansion of the dorsal *Pax6* expression into the ventral LGE territory, whereas *Gsx2* misexpression represses the dorsal

marker *Pax6* and upregulates the ventral markers, *Dlx* and *Ascl1*. These data indicate that *Gsx2* regulates dorsal/ventral marker expression and LGE specification (Kyuson et al., 2003).
Several other transcription factors have also been linked to different phases of neuronal development within the ventral telencephalon, some of them are shown in Table 3 below.

Gene	Phenotype	References
*Dlx1/Dlx2**	Defective tangential migration of cortical interneurons	Anderson et al., 1997a
	Defective differentiation of late-born striatal neurons	Anderson et al., 1997b
Ebf1	Altered gene expression patterns in the LGE and defective differentiation of striatonigral projection neurons	Lobo et al., 2006
Gsh2	Mis-specification of LGE progenitors	Toresson et al., 2000; Corbin et al., 2000; Yun et al., 2001
Lhx7/8(L3)	Defective differentiation but not survival of cholinergic neurons in the basal forebrain and the striatum	Zhao et al., 2003; Mori et al., 2004
Mash1	Precocious differentiation of LGE progenitors	Horton et al., 1999; Casarosa et al., 1999
Notch1	Reduction of early-born patch neurons in the striatum	Mason et al., 2005
*Notch1/3**	Reduction of both early-born patch and late-born matrix neurons in the striatum	Mason et al., 2005
Nkx2.1	Molecular re-specification of the pallidum into the striatum	Sussel et al., 1999
RARβ	Defective patterning of striatal compartmentation	Liao et al., 2003
*RARβ/RXRγ**	Reduction of striatal dopamine D1 and D2 receptors	Krezel et al., 1998
*RARβ/RXRβ**		
*RXRβ/RXRγ**		
Sp8	Loss of olfactory bulb interneurons	Waclaw et al., 2006
Tlx	Defective proliferation in LGE progenitors	Stenman et al., 2003c
Vax1	Dysgenesis of the optic nerve and defects in the basal telencephalon	Hallonet et al., 1999
	Defective axonal guidance and tract formation in developing forebrain	Bertuzzi et al., 1999
	Decrease of GABAergic cortical interneurons	Taglialatela et al., 2004

*double null mutations.

Table 3: Neural phenotypes of mutant mice carrying null alleles of genes enriched in the ventral telencephalon (Takahashi & Liu, 2006).

Within the subpallium, the MGE, LGE, and CGE produce distinct groups of neurons and interneurons that populate the entire dorsal and ventral telencephalon. Similar to the patterning of the dorsal telencephalon, morphogenetic molecules and transcription factors are engaged in patterning and specification of LGE, MGE, and CGE (Takahashi & Liu, 2006) (Figure 17).

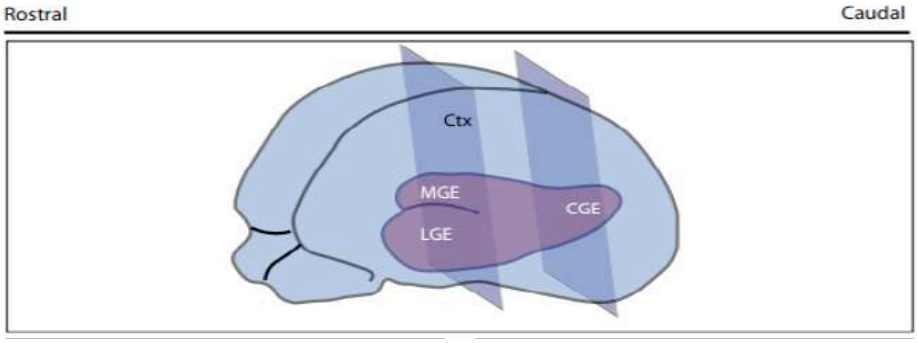

Figure 17: Morphogenetic molecules engaged in patterning and specification of the ventral telencephalon (modified from Greenberg et al., 2015).

3.3.1. MGE

The MGE is a very heterogeneous structure, giving rise to progenitors of interneurons from the cerebral cortex and the hippocampus, and progenitors of the globus pallidus (Marin et al., 2000; Wichterle et al., 2001).

Otx2 expression in the E9.5–E12.5 subpallium is restricted to the ventricular zone (VZ) and sub-ventricular zone (SVZ), where in the MGE it is required to generate normal numbers of SVZ progenitors and mantle zone (MZ) neurons (Casarosa et al., 1999; Yun et al., 2001). Furthermore, *Otx2* promotes oligodendrogenesis through positive regulation of *Olig1* and *Olig2* (Hoch et al., 2015; Petryniak et al., 2007; Yuen et al., 2014). Within the MGE, *Otx2* is required for the production of specific MGE derivatives (Hoch et al., 2015). In fact, *Otx2* may be involved in regulating and responding to FGFs. This signalling is essential for the generation of ventral cell types in the telencephalon. In fact, disruption of the gene that encodes FGF receptor 1 (*Fgfr1*) leads to a loss of expression of LIM homeobox protein 6 (LHX6) and LHX7, two LIM-domain transcription factors that are expressed in the MGE and are necessary for the differentiation of MGE-derived interneurons. In these mutants, *Nkx2.1*, which is normally expressed in the MGE and is necessary for its development is no longer expressed (Hébert & Fishell, 2008). *Nkx2.1* encodes a homeodomain transcription factor that is expressed in the VZ, SVZ and in a subset of neurons in the MZ of the MGE (Sussel et al., 1999). Several lines of evidence demonstrated that *Nkx2.1* function is essential for the specification of ventral identities and required for the specification of major subgroups of cortical interneurons of the MGE. In fact, *Nkx2.1*$^{-/-}$ mouse mutants, show molecular features of the LGE inside the MGE domain and generates striatal rather than pallidal neurons (Elias et al., 2009; Sussel et al., 1999). However, the human fetal brain development study had shown the expression of *NKX2.1* also in the developing striatum. At 7–8 w in human embryos, in fact, ~74% of the total striatal cells was NKX2.1^{+} and most NKX2.1^{+} cells co-expressed ISLET1 and CTIP2 (80.7 ± 6% and 95.9 ± 0.9%, respectively). At 20w NKX2.1 and ISLET1 were restricted to a few scattered cells (6.3 ± 2.7%). These observations suggested that the co-expression of NKX2.1 identifies the majority of striatal precursors, which later switch off the expression of NKX2.1 and ISLET1, and only CTIP2 expression is maintained (Onorati et al., 2014).

3.3.2. LGE

Within the LGE, the ventral part contains progenitors of GABAergic projection neurons in the striatum and the nucleus accumbens, while the dorsal part contains interneuronal progenitors that will migrate to the olfactory bulb (Rubenstein et al., 1998; Stenman et al., 2003; Wichterle et al., 2001). Working downstream the dorsal-ventral patterning are domain-specifically expressed transcription factors (TFs), whose expression is critical for the proper establishment of the LGE (Fjodorova et al., 2015) (Figure 18).

Despite expression in both the LGE and MGE, *Gsx2* encodes for a protein involved in delineating dorsal-ventral cell fate, and it seems to be intimately involved in LGE development (Szucsik et al., 1997). This gene is present in large amounts in the developing ventricular eminences of the mouse brain, and mice with a targeted mutation of *Gsx2* show aberrant LGE development, as outlined by a reduction in size and the lack of *Dlx2*, *Ascl1* and *Ebf1* expression (Corbin et al., 2000; Szucsik et al., 1997; Toresson & Campbell, 2001). Using conditional gain-of-function and loss-of-function approaches in mice, different studies have demonstrated the temporally distinct roles for *Gsx2* in the specification of ventral LGE (vLGE) and dorsal LGE (dLGE). In particular, at early stages of telencephalic development, *Gsx2* is necessary and sufficient to correctly specify the vLGE and its major derivatives: the striatal projection neurons. However, at later stages, high levels of *Gsx2* specify LGE progenitors towards a dLGE fate including olfactory bulb interneurons (Waclaw et al., 2009).

Gsx2 together with *Gsx1* is essential for specifying LGE precursors. In *Gsx1*$^{-/-}$; *Gsx2*$^{-/-}$ mouse mutants, LGE precursors are dorsalized and fail to express *Ascl1*, which acts as an effector of GSX2 function (Toresson & Campbell, 2001; Waclaw et al., 2009a). *Gsx2* is upstream of *Ascl1* (*Mash1*), a bHLH transcription factor, which is expressed in the SVZ and a subset of VZ cells in the ganglionic eminences (Guillemot et al., 1993; Lo et al., 1991). *Ascl1* null mice show a severe loss of neuronal precursors, especially in the SVZ of the MGE, additionally, the VZ shows premature differentiation and results in discrete neuronal populations of the basal ganglia being absent. Thus, it appears that *Ascl1* is important in maintaining distinct the two cell populations that make up the VZ and SVZ, and also for specification of neuronal precursor cells in the MGE (Casarosa et al., 1999).

Another group of transcription factors important for ventral telencephalic development are the *Dlx* genes. *Dlx* act downstream of both *Gsx2* and *Ascl1* (Casarosa et al., 1999; Toresson et al., 2000; Waclaw et al., 2009; Yun et al., 2001). There are four *Dlx* genes expressed in the developing forebrain: *Dlx1*, *Dlx2*, *Dlx5*, and *Dlx6* (Panganiban & Rubenstein, 2002). *Dlx1/2* and *Dlx5/6* form big gene clusters that are regulated coordinately by intragenic and extragenic enhancers following a specific temporal sequence (Eisenstat et al., 1999; Ghanem et al., 2003).

Dlx1/2 are co-expressed within subsets of *Gsx2* and *Ascl1* progenitor cells; loss of *Dlx1/2* function results in maintenance of *Gsx2* and *Ascl1* expression but failure to express *Dlx5/6* (Anderson et al., 1997; Long et al., 2007; Long et al., 2009; Yun et al., 2002). More recent studies suggest that *Dlx2* expression may in fact, precede that of *Dlx1*. Whilst *Dlx5/6* are expressed in the same forebrain regions as *Dlx1/2*, their transcripts are found in more differentiated cells (Long et al., 2009).

Striatal differentiation is also associated with the expression of *Ebf1* (Garel et al., 1999). *Ebf1* is a member of the *Ebf* gene family and encodes for a transcription factor that is expressed in both the LGE and MGE between E11 and E17.5 in mice (Garel et al., 1999). In *Ebf1* deficient mice, cells at the SVZ/mantle transition zone in the embryonic LGE show an inability to downregulate SVZ specific genes such as *Dlx5*, and they are unable to activate mantle-specific genes such as *Cadherin 8* and *CRABP1*. Thus, *Ebf1* acts in the regulation of the SVZ–mantle transition and it may be specifically involved in striatal differentiation since tangentially migrating interneurons are not affected in homozygous *Ebf1* knockout embryos.

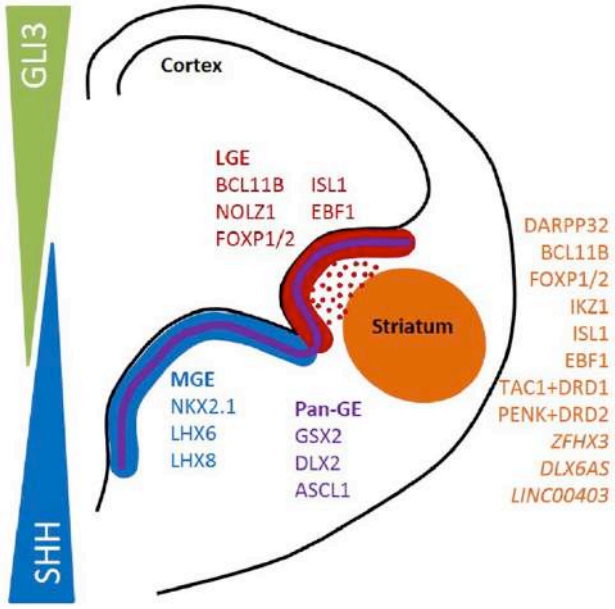

Figure 18: Summary of markers specific for subpallium development (Fjodorova et al., 2015).

3.3.3. CGE

The CGE gives rise to a diversity of GABAergic interneurons that populate different CNS regions, including supragranular layers of the cortex, consist of layers I to III, the nucleus accumbens, the bed nucleus of the stria terminalis, the hippocampus, the amygdala, the caudal striatum, and the globus pallidus (Bartolini & Ciceri & Marín, 2013; Kepecs & Fishell, 2014; Nery et al., 2002).

Analysis of CGE specification is less well developed, although *Gsx2* and *Dlx1/2* are required (Long et al., 2009). Given the strong expression of *COUP-TFI* and *COUP-TFII* (Kanatani et al., 2008; Long et al., 2009), it is likely that these genes contribute to CGE early development.

3.4. Medium-sized Striatal Projection Neurons

The principal neuronal subtype of the basal ganglia is the GABAergic medium-sized striatal projection neuron (MSN), which derives exclusively from the ventral LGE (Campbell et al., 1995; Deacon et al., 1994; Stenman et al., 2003) and from a portion of the CGE that likely represents a caudal extension of the ventral LGE (Nery et al., 2002).

These neurons convey the output of the striatum by projecting to the output nuclei of the basal ganglia through a 'direct' pathway that connects to the SNr/GPi and an 'indirect' pathway which projects to the GPe (Gerfen, 2000), as shown in Figure 19.

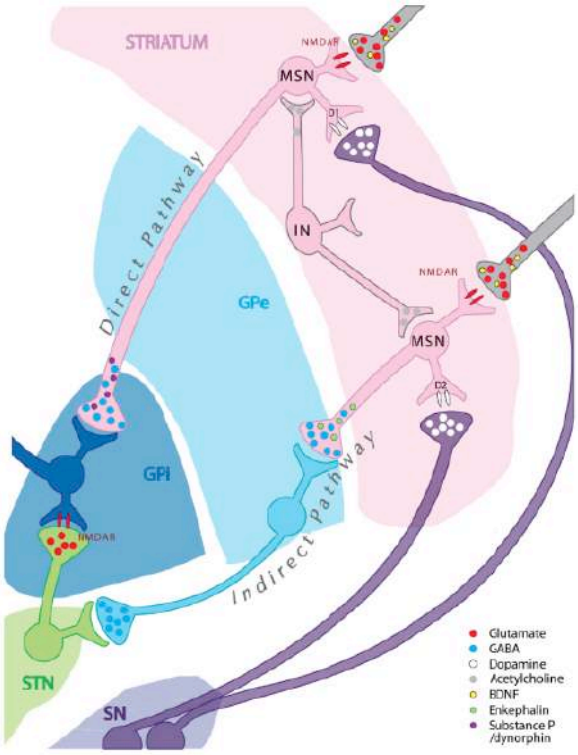

Figure 19: Schematic representation of direct and indirect pathways (Han et al., 2010).

Gsx2 expression is important for the maintenance of the pool of LGE progenitors (Corbin et al., 2000; Toresson et al., 2000; Yun et al., 2001) and for their specification toward MSN fates. This specification takes place at early stages of telencephalic neurogenesis, prior to E10.5 in mice (Corbin et al., 2000; Toresson et al., 2000; Waclaw et al., 2009; Yun et al., 2002), and from 7 w in the VZ, as demonstrated from the analysis of human fetal brain development (Onorati et al., 2014). The role of *Gsx2* in the correct formation of MSNs was demonstrated in *Gsx2* mutant mice, where the numbers of early born MSNs were severely reduced (Toresson & Campbell, 2001; van der Kooy & Fishell, 1987).

Following the specification of MSNs in the developing striatum, the *Dlx* genes (*Dlx1*, *2*, *5*, and *6*) are expressed in the SVZ and also detected between 7 w until 11 w of human brain development (Onorati et al., 2014). As described in several mutants, loss of function of these genes causes striatal differentiation defects (Corbin et al., 2000; Toresson et al., 2000; Yun et al., 2001). In particular, *Dlx1/2* mutant mice show a strikingly reduced expression of MSN markers in the striatum, including dopamine receptors DR1/DR2 (Long et al., 2009).

For the subsequent migration of the striatal precursors from the SVZ to the MZ *Ebf1* expression is required. This TF is essential for the survival and differentiation of precursors toward MSNs fate, and also for the formation of the matrix and patch regions in the developing striatum (Garel et al., 1999). After migrating radially into the developing striatum, in fact, MSNs segregate into two principal compartments: the patches (also known as striosomes) and the matrix that surrounds them (Gerfen et al., 1990). The first MSN to migrate into the developing striatum aggregate into the patches, whereas later generated neurons form the matrix (Krushel et al., 1989, 1995; Song & Harlan, 1994; van der Kooy & Fishell, 1987). Striatal patches develop concomitantly with the arrival of dopaminergic afferents from the substantia nigra (Herkenham et al., 1984). In addition, *Ebf1* has been implicated in the development of the direct pathway MSNs. In the *Ebf1* mutants, in fact, the most affected region is the MSNs in the striatal matrix compartment, which projects through the direct pathway (Lobo et al., 2008). The expression of EBF1 was detected also in the human fetal brain development in the MZ at 8 w in combination with IKAROS (Onorati et al., 2014).
This zinc finger transcription factor, in fact, is expressed in the MZ of the LGE (Agoston et al., 2007; Martín-Ibáñez et al., 2010) and requires DLX1/2 for its expression (Long et al., 2009; Martín-Ibáñez et al., 2010). *Ikaros* regulates differentiation of striatal projection neurons in the developing striatum (Arlotta et al., 2008; Garcia-Dominguez, 2003; Lobo et al., 2008; Martín-Ibáñez et al., 2010).

To become post-mitotic and to mature, striatal precursors in the MZ need to express the COUP-TF1-interacting protein 2 (CTIP2) (Arlotta et al., 2008). Loss-of-function studies have shown that *Ctip2* is required for MSN differentiation as well as for the normal formation of the patch compartment (Arlotta et al., 2008). There is evidence that these defects result from a failure of aggregation between patch compartment MSNs, in fact, *Ctip2* controls the expression of cell surface molecules that are involved in sorting MSNs into the patch and matrix compartments (Arlotta et al., 2008). In human fetal development, the expression of *CTIP2* was detected at 8 w,

11 w and 20 w in the MZ, but also in the cortical plate, where this TF has shown co-expression with DARPP32, but this neural population CTIP2^{+}/DARRP32^{+} of cortical plate did not display GABAergic identity, that is peculiar of MSNs resident in the striatum (Onorati et al., 2014).

4. How to obtain authentic MSNs *in vitro* from human pluripotent stem cells (hPSC)

Based on the information gathered in the study of embryonic development summarized above, various differentiation protocols have attempted to recreate striatal developmental features *in vitro* in order to differentiate human pluripotent stem cells into striatal MSNs with characteristic expression of gamma-aminobutyric acid (GABA), along with other known regional markers (Table 4).

Protocol	Cell source	Results	Transplant
1. Aubry et al. (PNAS, 2008)	hESCs (SA01, H9)	22% of cells are Map2^{+} neurons. Among the Map2^{+} neurons, 36% are GABA^{+} and 53% are Darpp32^{+}. Cells are Ki67^{+}	Quinolinic acid-lesioned rats. Integration, maturation, overgrowth, no functioal assessment. Generated teratoma-like region
2. Ma et al. (Cell Stem Cell, 2012)	hESCs (H9)	93% of cells are process-bearing neurons. 90% of Gaba^{+} neurons are Darpp32^{+}. No other markers	Quinolinic acid-lesioned mice. Integration, maturation, connection, no overgrowth, functional recovery on rotarod
3. Delli Carri et al. (Development, 2013)	hESCs (H9, HS401) hiPSCs (DF3F)	51% of cells are Map2^{+} neurons. With respect to the Map2^{+} neurons, 78% are GABA^{+}, 60.3% Ctip2^{+},and 20% Darpp32^{+}	Quinolinic acid-lesioned rat. Integration, some maturation, some connection, no overgrowth
4. Nicoleau et al. (STEM CELLS, 2013)	hESCs (H9), hiPSCs (190c17)	Quantification by qPCR analyses of these markers:Map2, Darpp32, Foxp1 and Foxp2	Quinolinic acid-lesioned rat. No motor analysis No ephys
5. Arber et al. (Development, 2015)	hESCs (H1,H7,H9), hiPSCs (2F8, 4FH)	80% of cells are Gaba, 45% Darpp32^{+}, no Ctip2 on section after transplantation	No rescue of apomorphine-induced rotations

Table 4: Summary of striatal protocols published

Previously published protocols have used different morphogens or transcription factor expression patterns to generate striatal neurons from human pluripotent stem cells (Arber et al., 2015; Aubry et al., 2008; Delli Carri et al., 2013; Ma et al., 2012; Nicoleau et al., 2013). These protocols encompass different stages that guide the differentiating cells towards a MSN fate. These steps include:

1) a neural lineage commitment stage,

2) a striatal precursor commitment phase,

3) a maturation stage of the striatal neuronal population.

For the first step, all the protocols used small molecules to block the TGF-β and BMP signalling, to promote the neural fate. For the second step, they administered morphogens that are able to promote the ventral telencephalic fate (for example SHH, that inhibits GLI3), and

also to inhibit the dorsal fate, for example Dickkopf-related protein 1 (DKK1) that inhibits the WNT pathway. For the maturation, they used neurotrophin factors, such as BDNF, the same that promotes the survival and the maturation of MSNs *in vivo*.

4.1. Overview on published MSN differentiation protocols

The first published attempt to derive human MSNs from pluripotent cells used a three-stage protocol on healthy human embryonic stem cells (hESCs) (Aubry et al., 2008). The hESCs were plated on a stromal feeder layer in neural induction media in order to induce rosette formation, which is an *in vitro* analogue of the neural tube (Wilson & Stice, 2006). Brain-derived neurotrophic factor (BDNF), sonic hedgehog (SHH) and DKK1 were added in order to induce the generation of striatal progenitors. Finally, BDNF, dibutyryl-cAMP (dbcAMP) and valproic acid were used in order to mature the cells into striatal neurons. The authors reported that this 62-day long protocol was able to generate 20% of the cells expressing MAP2. Of these neural cells, 50% also expressed DARPP32, a marker of a MSN. Most cells were able to generate induced action potentials, demonstrating their neuronal functionality (Figure 20, row n°1).

In 2012, Ma et al. published a 47-day long protocol using Embryoid Bodies (EBs) formation that used similar growth factors for neuronal maturation as Aubry et al., with the addition of glial cell line derived neurotrophic factor (GDNF) and interleukin growth factor (IGF). GDNF is implicated in the survival and maintenance of neurons (Lin & Tseng, 2015); IGF has a role in neuronal signalling, neurotrophic mechanisms, and neuroprotection (Hoshaw et al., 2005; Szczêsny et al., 2013). According to the paper, at day 27, 93% of the cells were positive for ßIII-TUBULIN, of which 90% were positive for GABA and this population was mostly DARPP32-positive. This is not sufficient to confirm that the neurons obtained *in vitro* are authentic MSNs. Indeed, no other molecular markers were analysed to better characterize the cells during *in vitro* differentiation, from the progenitors following neural induction until the mature neuronal populations at the end of differentiation, to confirm the striatal neuron identity (Ma et al., 2012)(Figure 20).

In 2013, the lab in which I performed this thesis work published a paper on the differentiation of human pluripotent stem cells into striatal neurons (Delli Carri et al., 2013), where they used the dual SMAD inhibition method to induce the neuro-ectodermal fate, by using NOGGIN and SB431542, to inhibit TGF-β and BMP signalling (Chambers et al., 2009). This step is followed by a differentiation paradigm similar to those previously described. In this study, several

molecular markers associated with the developing human ganglionic eminence were analysed to gauge the differentiation and maturation of the cells. At day 80 cultures contained 25% GFAP-positive cells and 51% MAP2-positive neurons, specifically 78% expressing GABA, 53% expressing CALBINDIN, 60% expressing CTIP2, and 20% expressing DARPP32. This is the only work that showed the co-expression of CTIP2 and DARPP32 in hES-derived neurons, that confirmed unequivocally the striatal identity of the obtained neurons (Delli Carri et al., 2013) (Figure 20, row n°3).

An analogous differentiation protocol based on dual SMAD inhibition (Chambers et al., 2009) is published by Nicoleau et al., in 2013. In this protocol, the authors tested the role of WNT-signalling in the generation of MSN *in vitro* (Nicoleau et al., 2013). The use of a WNT-antagonist, DKK1, and SHH together produced human ventral-telencephalic neurons that were 50-60% MAP2 positive, of which 25-30% were DARPP32-positive, indicating that sequentially organized WNT signals play an important role in striatal development (Figure 20, row n°4). However, also in this work the authors didn't characterize the obtained neurons at the end of protocol.

The dual SMAD inhibition (Chambers et al., 2009) was also used by Arber and colleagues in 2015. In this protocol, the authors used ACTIVIN A, a member of the transforming growth factor beta (TGF-β) family of proteins, rather than traditionally used DKK1, to induce an LGE phenotype (Arber et al., 2015). Following ACTIVIN A treatment, ~50% cells expressed CTIP2 and GSX2 at day 22, indicative of a correct LGE-fate acquisition. In addition, neurons were $DARPP32^{+}$ (40%), $CTIP2^{+}$ (80%) with GABAergic electrophysiological properties at day 43. However, after transplantation, the authors didn't show any kind of characterization of the cells transplanted. Also in this work was missing the specific identification of MSNs by the analysis of striatal neurons' typical markers (Figure 20, row n°5).

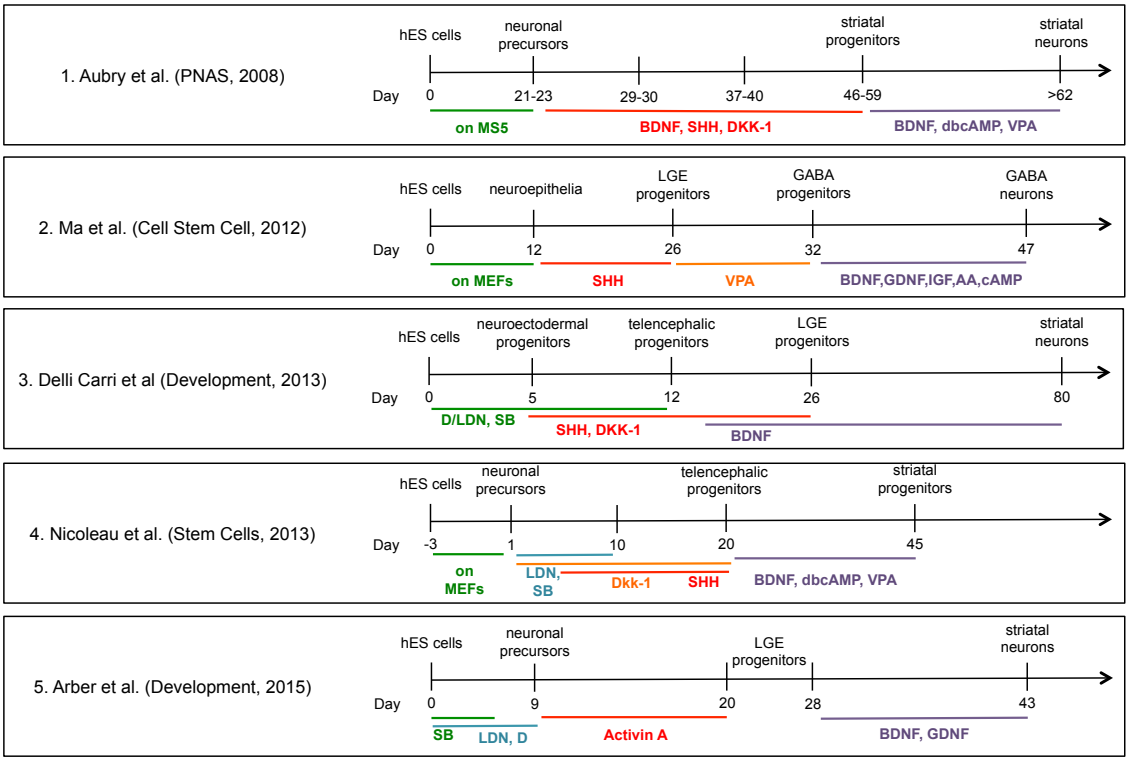

Figure 20: Details of striatal protocols published.

During my PhD I have used the Delli Carri (Delli Carri et al., 2013) protocol for MSN generation. This protocol is actually the only one that unequivocally follows the phases of neural differentiation starting from hPSC cells to MSNs, and compares these populations *in vitro* with the developing human fetal brain (Onorati et al., 2014). Indeed, thanks to detailed gene-expression information obtained by the study of human fetal brain development performed by Onorati et al., in 2014, we are now able to identify and characterize every stage of human striatum development *in vivo*, and to understand if hPSC lines, differentiated towards a striatal fate, are able to recapitulate the principal stages of striatal development *in vitro*.

4.2. Focus on Delli Carri et al. protocol, 2013

As for the majority of the directed differentiation protocols, Delli Carri et al induced three phases encompassing neural induction, neural patterning and terminal differentiation of MSNs. These steps closely recapitulate what occurs *in vivo i*n the developing striatum (Figure 21).

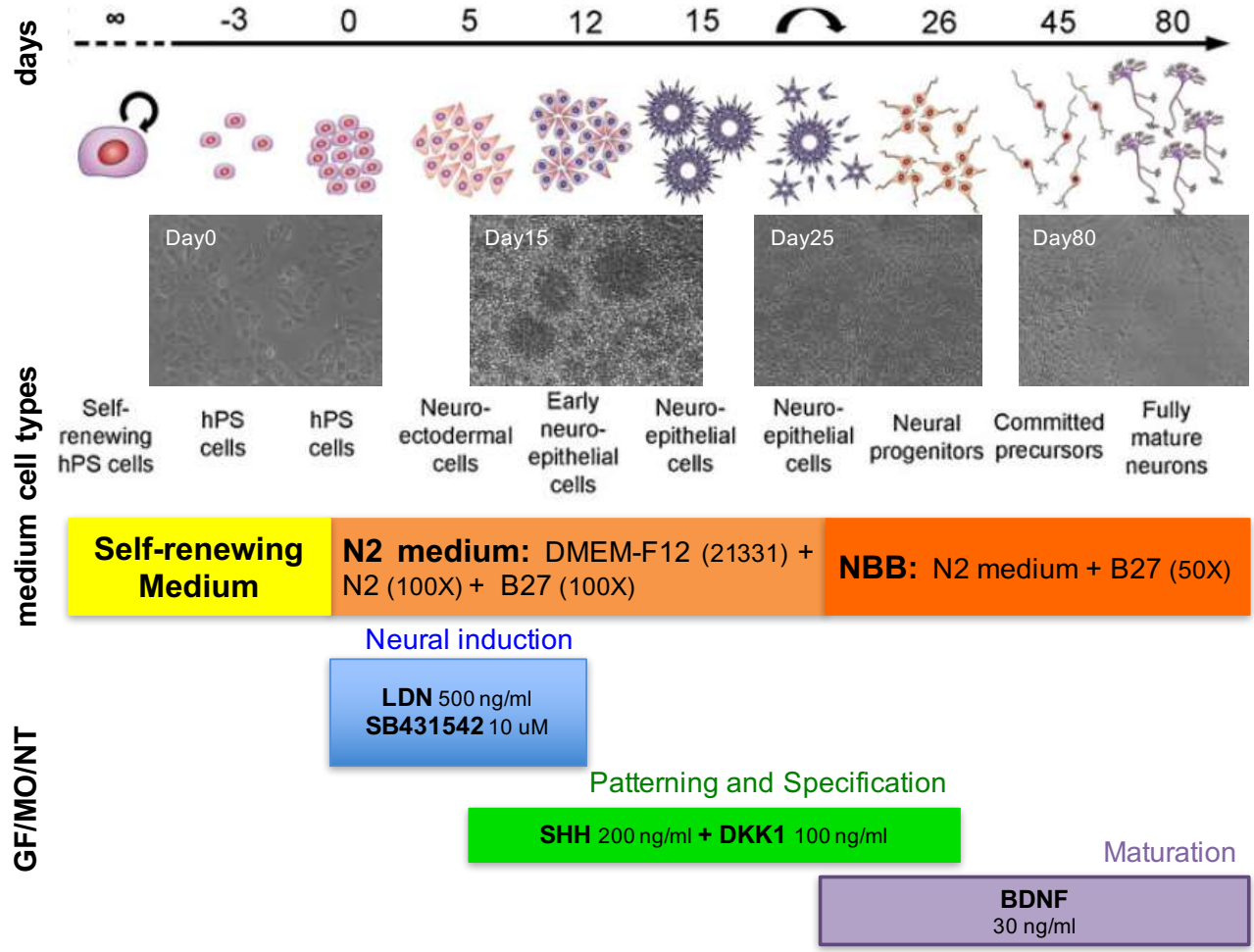

Figure 21: Diagram of Delli Carri protocol (2013).

(i) Neural induction

Dual inhibition of SMAD signalling by NOGGIN (N) and SB431542 (SB) is used for neural induction from hPSC cells in order to achieve efficient neuroectodermal fate acquisition, as described in Chambers et al., published in 2009.

For neural induction, 500nM of LDN-193189 (LDN), a NOGGIN analogue, was used to block the BMP pathway, which drives toward trophectoderm and ectoderm fate, in combination with 10μM SB431542 (SB), to block TGB-β signalling, which promote mesendoderm fate. NOGGIN or LDN treatment in combination with SB (N+SB or LDN+SB) showed comparable neural conversion efficiency of hESCs.

Neural induction of hPSC cells was achieved by exposure to LDN+SB for 12 days demonstrated by the formation of neural rosettes (Zhang et al., 2010) at day 15. At this stage neuroepithelial cells begin to express NESTIN, SOX2, OTX2 and PAX6, and show a down-regulation of OCT4 and NANOG, which are typical markers of the pluripotent state (Figure 22).

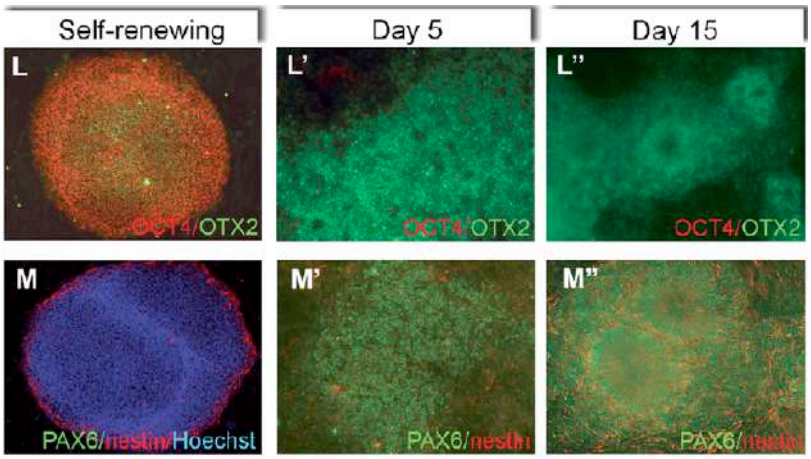

Figure 22: Immunofluorescent analysis for markers for pluripotency OCT4, and for markers of neural induction PAX6, NESTIN, and OTX2.

Interestingly, in the Onorati study at 2-3 weeks post-conception, we observed, in the human embryo the same immunoreactivity at day 5 of *in vitro* differentiation. In particular, OTX2 gene was expressed in N-CADHERIN^{+} neural folds and in the more posterior region of the closing neural tube (Onorati et al., 2014).

From the day 15 of *in vitro* differentiation, the cells started to show also BF1 (FOXG1) expression, a gene that is highly expressed in the subpallium, as a result of the inhibition of the BMP pathway.

(ii) Patterning and Specification

To recapitulate *in vitro* ventralization of the telencephalon, two different pathways are modulated *in vitro*, SHH and WNT signalling. The former is important for the correct regionalization of the LGE and MGE, in a dose-dependent manner. The inhibition of the latter is essential to repress cortical fate. Experimentally, starting from day 5, regional patterning was achieved by treatment with DKK1 (100ng/ml) and a modified version of SHH (SHH C-25II) (200ng/ml) treatment. The SHH modification is necessary to make the morphogen more stable in the culture media. In particular, as outlined in Figure 23, DKK1 inhibits the WNT pathway, represented in red line, and SHH targets GLI3, which would otherwise activate WNT signalling, represented in green line (Figure 23).

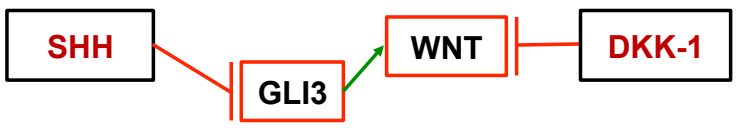

Figure 23: Schematic representation of SHH, that inhibits GLI3, and DKK1, that inhibits WNT signalling.

WNT inhibition, by means of SHH and DKK1 administration, led to GXS2 and ASCL1 positive cells around day 25, which identify respectively neurons of VZ and SVZ proliferative progenitor zones. *In vivo*, GSX2 is detected mainly in the VZ while ASCL1 expression is restricted to the SVZ of the LGE (Onorati et al., 2014). Cells positive for PAX6 were also observed in our differentiated cells. The presence of PAX6 and GSX2 positive neurons *in vitro* at day 25 recapitulate the formation of the pallial-subpallial boundary in human embryo, occurring at about 3 weeks post-conception

In the Delli Carri protocol few cells showed NKX2.1$^+$-ISLET1$^+$ co-expression, indicating possible presence of cholinergic interneuronal precursors (Onorati et al., 2014) This is in line with findings from Onorati et al., who identified neurons co-expressing NKX2.1$^+$-ISLET1$^+$ at 8 weeks of human embryo development. As we already know from previous studies, ISLET1 is initially expressed in post-mitotic striatal precursors and is later restricted to cholinergic interneuron populations (Wang & Liu, 2001).

(iii) Maturation

The patterning stage was extended until day 26, followed by the terminal differentiation period (from day 26 to day 80) where the cells are exposed to 30ng/ml BDNF, a neurotrophin that promotes cell survival *in vitro* (Altar et al., 1997; Canals, 2004; Cattaneo et al., 2001; Crook & Housman, 2011; Fusco et al., 2003; Gauthier et al., 2004; Zuccato & Cattaneo, 2007).

At day 45 of neural differentiation, βIII-TUBULIN$^+$ neuronal cells with branched MAP2$^+$ dendrites appeared in the culture (Figure 24, E and F). The majority of these neurons exhibited a GABAergic phenotype, as confirmed by immunocytodetection of glutamic acid dehydrogenase-67 (GAD67) staining, the limiting enzyme for GABA synthesis (Behar et al., 1994)(Figure 24, F and G).

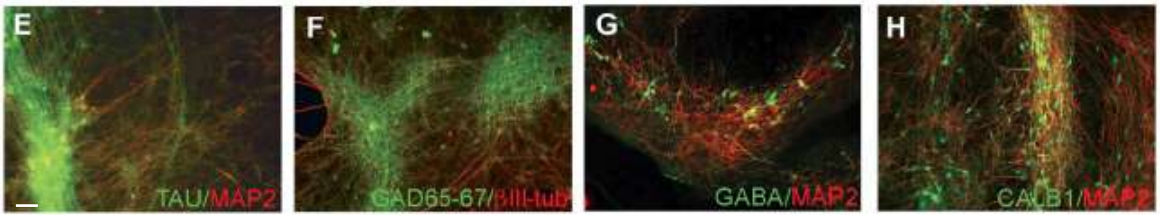

Figure 24: Immunofluorescent analysis for neuronal markers at day 45. (Panel E**)** Expression of the pan-neuronal markers MAP2 (red) and TAU (green) (scale bar=50 μm); (Panel F) Immunodetection of GAD65/67 (green) and βIII-tubulin (red) (scale bar=50 μm); (Panel G) MAP2$^+$(red) neurons express GABA (green) (scale bar=50 μm); (Panel H) Calbindin (CALB1) (green) with MAP2$^+$(red) (scale bar=50 μm) (Delli Carri et al., 2013).

At day 45 of the differentiation period, the cells matured and acquired expression of striatal markers, and in particular, of MSNs. The transcription factors FOXP2 and FOXP1 were

expressed in mature striatal neurons in combination with CALBINDIN (CALB), a calcium-binding protein (Garcia-Calero et al., 2013; Hisaoka, Nakamura et al., 2010).

There are indeed numerous DARPP32, CTIP2, FOXP2 and FOXP1 positive cells at these later stages (Figure 25).

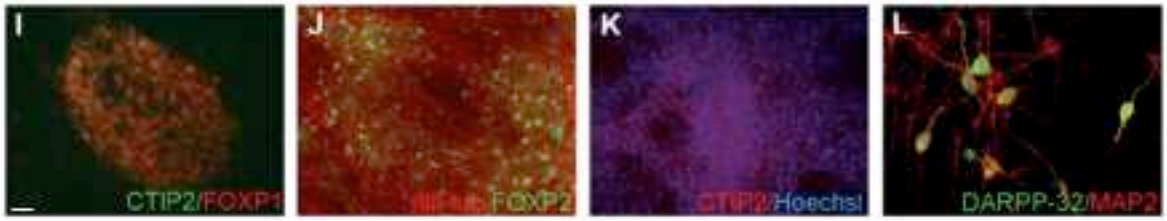

Figure 25: Immunofluorescent analysis for markers specific to identify authentic MSNs at day 45. (Panel I) The early post-mitotic striatal marker CTIP2 (green) and FOXP1 (red) is expressed in neuronal cells (scale bar=50 μm); (Panel J) Immunodetection of FOXP2 (green) and βIII-tubulin (red) (scale bar=50 μm); (Panel K) CTIP2 (red) in combination with Hoechst (blue) staining (scale bar=50 μm); (Panel L) Confocal image of $MAP2^+$(red) neurons expressing DARPP32 (green) (scale bar=25 μm) (Delli Carri et al., 2013).

MSN identity was also corroborated by analysis for DARPP32 and CTIP2 co-expression (Figure 26).

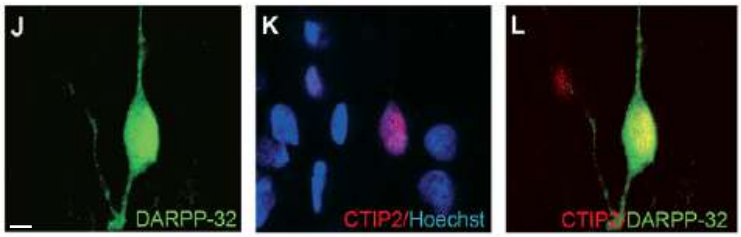

Figure 26: Crop of DARPP32 and CTIP2 double staining at day 45. Confocal analysis confirming MSN identity by co-expression of CTIP2 (red) and DARPP32 (green) (scale bar=25 μm) (Delli Carri et al., 2013).

Fifty-one percent of the cells at this stage were $MAP2^+$ neurons (Figure 27), and 17% of the total were positive for NESTIN, suggesting the presence of cells with a neuronal precursor identity at this late stage *in vitro*.

With respect to the $MAP2^+$ neurons, 78% were $GABA^+$, 60,3% $CTIP2^+$ (86% of which co-expressed GABA) and 53% $CALB1^+$ neurons. 70,6% of the $CALB1^+$ neurons co-expressed CTIP2, and 20% of the neurons were immunopositive for DARPP32, thus confirming the general acquisition of an MSN fate (Delli Carri et al., 2013).

The protocol also showed a percentage of astrocytes, as $GFAP^+$ cells, that appeared only around day 80 in culture (25% of cells) (Figure 27).

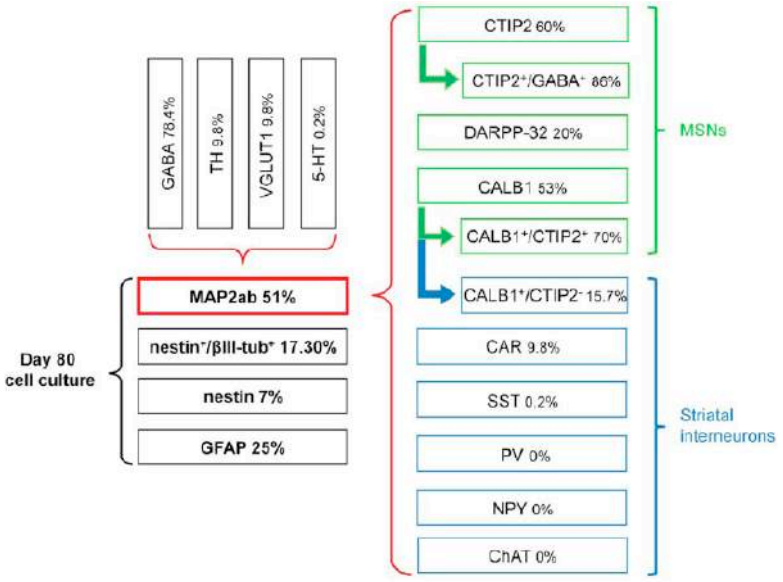

Figure 27: Quantification of different cells subtypes after 80 days of striatal protocols. Description of the different neuronal populations. MAP2$^+$ 51±3%, *n*=1126 cells; GFAP$^+$ 25±0.03%, *n*=712; nestin$^+$/βIII-tubulin$^+$ 17.3±5.03%, *n*=208; nestin$^+$ 7±4.9%, *n*=220; GABA$^+$ 78.4±9.8%, *n*=1242; tyrosine hydroxylase (TH)$^+$ 9.8±0.98%, *n*=826; VGLUT1$^+$ 9.8±0.6%, *n*=1005; 5- hydroxytryptamine (5-HT)$^+$ 0.2±0.02%, *n*=775; CTIP2$^+$ 60.3±14.1%, *n*=320; CTIP2$^+$/GABA$^+$ 86±7.6%, *n*=320; CALB1$^+$ 53±5%, *n*=1020; CALB1$^+$/CTIP2$^+$ 70.6±19.5%, *n*=770; DARPP-32$^+$ 20±3.9%, *n*=987; CALB1$^+$/CTIP2$^-$ 29.4±19.5%, *n*=770; calretinin (CAR)$^+$ 9.8±3.9%, *n*=956; SST$^+$ 0.2±0.02%, *n*=810; PVALB$^+$ 0%, *n*=790; NPY$^+$ 0%, *n*=680; ChAT$^+$ 0%, *n*=540) (mean ± SD) (Delli Carri et al., 2013).

All these human-specific gene expression transition patterns are essential tools to follow the progression of the differentiation and the maturation of the human neural progenitors *in vitro*. Due to the scarcity of human embryo developmental data these aspects had not been previously investigated.

The aim of this thesis is to further analyze human embryonic striatal development *in vitro* using the Delli Carri et al. protocol, and to generate an improved protocol for MSNs production that reliably characterizes and describes all progenitor and neuronal populations generated and their maturation *in vitro*.

After the thorough characterization of the various stages of neural differentiation, the aim is to identify the different subpopulations during striatal differentiation, and to increase the percentage of these populations in the culture in order to increase the efficiency of authentic MSNs generation *in vitro*.

Aim of the project

Aim of the project

Mimicking striatal development during *in vitro* differentiation of human Embryonic Stem cells (hESC) and pluripotent stem cells (hPSCs) is an invaluable method to investigate different aspects of striatal formation, model HD in a dish and generate cells for future cell replacement strategies. HD specifically affects medium spiny neurons (MSNs) that are located in the striatum of the adult brain. Our goal is to generate MSNs *in vitro* in a controlled and reproducible manner that mimics normal striatal development with a high degree of precision. To reach this goal I exploited the protocol published in 2013 to generate authentic MSNs (Delli Carri et al., 2013) and, during my PhD, I further characterized and improved the generation of these neurons by implementing three fundamental approaches:

i) Characterize the stability and reproducibility of the directed differentiation protocol and study the differentiation potential into MSNs of a very diverse set of human pluripotent cell lines. This part was performed on human non-integrating iPS cell line (produced at Cedars Sinai, Los Angeles), hES Roslin Cells (generated by Roslin Cell Institute, Edinburgh), hESC H9 (produced by WiCell Research Institute in 2001) and hESC RUES2 (generated at Rockefeller Foundation in Ali Brivanlou lab, New York).

ii) Outline specific cell transitions occurring *in vitro* to pinpoint potential pivoting moments during MSNs generation *in vitro*. This aim was reached by developing a highly automated pipeline for image acquisition that enabled us to characterize and quantify cell states present during differentiation with a high level of accuracy.

iii) Identify transcription factors that are highly specific for MSNs generation and exploit their function to increase and optimize MSNs turnover. This part of the project involved developing a system to overexpress Gsx2 and Ebf1 during differentiation.

Main Results

Main Results

1. Reproducibility of the Delli Carri protocol: monitoring striatal differentiation phases in four hPSC lines
   1.1. Neural induction
   1.2. Patterning: LGE progenitor markers
   1.3. Specification: Striatal precursor
   1.4. Maturation: authentic MSNs

2. Quantification of neuronal subpopulation during differentiation
   2.1. VZ-SVZ transition
   2.2. SVZ-MZ transition
   2.3. Striatal precursor in MZ
   2.4. Identification of authentic MSNs
   2.5. Role of cell cycle state during differentiation

3. Forced gene expression applied to Delli Carri protocol
   3.1. Inducible overexpression of key transcription factors during neuronal differentiation
   3.2. Generation of inducible hES cell line for Gsx2 and Ebf1
   3.3. Gsx2 and Ebf1 Regulate Cell-Cycle Kinetics
   3.4. Evaluating effects of the TFs on the MSN identity acquisition
   3.5. Modified mRNA as non-integrating strategy for TF expression: preliminary results
   3.6. Evaluation of survival and maturation of iGOF-derived MSNs after transplantation

Main Results

1. Reproducibility of the Delli Carri protocol: monitoring striatal differentiation phases in four hPSC lines

In the first part of my thesis I applied the striatal differentiation protocol published from the lab in 2013 and defined as "Delli Carri protocol" to different human pluripotent stem cell (hPSC) lines. The aim was to test the robustness and the reproducibility of the published protocol, assessing cell-line dependent differences in the efficiency of *in vitro* differentiation.

An important contribution to develop our striatal differentiation protocol was provided by recent data published in 2014 about human fetal brain development (Onorati et al., 2014). This study performed on human brain from 6 to 11 weeks of gestational age highlighted the progressive expression of a set of transcription factors (TFs) that distinguish the ventricular zone (VZ) of the LGE from the subventricular zone (SVZ) and the mantle zone (MZ), providing a complete map of markers to monitor striatum development *in vitro* and *in vivo* (Figure 28).

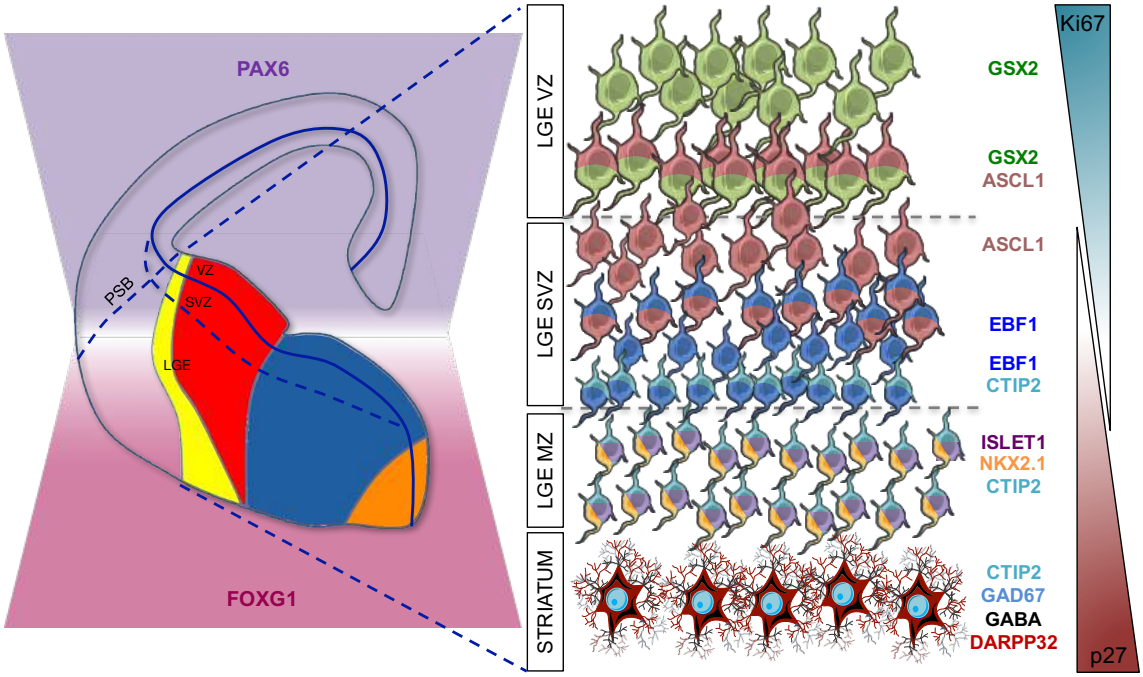

Figure 28: Most important markers specific for subpallium development toward striatal fate acquisition.

The Delli Carri protocol was applied to four human pluripotent cell lines:

- a human non-integrating iPS cell line (Mattis et al., 2015), from Svendsen's Lab (Cedars Sinai, Los Angeles),
- the Roslin hES Cells, a good manufacturing practice (GMP) human embryonic stem cells from Roslin Cell Institute in Edinburgh,
- the H9 hES cells from the WiCell Research Institute,

- the RUES2 hES parental cell line from the Ali Brivanlou lab at the Rockefeller University. This last hES cell line is important in the context of the study of HD. In fact, Brivanlou's lab has worked to create an isogenic allelic series of hESCs carrying different CAG expansions to study the effect of these mutations on neuronal differentiation.

At first, the pluripotency state of the different cell lines was assessed by immunocytochemistry for OCT4 and SOX2. All the lines show positivity for these pluripotency markers with lower intensity in SOX2 staining, especially in RUES2 cell line (Figure 29). This could suggest a slightly different basal state of pluripotency between the lines that may have significant effect at the end of differentiation.

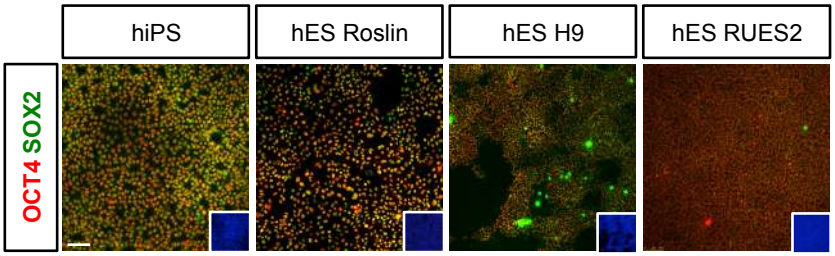

Figure 29: OCT4 and SOX2 immunocytochemistry, inset: Hoechst nuclear counterstaining in hPSCs (scale bar=100 µm).

1.1. Neural induction

For neural induction, cells were exposed to dual-smad inhibition (Chambers et al., 2009). To evaluate whether upon losing pluripotency the cells acquire a neuroectodermal identity, we analysed the expression of PAX6 and FOXG1 (see diagram in Figure 28). PAX6 is the earliest neuroectodermal marker expressed in the developing human CNS (Zhang et al., 2010), becoming at later stages a general pallial marker (Bayatti et al., 2008)(Onorati et al., 2014). Instead, FOXG1 is expressed in the prosencephalic primordium, and in the neuroepithelial progenitors (NEPs) of the VZ (Onorati et al., 2014). Here we monitored the expression of these two markers at day 15 of neural differentiation as a control for efficient neural induction (Figure 30). We found that all the four hPSC lines at day 15 exhibit a correct neuroectodermal induction in terms of PAX6 and FOXG1 expression.

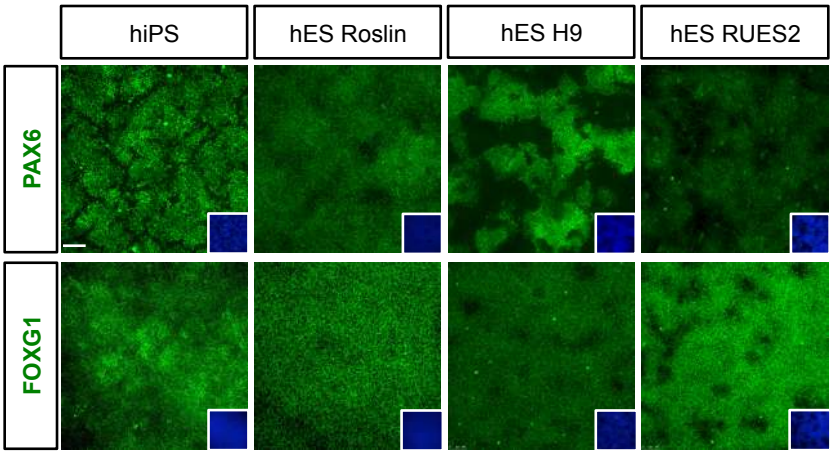

Figure 30: Immunodetection of FOXG1 and PAX6, inset: Hoechst nuclear counterstaining at day15 (scale bar=100µm).

1.2. Patterning: LGE progenitor markers

To follow the neural progression and to identify the neural progenitors, we monitored the patterning *in vitro* by assessing the expression of selected transcription factors. The first important step was to evaluate the presence of $GSX2^+$ neural progenitors, localized *in vivo* in the VZ, and their maturation by monitoring ASCL1 expression. $GSX2^+/ASCL1^+$ cells represent those striatal precursors that move to SVZ during development (see diagram in Figure 28). We focused on cells at day 25 of neural differentiations following of the Delli Carri protocol (Figure 21), since it corresponds to the end of the patterning phase (induced by SHH and DKK administration) and therefore we could evaluate their effect on the differentiation progression (Figure 31). Indeed, all the hPSC lines showed expression of GSX2 and ASCL1, suggesting that patterning had been completed successfully to obtain striatal progenitors.

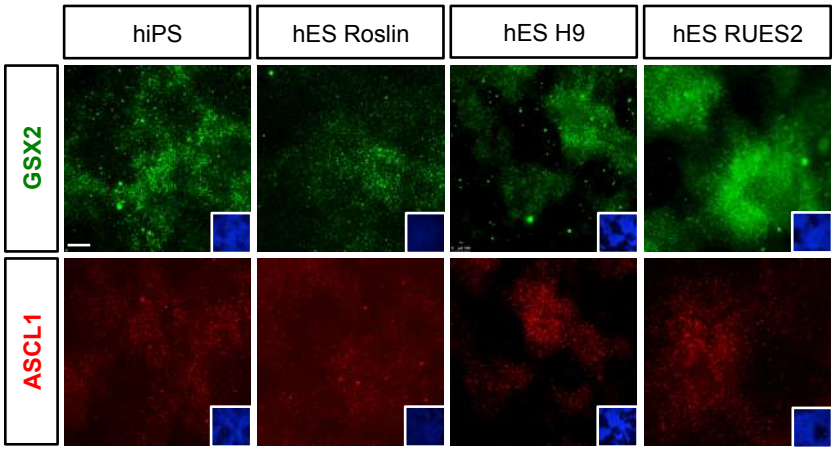

Figure 31: Immunodetection of GSX2 and ASCL1, inset: Hoechst nuclear counterstaining at day25 (scale bar=100µm).

1.3. Specification: Striatal precursor

To monitor the striatal specification phase of the four hPSC lines we performed immunocytochemistry for NKX2.1, ISLET1 and CTIP2, which are markers of the precursors of striatal neurons (see diagram in Figure 28). To identify these precursors during *in vitro* differentiation, we performed immunocytochemistry for these markers at day 30, selected because preliminary experiments have exhibited the expression of these markers at this time point. Figure 32 shows that hiPS, hES Roslin, hES H9 and hES RUES2 cells were all able to express NKX2.1, CTIP2 and ISLET1. Confirming the cells are maturating and acquiring a ventral MZ fate.

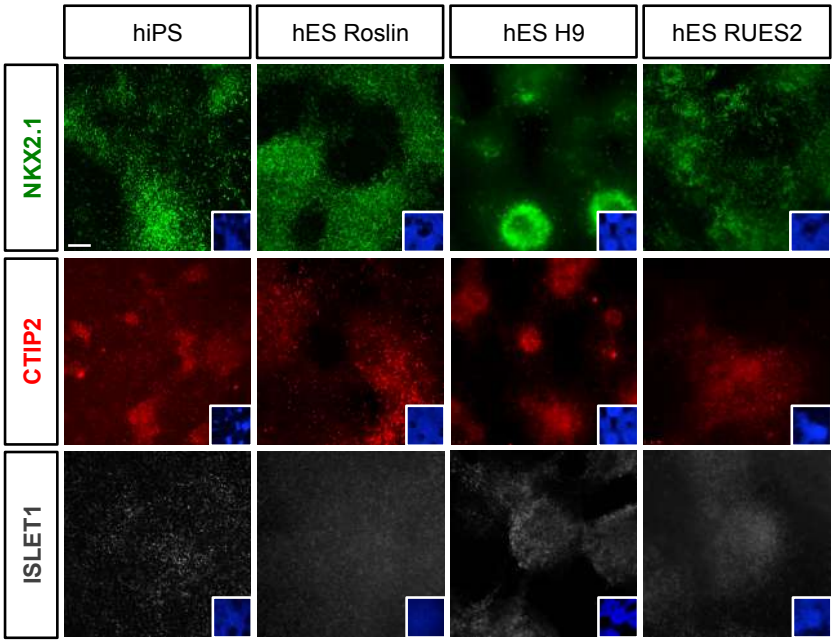

Figure 32: Immunodetection of NKX2.1, CTIP2, and ISLET1. Inset: Hoechst nuclear counterstaining at day 30 (scale bar=100µm).

Notably, we observed in our experiments some ISLET1^{+} cells that did not co-localize with CTIP2 at this stage, suggesting that they could differentiate into interneurons. This cell population was also observed in the developing rodent brain, where ISLET1 is initially expressed in all striatal precursors and later restricted to cholinergic interneurons (Wang & Liu, 2001).

Indeed, in *in vivo* studies, a subpopulation of striatal cells was found to be double positive for NKX2.1 and ISLET1, which would confirm the presence of cholinergic interneuronal precursors (Onorati et al., 2014).

1.4. Maturation: Authentic MSNs

MSNs represent more than 90% of striatal neurons in rodents and are identified by co-expression of CTIP2 and DARPP32 (also known as PPP1R1B) (Arlotta et al., 2008). We therefore decided to identify the prospective MSN neurons by evaluating co-expression of GABA together with CTIP2 and DARPP32 (Figure 33).

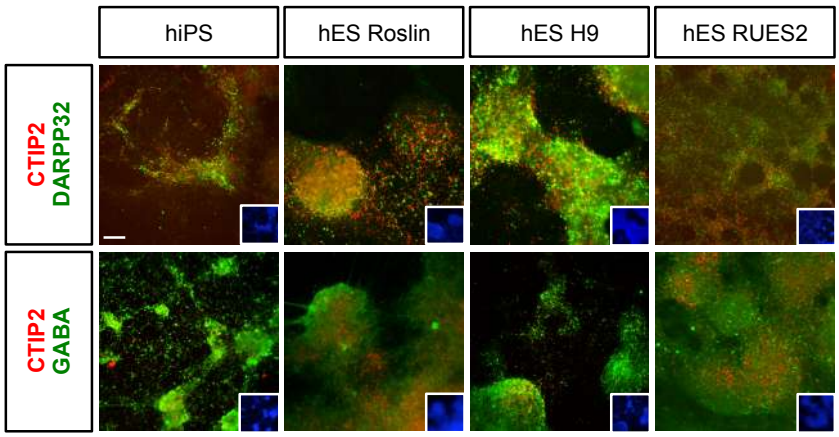

Figure 33: Double labelling of cells for CTIP2 and DARPP32, and for CTIP2 and GABA, inset: Hoechst nuclear counterstaining at day 50 (scale bar=100µm). For each cell line, we performed at least four independent differentiation experiments, and the images showed are the most representative**.**

All cell lines at day 50 showed expression of cells that were $CTIP2^{+}/GABA^{+}$. The more striking difference between the lines lies in the expression of DARPP32 which remains undetectable in differentiated RUES2, indicating that the striatal potential of this line (or its requirements to reveal such phenotype) is different from the other lines.

We demonstrated that different types of hPSC, in particular hES and hiPS cell lines, are able to correctly respond to Delli Carri differentiation protocol. Only the hES RUES2 line showed problems in the acquisition of MSN fate, evaluated by the expression of DARPP32 and CTIP2 markers at the end of differentiation.

2. Quantification of neuronal subpopulation during differentiation

To better characterize the different subpopulations during the later phase of differentiation and to quantify the expression of the markers that identify each neurodevelopmental stage *in vitro*, we worked to improve the acquisition and quantification methods. However, the quantification was hindered the formation of dense clusters of cells during the maturation phase of the differentiation protocol. Indeed, mature $CTIP2^{+}/DARPP32^{+}$ formed clusters that allowed the cells to interconnect, facilitating neuronal maturation. Unfortunately, standard wide-field microscopy is not sufficient to resolve individual cells within these structures, in order to count them and evaluate the expression of protein markers. To better quantify the cells in these

clusters, we first tried to dissociate them and re-plate the cells as a monolayer. Unfortunately, most of the cells died after dissociation and the few cells that survived were not able to express markers of mature neurons (data not shown). Since cell-to-cell contact is required for optimal neuronal maturation, we worked to set up an imaging pipeline to capture and quantify cells within the clusters (Figure 34).

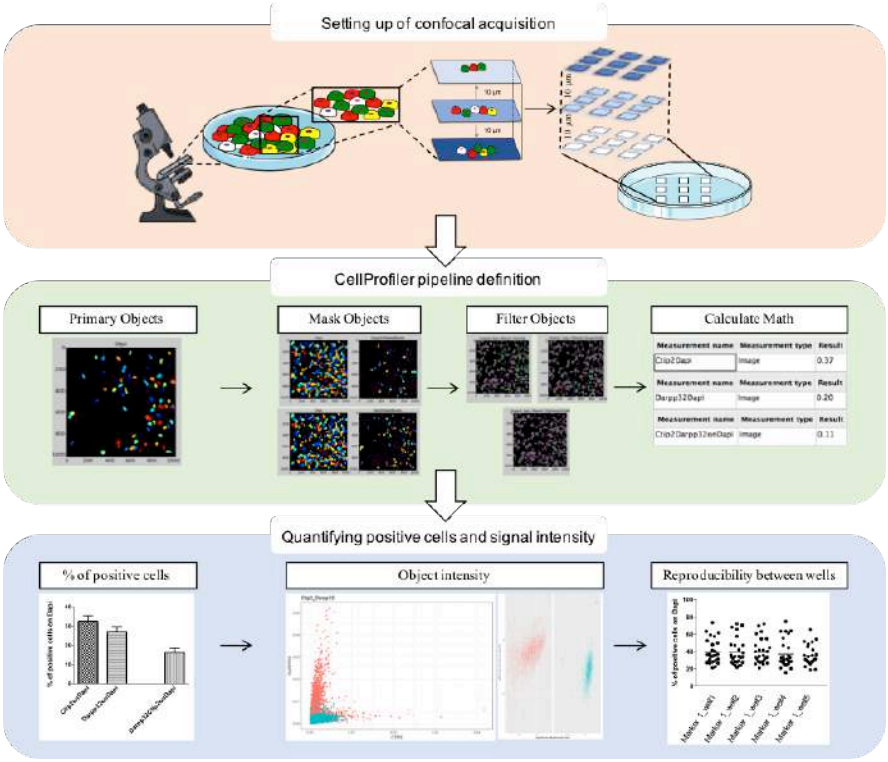

Figure 34: Pipeline for images acquisition and analysis.

To solve this issue, we evaluated two different types of acquisition method based on confocal microscopy or a Nikon wide-field microscopy. The Nikon Eclipse Time Lapse is a platform for automated acquisition with a built-in software for analysis. For this reason, we have tried the Nikon wide-field instead our standard wide-field. With this Nikon platform, in fact, we are able to acquire a lot of images which are quantified at the same time. Images were acquired and then a deconvolution filter (image-based mathematical approach designed to reduce out-of-focus light) with 50 iterations was applied to obtain countable nuclei (Figure 35, panels in the center). In parallel we tested a Leica SP5 Confocal system and, to optimize image output, we applied noise reduction filter with two iterations after image acquisition (Figure 35, right panels).

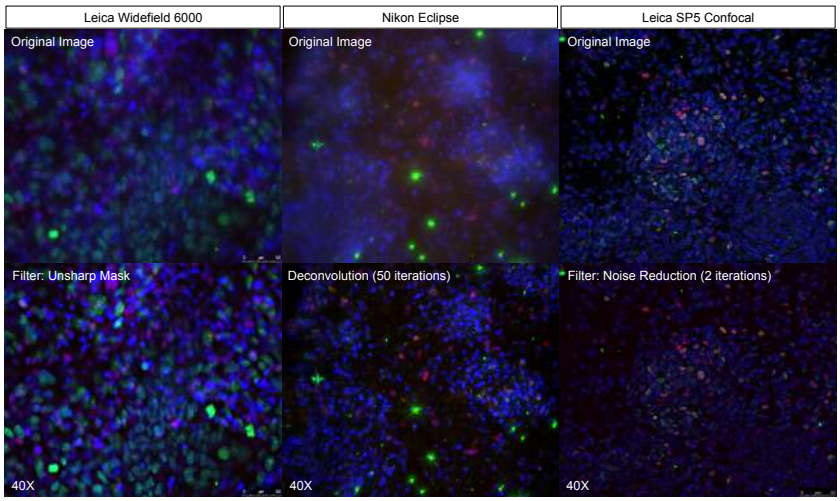

Figure 35: Original images and modification after Leica Widefield 6000, Nikon Eclipse and Leica SP5 Confocal (scale bar= 25 µm).

We found that the best system for our experimental purposes is represented by the Leica SP5 Confocal coupled with a 40x objective. In fact, images acquired with this system appeared more defined and quantifiable than the ones provided by the Nikon Eclipse Time Lapse. To capture cells along the vertical extension of these clusters and to assure that each cell will be represented only in one layer, we acquired three z stack planes, one every 10 µm for each field. We color-coded nuclei in each z stack plane to avoid double counts and made the merge of images to identify the counted object (Figure 36).

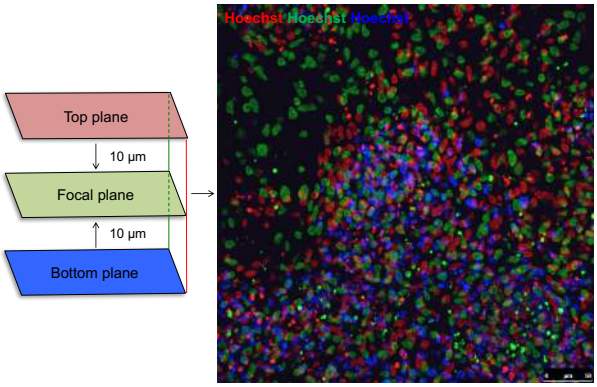

Figure 36: Merge of images obtained after the application of pseudo-colours to three z stacks counted (scale bar= 25 µm).

With this type of acquisition in z stack, we were able to section the thickness of clusters and also to acquire a representative fraction of the cells that form the cluster itself.

After acquisition, we applied noise reduction filter with two iterations to remove background and spots of secondary antibody. For a good representation of cells presented in each analyzed well, we decided to acquire nine fields (three in the top, three in the middle and three in the bottom side of the well) and for each field to acquire three z stack planes.

After improving the capturing procedure, then we worked to set up the pipeline for cells and protein markers quantification. To do that, we tested softwares for the quantification, and we compared the results to the manual counting method.

For manual counting, we used ImageJ, a public domain Java image-processing program inspired by NIH Image for the Macintosh and PC. As a plugin to count the processed images we used Cell Counter. The plug-in is very simple and it basically assists the manual click-and-count by scoring the number of counts into different user-selected categories. With this plugin, we have manually analysed part of the pictures to be able to compare the number of positive cells obtained with the other methods.

For automatic counting, we decided to use CellProfiler, the software that we found most suitable for our application. In fact, the same image analysed using the manual and the automatic method did not reveal any difference (see Figure 37).

CellProfiler is a versatile, open-source software tool for quantifying data from biological images. It is designed for modular, flexible, high-throughput analysis of images, measuring size, shape, intensity, and texture of every cell (or other object) in every image. Using the point-and-click GUI, users can construct an image analysis "pipeline", a sequential series of modules that each one performing an image processing function such as illumination correction, object identification (segmentation), and object measurement. We mixed and matched modules and adjusted the settings to measure the phenotype of interest. For our purpose, all the images carrying the different immunocytochemical staining were analysed starting from a 12 bits grey-scale picture of the individual channels (blue, green, red and magenta– three colours staining). Images were filtered so that each channel was analysed for the appropriate marker.

For the images processing we adopted the following modules: “Apply Threshold” to increase signal-to-noise ratio using three-classes “Adaptive” “Entropy” thresholding method; “Identify Primary Object” in the size range of 20 to 80 pixels using “Adaptive” thresholding strategy with three-classes “Entropy” and “Custom” smoothing method (Figure 37), because using these settings counted cells were more similar to the manual count. “Intensity” was used as method to distinguish clumped object and “Shape” as method to divide clumped objects (Figure 37).

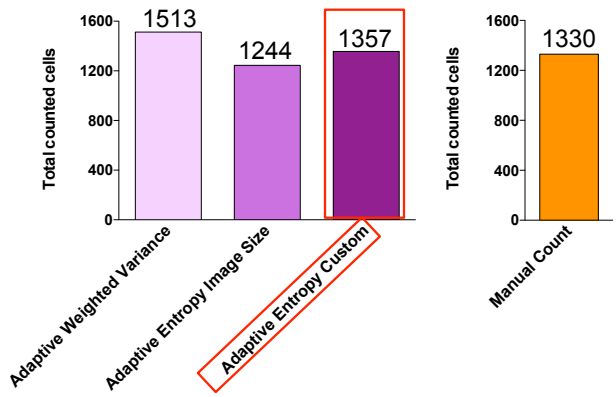

Figure 37: Comparison between the counted cells with different types of CellProfiler threshold.

This pipeline allowed us to obtain the percentage of cells positive for two or three given protein markers on the total number of DAPI positive cells (for the pipeline details see the Materials and Methods section). Moreover, expression level of each analysed protein marker can be accurately quantified.

Using the new acquisition method and type of analysis for the quantification described above, we were able to follow *in vitro* the cells' progression and maturation toward the acquisition of the striatal identity. In the following sections, we are going to focus our analysis on hES H9, because it showed higher consistency of marker expression between different biological replicates.

2.1. VZ-SVZ transition

The first important step was to evaluate if $GSX2^+/ASCL1^+$ cells represent those striatal precursors that move to the SVZ during development *in vivo*.

To closely monitor the evolution of the cultures during the differentiation protocol, we analyzed them every 5 days from day 20 to day 50 with the aim to understand if they are able to recapitulate the VZ to SVZ transition *in vitro.* (Figure 38, Panel A). With the method described above, we quantified the percentage of positive cells for GSX2, ASCL1 and the co-expressing cells on the total number of DAPI counted cells. The obtained number was expressed with the mean with standard error (mean ± SEM).

As we can observe in Figure 38 panel C, in parallel to a peak of $GSX2^+$ cells at day 25 (15.49 ± 1.24%) we detected an increase in the number of $ASCL1^+$ cells which reaches the maximum peak at day 35 (30.21 ± 4.08%). In line with this, at day 35 we found the highest number of cells co-expressing $GSX2^+/ASCL1^+$ (3.70 ± 0.35%, represented in the graph with the orange line) (Figure 38, Panel C).

Quantification of the fluorescent signal of GSX2 and ASCL1 staining (object intensity) confirmed this data. Specifically, the diagram in Panel B of Figure 38 illustrates GSX2 (y-axis) versus ASCL1 (x-axis) signal. Each dot represents a cell with the relative expression of both markers. The intensity of the color in each panel is proportional to the number of cells expressing each intensity value (Figure 38, Panel B).

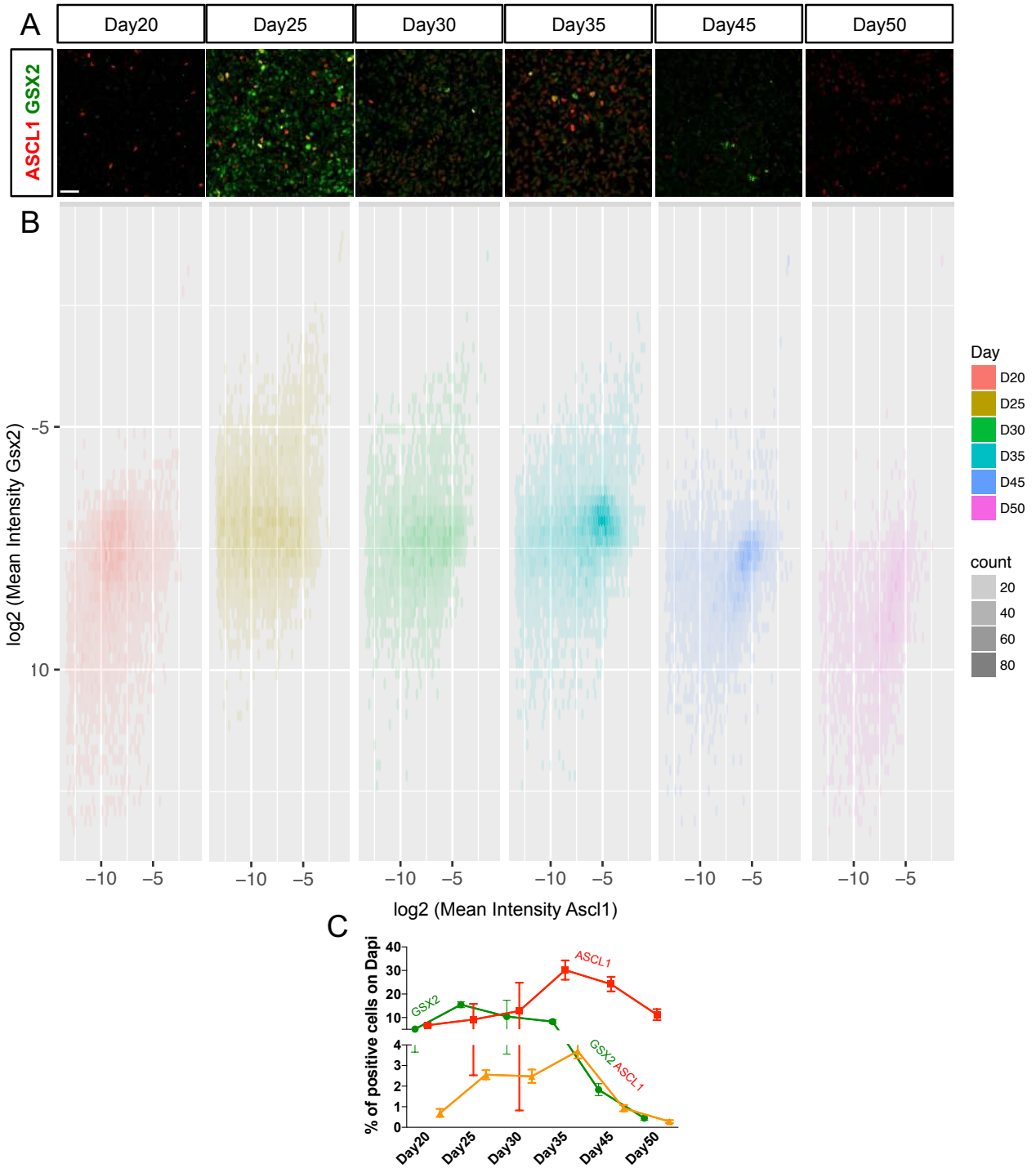

Figure 38: (Panel A) Immunofluorescence on hES H9 for GSX2 and ASCL1 (scale bar=25µm), (Panel B) Measurement of the intensity of the fluorescent signal (object intensity) of GSX2 and ASCL1 in each cell (x-axis = mean intensity of ASCL1 signal; y-axis mean intensity of GSX2 signal in the log_2 scale), (Panel C) Percentage of markers quantification on the number of the total counted cells (Dapi positive) (data are represented as means ± SEM).

Our experiments indicate that GSX2 intensity level reaches its peak at day 25 and then it gradually decreases until day 50. Instead, the level of ASCL1 signal reaches its maximum at day 35 and then decreases from day 45 to 50.
We concluded that *in vitro* the time-window between day 25 and 35 represents the temporal evolution of an "SVZ like" domain where we can clearly observe an increasing number of GSX2 and ASCL1 double positive cells.

2.2. SVZ - MZ transition

An additional critical step in the progression of neural progenitor maturation is the transition from SVZ toward the MZ.
The study performed in mouse by Garel et al. published in 1999 had demonstrated that *ebf1* inactivation affects the differentiation of striatal cells while they migrate from the SVZ to the MZ, resulting in the expression of an abnormal combination of regulatory genes in the mantle zone. Based on this evidence, we decided to monitor in EBF1 in hES H9 cells at differentiation days 20, 25, 30 and 50. EBF1 was visualized in combination with PAX6 and CTIP2, specifically labeling neuronal population of MZ from early post mitotic stages in hES H9 cell line.
We found that the number of $PAX6^+$ cells increases from day 20 until day 50, probably due to the persistency of neural progenitors in our cultures. The presence of PAX6 at later time points (as day 50) could also indicate persistence of neurons with cortical identity as demonstrated by expression of cortical markers TBR1 and TBR2 (data not shown) (Figure 39, Panel A).

The hES H9 cell line started to show EBF1 positive cells at day 20 (6.37 ± 0.60%). This number progressively increases (day 25: 14.15 ± 1.30% and day 30: 24.59 ± 2.15%) and it reaches a peak at the last time point analyzed (day 50) (33.70 ± 1.43%) (Figure 39, Panel C).

In order to monitor the transition from SVZ to MZ we analysed CTIP2 expression. At day 20 we observed very few $CTIP2^+$ cells (0.95 ± 0.19%), which progressively increased from day 25 (7.07 ± 1.29%), day 30 (8.38 ± 1.48%), until day 50 when it reached the highest numbers (34.63 ± 3.23%) (Figure 39, Panel C). The graphs reported in Figure 45 Panel B represents the strength of the intensity of each marker described. The graphs show the mean intensity of CTIP2 (x-axis), PAX6 (y-axis) and EBF1 (z-axis), at each point representing the three values of each measured cell. The graphs show that as the differentiation progresses the intensity signal of CTIP2, EBF1 and PAX6 gradually increases. Accordingly, CTIP2 signal level reaches a

maximum towards terminal differentiation at day 50 as expected in mature post-mitotic neurons (Figure 39, Panel B).

To confirm this transition, we also counted the number of cells that exhibited co-expression of EBF1 and CTIP2. At day 25 we observed very few cells co-expressing these markers (1.11 ± 0.21% represented in the graph with the orange line). However, this percentage increased gradually until day 50 where we could observe 18.3% ± 1.21% of double positive cells (Figure 39, Panel C). The data collected indicates that at day 50 of *in vitro* differentiation we identified a high percentage of EBF1^{+}/CTIP2^{+} maturing neurons that are mimicking the *in vivo* migration from SVZ toward MZ.

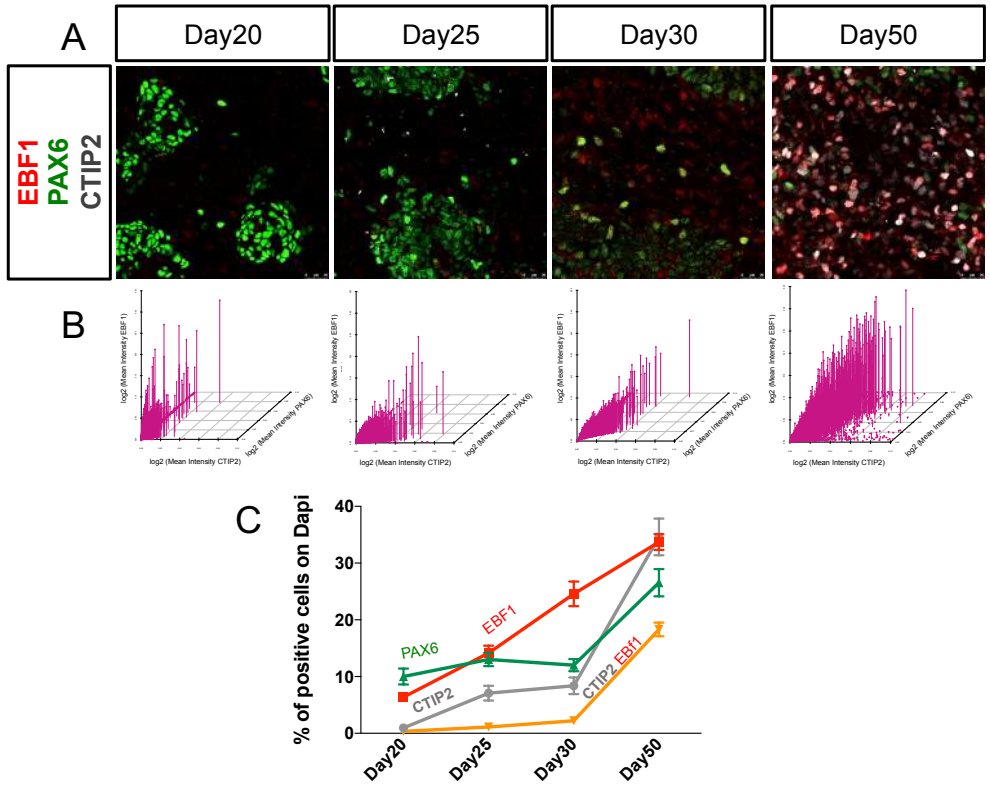

Figure 39: (Panel A) Immunofluorescence in hES H9 for PAX6 (green), EBF1 (red) and CTIP2 (grey) (scale bar=25µm), (Panel B) Measurement of the intensity of the fluorescent signal (object intensity) of CTIP2, PAX6 and EBF1 in each cell (x-axis = mean intensity of CTIP2 signal; y-axis = mean intensity of PAX6 signal; z-axis = mean intensity of EBF1 signal, in the $\log_2$ scale), (Panel C) Percentage of markers quantified on the number of the total counted cells (Dapi positive) (data are represented as means ± SEM).

2.3. Striatal precursor in MZ

The neurons identified in the previous analysis could mature and acquire a striatal precursor identity, characterized by the co-expression of NKX2.1, CTIP2 and ISLET1 markers.

In fact, at 7–8 w in human embryos, ~74% of the total striatal cells was NKX2.1^{+} and most NKX2.1^{+} cells co-expressed ISLET1 and CTIP2 (80.7 ± 6% and 95.9 ± 0.9%, respectively).

At 20w NKX2.1 and ISLET1 were restricted to a few scattered cells (6.3 ± 2.7%) (Onorati et al., 2014). These observations suggested that the co-expression of these three TFs identifies the majority of striatal precursors, which later switch off the expression of NKX2.1 and ISLET1, and only CTIP2 expression is maintained.

To detect this neuronal precursor population, we have monitored CTIP2, NKX2.1 and ISLET1 every 5 days of differentiation in hES H9 cell line from day 20 to day 50 (Figure 40, Panel A). After quantification, we observed an increase in NKX2.1^{+} cells starting from day 25 (38.10 ± 3.09%) detecting a peak at day 35 (45.17 ± 3.11%) that decreases at day 50 (9.01 ± 1.71%). At day 35, NKX2.1 expression is also correlated to a very high percentage of ISLET1^{+} cells (36.20 ± 5.53%), which decreased until day 50 (4.27 ± 0.74%). When we analyzed CTIP2 staining we found that at day 35, 53.11 ± 5.70% of the cells were positive for this TF, and this proportion remained unchanged until day 50 (48.20 ± 3.63%).

The highest percentage of striatal neuronal precursors co-expressing NKX2.1, CTIP2 and ISLET1 was detected at day 35 (18.23 ± 3.10%, represented in the graph with the orange line) and this data was also confirmed by the signal intensity analysis. Specifically, the diagram in Panel B of Figure 45 illustrates the signals for ISLET1 (y-axis), CTIP2 (x-axis) and NKX2.1 (z-axis) (Figure 45, Panel C), and indicates that highest level of intensity for the 3 markers was reached at day 35 (Figure 40, Panel B).

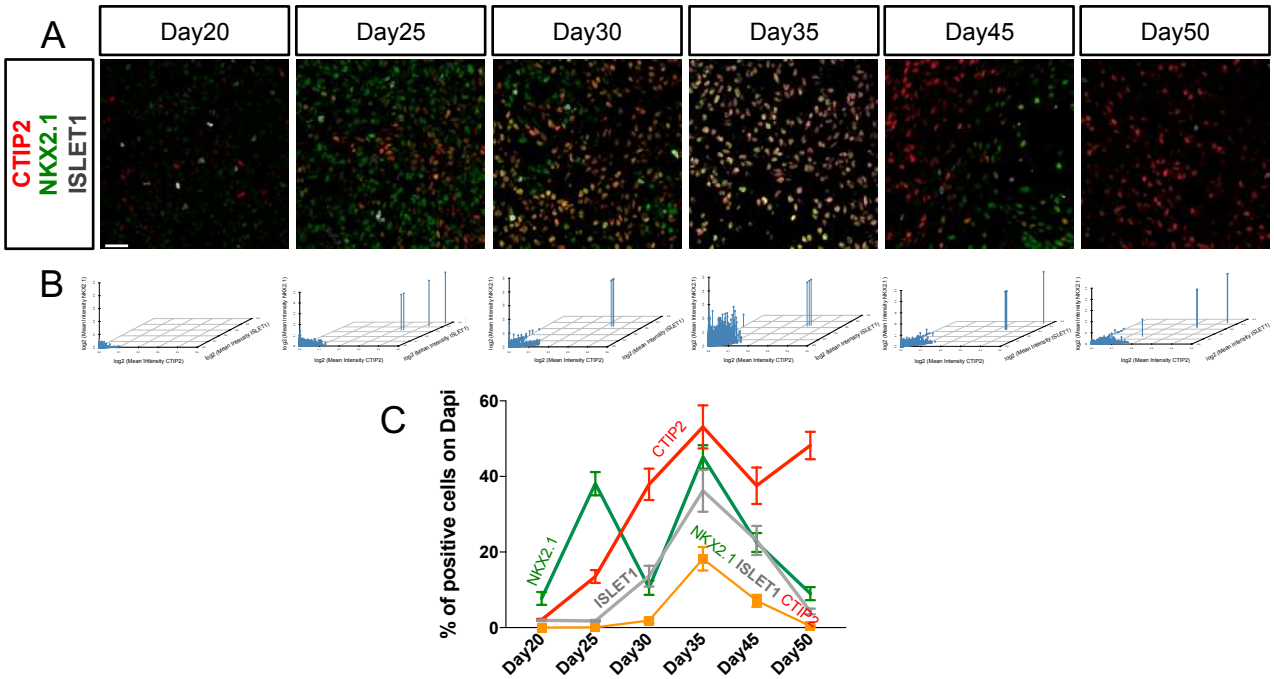

Figure 40: (Panel A) Immunofluorescence in hES H9 for CTIP2 (red), NKX2.1 (green) and ISLET1 (grey) (scale bar=25µm), (Panel B) Measurement of the intensity of the fluorescent signal (object intensity) of CTIP2, NKX2.1 and ISLET1 in each cell (x-axis = mean intensity of CTIP2 signal; y-axis = mean intensity of ISLET1 signal; z-axis = mean intensity of NKX2.1 signal, in the $\log_2$ scale), (Panel C) Percentage of markers quantification on the number of the total counted cells (Dapi positive) (data are represented as means ± SEM).

This data indicate day 35 as the time point *in vitro* with the highest percentage of striatal precursors i.e. cells NKX2.1^{+}/CTIP2^{+}/ISLET1^{+}. The persistence of a NKX2.1^{-}/CTIP2^{+}/ISLET1^{-} population at day 45 and day 50 suggests the appearance of mature striatal neurons (Onorati et al., 2014). To understand if this population corresponds to authentic MSNs we further analysed these cells.

2.4. Identification of authentic MSNs

Co-expression of CTIP2 and DARPP32 is not a sufficient criterion to determine the presence of authentic MSNs. In fact, DARPP32 is expressed also in neurons of layer VI of the adult cerebral cortex (Hisaoka et al., 2010), where also CTIP2 was detected, albeit at low levels (Alcamo et al., 2008). We therefore decided to analyse the expression of glutamic acid dehydrogenase-67 (GAD67) staining, the limiting enzyme for GABA synthesis (Behar et al., 1994), which is also expressed in the embryonic striatum.

Previous studies highlighted that hESC-derived DARPP32 neurons expressed GAD67, which is consistent with the medium-sized spiny neurons being GABAergic (Danjo et al., 2011). At day 50, in three independent experiments we observed 12.4 ± 7.23% of DARPP32^{+} cells and 57.5% of them showed co-expression with CTIP2 (Figure 41, Panel A and B).

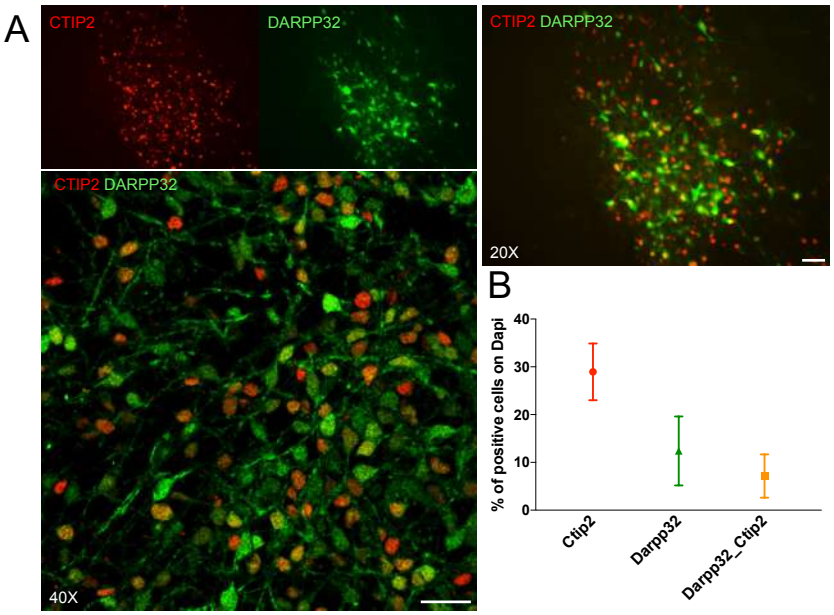

Figure 41: (Panel A) Immunofluorescence in hES H9 at day 50 for CTIP2 (red) and DARPP32 (green) (scale bar=50µm and 25µm), (Panel B) Measurement percentage of markers quantification on the number of the total counted cells (Dapi positive) (data are represented as means ± SEM, n= 3 independents experiments).

The striatal identity of these neurons was confirmed by immunostaining with GAD67 (Figure 42, Panel A) and with the measurement of the signal intensities of GAD67 (y-axis), CTIP2 (x-axis) and DARPP32 (z-axis) (Figure 42, Panel B). In particular, the latter analysis portrayed

high intensity values for each marker, suggesting a population of mature striatal MSNs (Figure 42, Panel B).

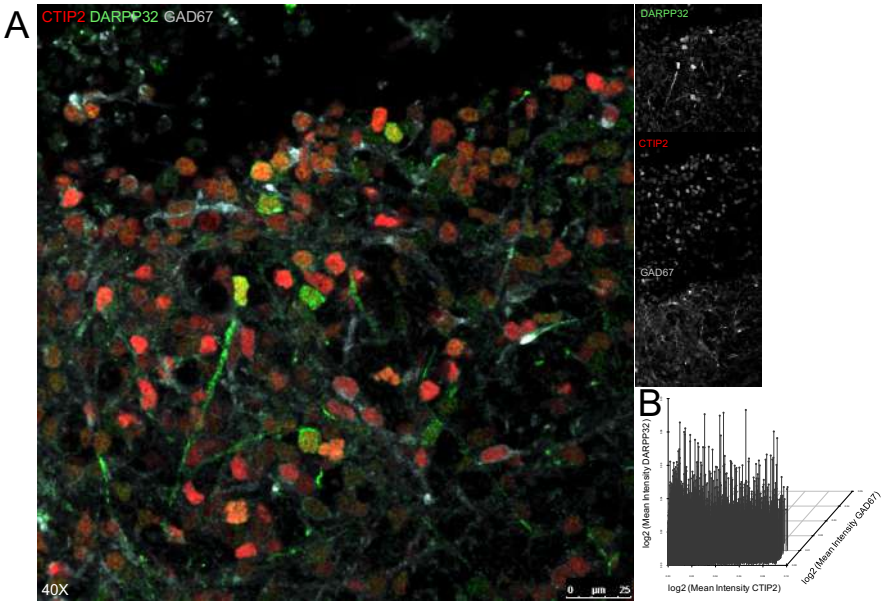

Figure 42: (Panel A) Immunofluorescence in hES H9 at day 50 for CTIP2 (red), GAD67 (grey) and DARPP32 (green) (scale bar=25µm), (Panel B) Measurement of the intensity of the fluorescent signal (object intensity) of CTIP2, DARPP32 and GAD67 in each cell (x-axis = mean intensity of CTIP2 signal; y-axis = mean intensity of GAD67 signal; z-axis = mean intensity of DARPP32 signal, in the log_2 scale).

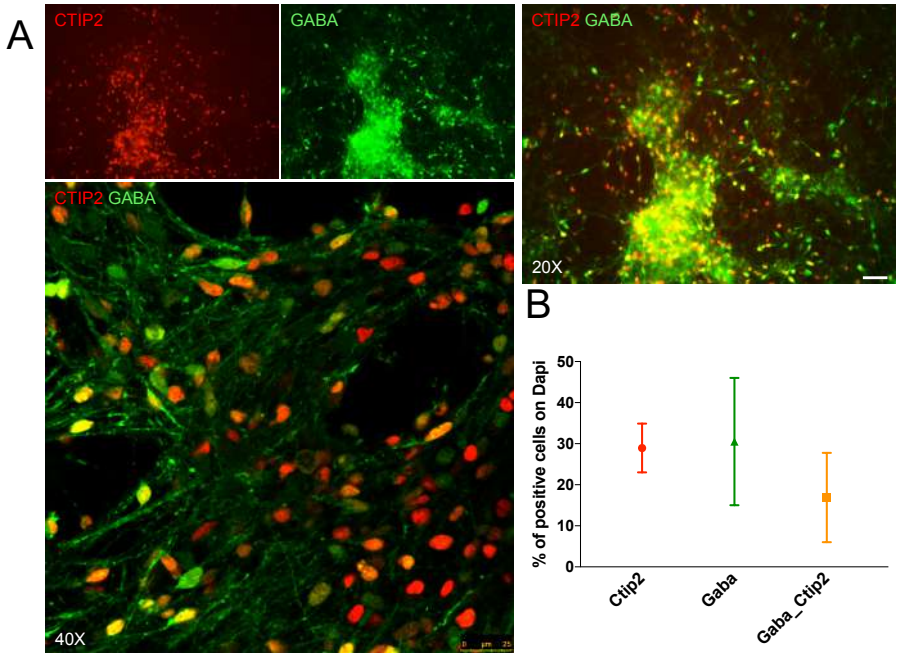

Figure 43: (Panel A) Immunofluorescence in hES H9 at day 50 for CTIP2 (red) and GABA (green) (scale bar=50 µm and 25µm), (Panel B) Measurement percentage of markers quantification on the number of the total counted cells (Dapi positive) (data are represented as means ± SEM, n= 3 independents experiments).

At day 50 30.52 ± 15.50% of cells exhibited GABA positivity and 16.09 ± 10.88% were also $CTIP2^+$, compared to a total of 28.95 ± 5.92% of CTIP2 positive cells (Figure 43, Panel A and B). To confirm the striatal identity of the cells, we checked the expression of GAD67 in parallel to the analysis of the signal intensity of these markers (Figure 44, Panel B): GAD67 (y-axis),

CTIP2 (x-axis) and GABA (z-axis) signal. We observed a high signal for these three markers, further confirming the striatal fate acquired by these cells. (Figure 44, Panel B).

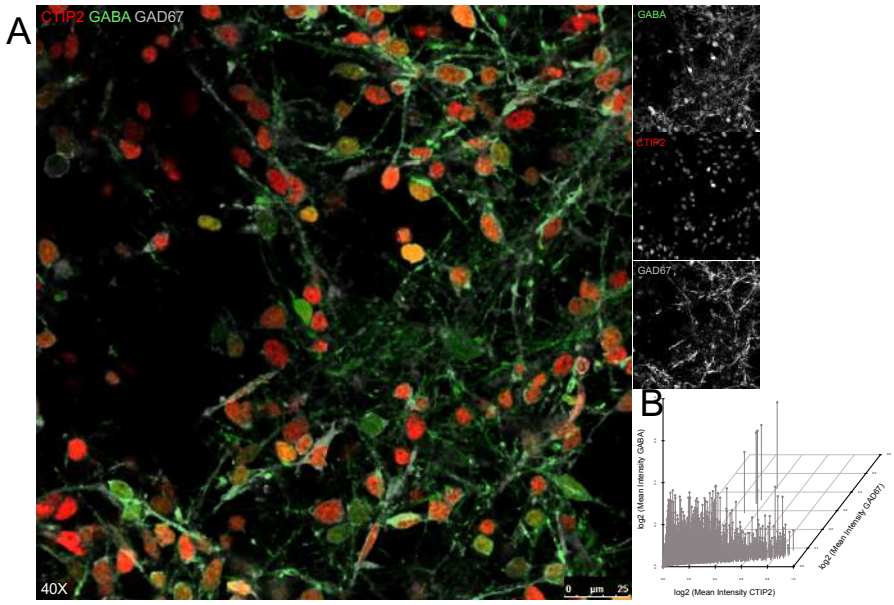

Figure 44: (Panel A) Immunofluorescence in hES H9 at day 50 for CTIP2 (red), GAD67 (grey) and GABA (green) (scale bar=25µm), (Panel B) Measurement of the intensity of the fluorescent signal (object intensity) of CTIP2, GABA and GAD67 in each cell (x-axis = mean intensity of CTIP2 signal; y-axis = mean intensity of GAD67 signal; z-axis = mean intensity of GABA signal, in the $\log_2$ scale).

2.5. Role of cell cycle state during differentiation

One alternative way to monitor cell differentiation is represented by the analysis of markers of the cell cycle, as Ki67, a marker of active cell cycle and cell proliferation.

Ki67 is preferentially expressed during late G1, S, G2 and M phases of the cell cycle, while non-cycling cells (G0 phase) lack Ki67 expression. Thus, Ki67 is commonly used as a proliferation marker.

Analysis of $Ki67^+$ cells had been performed also in the human fetal brain development (Onorati et al., 2014). The authors studied the co-expression of the proliferation marker Ki67 with MAP2, GABA, CTIP2, ISLET1, GSX2 and ASCL1 and they found that it delineates the VZ, SVZ and MZ compartments in the LGE at 7–8 w, confirming that Ki67 is a marker of the neural precursors only (Onorati et al., 2014).

In parallel, to identify the mature post-mitotic neurons, we used p27 staining. Several reports demonstrated that p27 regulates many aspects of neurogenesis, including neural progenitor proliferation, migration and/or differentiation (Cunningham et al., 2002; Doetsch et al., 2002; Fero et al., 1996; Goto et al., 2004; Nguyen et al., 2006; Sakaue-Sawano et al., 2008; Zezula et al., 2001). All these studies indicate that p27 plays critical roles in the development of the central nervous system (Cunningham et al., 2002). The function of cell proliferation inhibitor of p27 is closely related with its subcellular localization (Reynisdóttir & Massagué, 1997; Tomoda

et al., 1999). Indeed, in the nucleus, p27 inhibits the activity of cyclin E/A-CDK2 and prevents the cell cycle progression (Sherr & Roberts, 1995). Conversely, p27 is exported to the cytoplasm after phosphorylation in Thr 187 or Ser 10 (Boehm et al., 2002). Cytoplasmic p27 decreases the level of nuclear p27, a regulatory step that is required for a cell to re-enter the cycle, and promotes cell migration, as demonstrated in HepG2, fibroblasts, lung cancer cells, mesangial cells and neurons (Assoian, 2004; Besson et al., 2004, 2006; McAllister et al., 2003; Nguyen et al., 2006; Zezula et al., 2001). Several *in vivo* and *in vitro* studies have demonstrated that p27 has a key role during neuronal differentiation (Galderisi & Giordano, 2003). For instance, in rat embryos a strong *p27* expression was observed also in the neurons located in the basal telencephalon and diencephalon (Lee et al., 1996) suggesting that high p27 expression is characteristic of post-mitotic neurons. Another study, from Casaccia-Bonnefil et al., 1997 highlights the role of p27 in cell cycle exit showing that p27 deficiency compromises the differentiation process of oligodendrocyte precursors.

Based on these data we investigated the cell cycle state of cells during differentiation by monitoring the expression Ki67 and p27, by immunofluorescent analysis, in two hES cell lines, H9 and RUES2, in three independent experiments for each line (Figure 45, Panel A and C).

In both cell lines the levels of Ki67 started to decrease from day 30 until day 50, conversely, the number of $p27^+$ cells increased and remained stable between day 30 and day (Figure 45, Panel B and D). In hES RUES2, in fact, at day 30 we detected 23.58 ± 18.19% of p27 positive cells, and at day 50, 35.15 ± 11.01% $p27^+$ (Figure 45, Panel B). At day 30, the hES H9 cell line showed 47.66 ± 4.81% and at day 50 45.79 ± 11.10% p27 positive cells (Figure 45, Panel D). This data suggested that only a portion of cells were able to maturate and become p27 positive. Between day 30 and day 50 this percentage did not increase suggesting that the number of post-mitotic cells had reached a plateau.

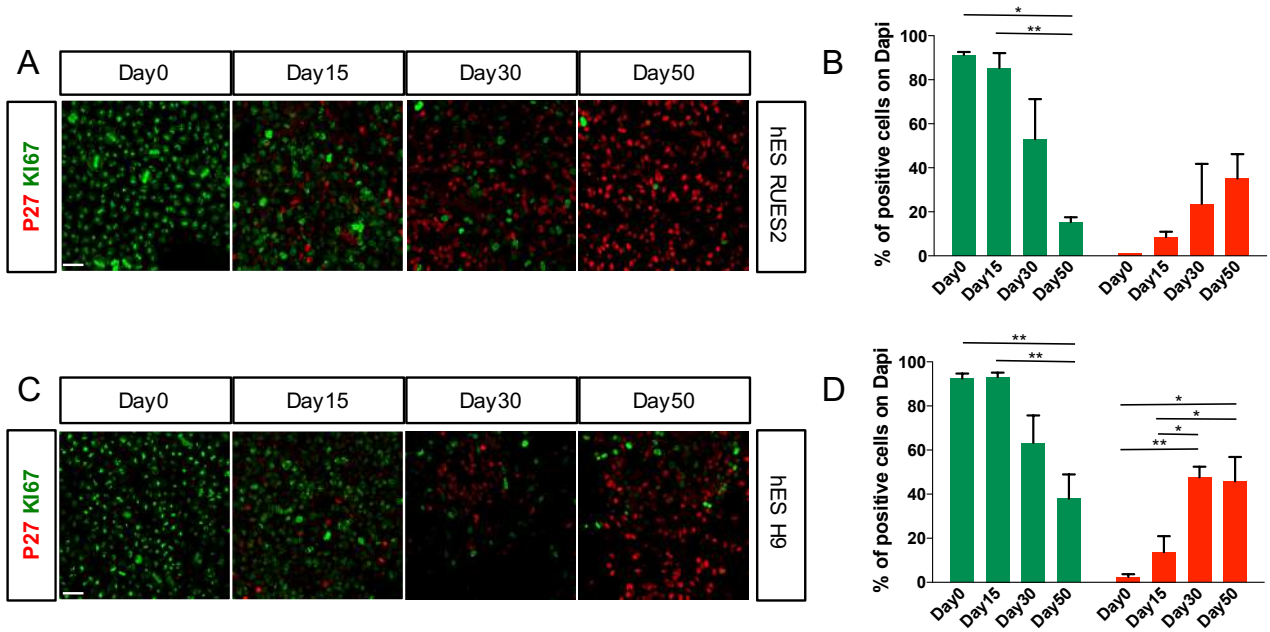

Figure 45: (Panel A) Immunofluorescence on hES RUES2 and (Panel C) H9 for p27 (red) and Ki67 (green) (scale bar=25µm), (Panel B) Measurement of percentage of markers quantification on the number of the total counted cells (Dapi positive) in hES RUES2 and (Panel D) in hES H9 (n=3 independent experiments for each cell line, with 27 images analysed for each time point; data are represented as means ± SEM; Anova One way, Tukey post-test *p<0.05, **p<0.01).

To further analyze the cell cycle state during *in vitro* striatal differentiation we focused on hES H9 line and fixed the cells every 5 days from day 20 to day 50, to monitor p27 and Ki67 levels (Figure 46, Panel B). To correlate the portion of p27 positive cells to a marker of mature neurons, we also monitored in parallel the percentage of CTIP2$^+$ cells (Figure 46, Panel A, B).
In fact, when we calculated the percentage of CTIP2$^+$/p27$^+$ cells on the total number of CTIP2$^+$cells, especially at day 45 and 50, we observed that almost all CTIP2$^+$ cells were also p27$^+$ (day 20: 54.56 ± 7.01%; day 25 82.67 ± 1.67%; day 30 83 ± 2.20%; day 35 82.74 ± 1.93%; day 45 91.85 ± 1.09%; day 50 83.78 ± 1.99%) (Figure 46, Panel C). P27 is a good marker of post-mitotic neurons as it matches the increase in the percentage of CTIP2 positive cells.

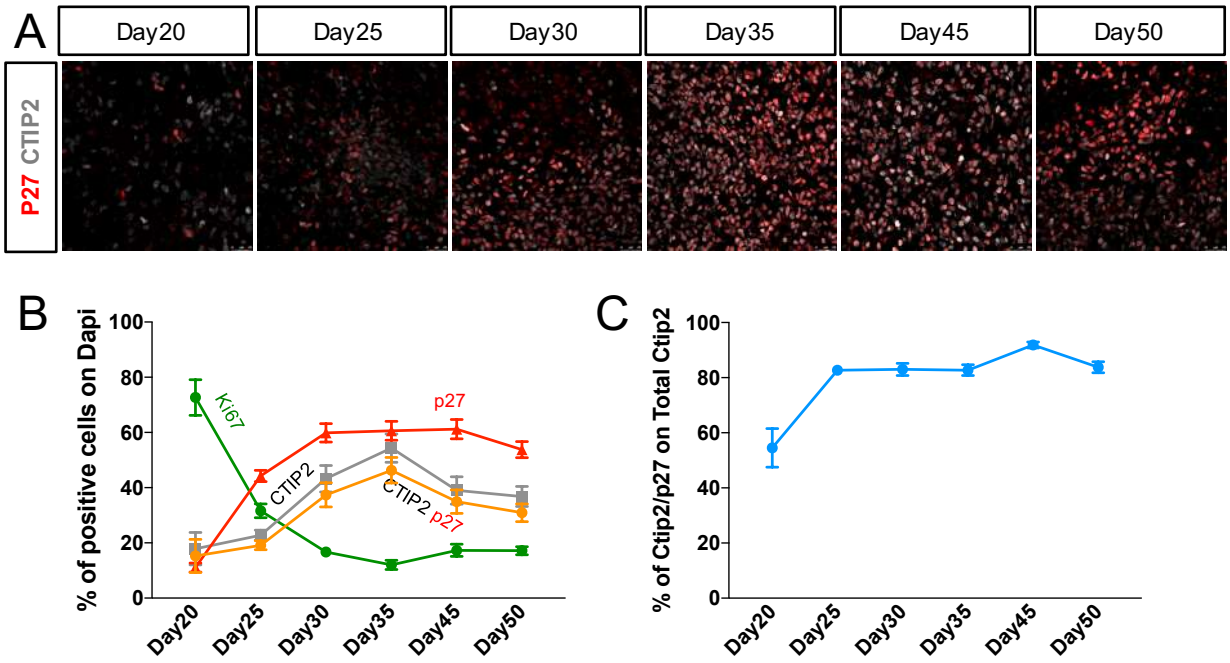

Figure 46: (Panel A) Immunofluorescence in hES H9 for p27 (red) and CTIP2 (grey), (Panel B) Percentage of markers quantification on the number of the total counted cells (Dapi positive), analysed every 5 days, (Panel C) Percentage of double CTIP2/p27 co-expressing cells on the total CTIP2 positive cells (data are represented as means ± SEM).

In summary, our *in vitro* analysis demonstrates that the striatal protocol published in 2013 is reproducible and is effective on different human pluripotent cell lines. Each cell line showed the appearance of the specific subpopulation of precursors and progenitors mimicking the *in vivo* striatum development. The new acquisition and quantification method allowed us to quantify more precisely the efficiency of the protocol highlighting new markers and also the possible problems in term of authentic MSN conversion. Therefore, we conclude that the efficiency to generate MSN neurons is partially cell line dependent because in hES RUES2 in particular we observed low efficiency in term of MSN conversion. This point will be under future investigation.

Three independent experiments performed with hES H9 had shown that only 7.13 ± 4.52% of the cells are able to become authentic MSNs (i.e., $DARPP32^{+}/CTIP2^{+}$). For this reason, we decided to improve the Delli Carri by using an inducible expression approach; in particular, we wanted to express specific TFs involved in specification and maturation of neural precursors both *in vivo* (Garcia-Dominguez, 2003; Garel et al., 1999; Méndez-Gómez & Vicario-Abejón, 2012) and *in vitro*, as we described.

3. Forced gene expression applied to the Delli Carri protocol

Our previous data demonstrated that human ventral telencephalic progenitors could be generated from hES cells by using a SHH-treatment coupled with WNT-inhibition. These progenitors eventually differentiate into electrophysiologically active and mature neurons after 80 days of differentiation, with 10-15% of them resembling authentic MSNs as demonstrated by the co-expression of the striatal markers DARPP32 and CTIP2 (Delli Carri et al., 2013). These data were confirmed in the experiments that I performed during my thesis on four independent hPSC.

To further improve recovery and quality of human MSN from hES/hiPS cells, we have recently generated doxycycline-inducible hES lines that overexpress critical combinations of TFs known to be important for striatal specification and differentiation.

In the first part of this thesis we described a set of transcription factors critical for establishing a dorsal-ventral and medial-lateral positional identity in striatal progenitor cells and for the specification of neuronal terminal differentiation. In particular, in the developing telencephalon, two TFs play a key role in contributing to the formation of the striatum: GSX2 and EBF1. GSX2 is first expressed in the ventricular zone (VZ) of the telencephalon, where it is involved in maintaining the identity of early striatal progenitors, while EBF1 controls cell differentiation in the murine embryonic striatum (Garel et al., 1999; Jain et al., 2001; Sussel et al., 1999). We therefore decided to establish a hES cell-based inducible gain-of-function (iGOF) system whereby TFs expressed in the developing striatum can be harnessed to improve MSN differentiation.

3.1. Inducible overexpression of key transcription factors during neuronal differentiation

We employed an inducible overexpression system commercially available (Clontech) that we adapted for transgene expression in hES cells. To this effect, the TetON cassette was moved into a chicken beta-actin promoter with a CMV enhancer-based plasmid (pCAG), which allows a persistent and stable expression of the gene of interest. This promoter was shown to be active after many passages in hES cells as confirmed by the continuous expression of the GFP protein after transfection of a pCAG-GFP vector (data not shown). pCAG-TetON was delivered by nucleofection in hES H9 cells along with a linear construct encoding for puromycin for selection of H9 cells stably expressing the pCAG-TetON. hES clones resistant to puromycin were picked, amplified, and tested for inducibility by transfecting a pTRE-Luciferase construct. We selected four clones: B5 and C6 showed no basal Luciferase activity while C4 and B6

exhibited a low-to-high luciferase activity after 48 hours of doxycycline treatment (for details see Materials and Methods) (Figure 47).

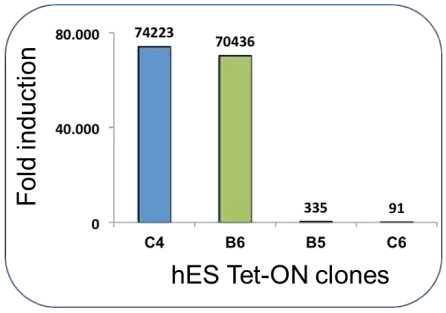

Figure 47: Testing inducibility of four of hES Tet-ON clones with luciferase assay.

Next, transient transfections were performed in these four clones using a pTRE responsive vector bearing cDNA for Gsx2 (pTRE-Gsx2). After 48 hours of doxycycline treatment transfected cells were fixed and analysed by immunofluorescence for GSX2 expression. C4 and B6 clones, but not B5, showed high GSX2 expression after transient transfection (Figure 48).

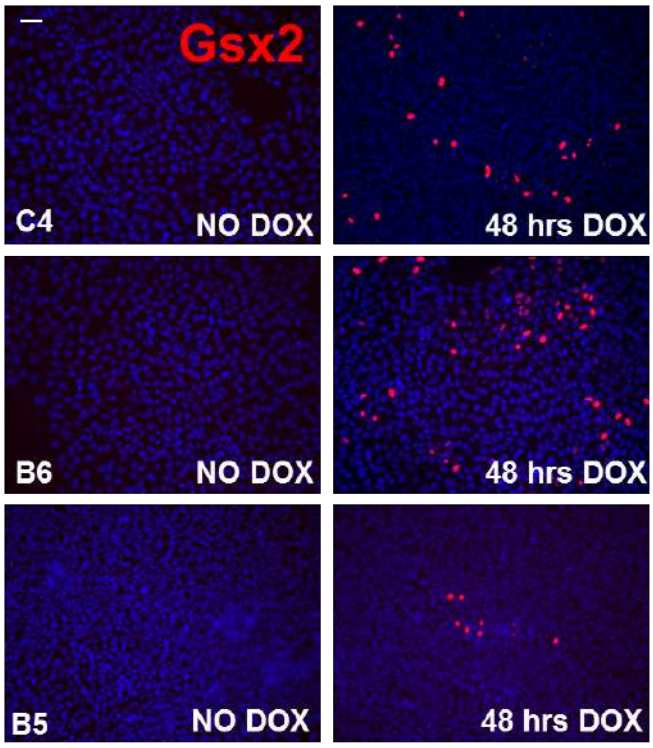

Figure 48: GSX2 in C4, B6 and B5 clones after 48 hrs of doxycycline administration (scale bar=50 µm).

C4 and B6 clones expressed OCT4 and SOX2 in pluripotency medium, and responded promptly to neural differentiation stimuli similarly to the original H9 cells (Figure 49 and data not shown).

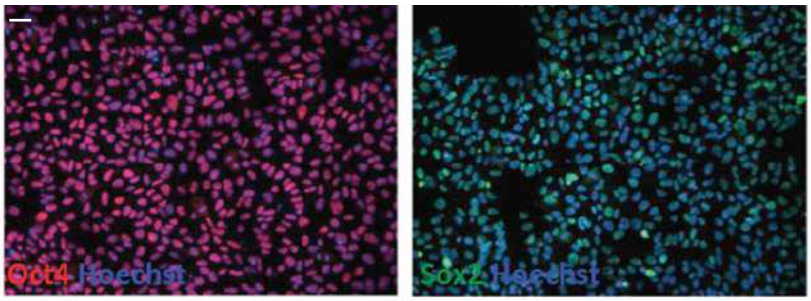

Figure 49: OCT4 and SOX2 in C4 clone (scale bar=50 µm).

3.2. Generation of inducible hES cell line for Gsx2 and Ebf1

To generate hES cell line with inducible expression of Gsx2, Ebf1 and a combination of the two TFs, we transfected pTRE3G-IRES responsive vector (Clontech) bearing Gsx2 alone, Gsx2 an IRES sequence and Ebf1, and Ebf1 alone. Gsx2 cDNA was a gift from Kenneth Campbell, Cincinnati Children's Hospital Medical Center, Cincinnati. Ebf1 cDNA was a gift from Giacomo Consalez, Division of Neuroscience, San Raffaele Scientific Institute, Milan.

Transfected cells without doxycycline treatment represented our control lines. Briefly, after nucleofection and selection, several stable hES cell clones were picked, amplified, and tested for TFs expression and those with mild overexpression were selected (Figure 50, Panel A). Next, transgenes expression was examined by a time-course analysis and transcription was induced for 8, 24, and 48 hours in Gsx2, Gsx2-Ebf1, and Ebf1 inducible lines. We found transgene expression as soon as after 8 hours of doxycycline treatment, with a peak of expression at around 48-72 hours. We found that 55 ± 3% of the cells expressed Gxs2 in Gsx2 iGOF (Figure 50, Panel D), 51 ± 19% and 48 ± 22% of the cells express Gsx2 and Ebf1, respectively, in Gsx2–Ebf1 iGOF (Figure 50, Panel G) while 60 ± 8% of the cells expressed Ebf1 in Ebf1 iGOF (Figure 50, Panel J).

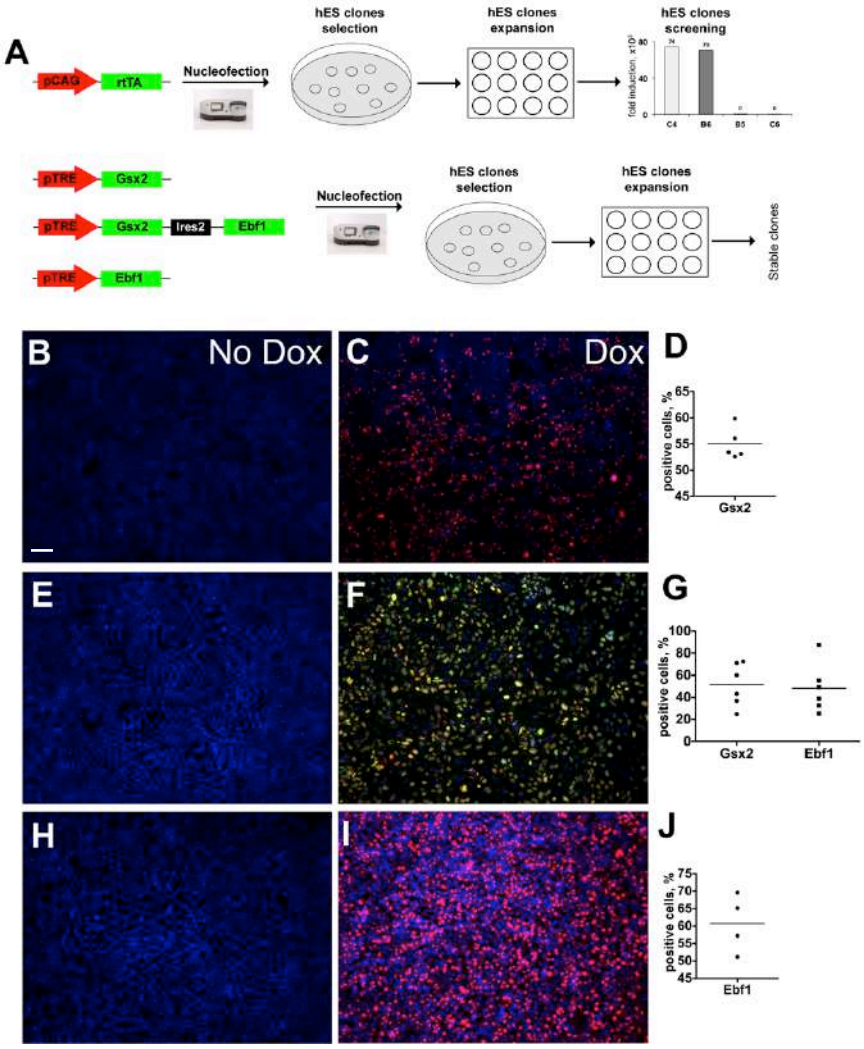

Figure 50: (Panel A) Schematic representation of generation of the three hES iGOF cell lines; (Panel C, F, I) Immunofluorescence of GSX2 (red) and EBF1 (green) (scale bar=100 µm); (Panel D, G, J) quantification of TFs overexpression after doxycycline treatment.

We then studied if the newly generated clonal lines were able to respond appropriately to the Delli Carri protocol and to generate authentic MSNs. We found that at day 40 of neural differentiation our cell lines expressed specific neuronal markers such as MAP2, CALBINDIN, FOXP2, CTIP2, and GABA (data not shown). Thus, the process of genetic modification and selection of the cells did not alter the capacity of these H9 sub-clones to differentiate toward a neuronal lineage. To determine the effects of Gsx2 and Ebf1 expression in human neural progenitors, we overexpressed Gsx2, Gsx2-Ebf1 and Ebf1 in different temporal windows during hES neural differentiation: day 10-15, day 15-20, and day 20-30. We observed that expression of the TFs between day 20-30, but not in the other temporal windows, reduced expression of cortical (PAX6) and MGE markers (NKX2.1) at day 30 (data not shown). This evidence suggested that, in this particular window of differentiation, overexpression of TFs could affect the differentiation rate. We therefore decided to expose cells to doxycycline from day 20 until

day 30. Cells were differentiated until day 80 in 5 different and independent experiments for each cell line. During differentiation, after 10 days of doxycycline treatment starting from day 20, we confirmed, at day 30, correct overexpression of TFs by Western Blot analysis (Figure 51, Panel A) in the three generated iGOF lines (Figure 51, Panel B).

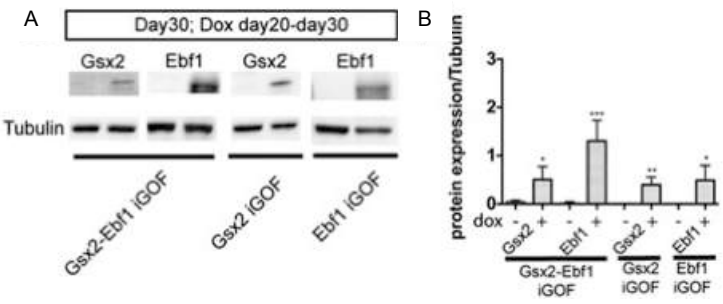

Figure 51: Protein levels of Gsx2 and Ebf1 at day 30. (Panel A) Western Blot for Gsx2 and Ebf1 at day 30 in the three hES iGOF cell lines; (Panel B) quantification of GSX2 and EBF1 protein levels (Error bars show SD, n = 5 independent experiments, *p< 0.05, **p< 0.005, ***p< 0.001).

3.3. Gsx2 and Ebf1 Regulate Cell-Cycle Kinetics

Cell proliferation in the developing telencephalon is a tightly regulated process, and it is essential to produce the correct number of post mitotic neurons. To examine the effects of Gsx2 and Ebf1 overexpression on the cell cycle in human progenitor cells, we first performed a cumulative bromodeoxyuridine (BrdU) analysis in the proliferating hES cell lines inducible for Gsx2, Gsx2–Ebf1 and Ebf1. BrdU is a halogenated thymidine analogue that is incorporated into DNA synthesized during S-phase. With this approach, we were able to detect the cells in S phase, that have incorporated BrdU and, therefore, resulted positive for BrdU staining.

After treating the cells with doxycycline for 5 days, we administered BrdU for either 30 min, 4, 8, or 20 hours. We found that the Gsx2 iGOF line showed a reduced BrdU incorporation compared with the untreated cells (Figure 52, Panel A and quantification in Panel B). These data indicate that overexpression of Gsx2 alters the cell cycle by arresting its progression; in fact, Gsx2 overexpressing cells are not able to pass the phase S, where they would incorporate BrdU.

In contrast, the Gsx2–Ebf1 inducible line showed a similar BrdU incorporation rate compared with the control line, suggesting that cell-cycle alteration by Gsx2 was rescued by Ebf1 expression (Figure 52, Panel C and quantification in Panel D). Finally, cell cycle analyses were performed in the Ebf1 iGOF line. In contrast with the previous results, a significant increase in BrdU incorporation was recorded after 20 hours of induction in Ebf1 iGOF (Figure 52, Panel E and quantification in Panel F). Taken together these data suggest that expression of Gsx2 and Ebf1 alone affects the cell cycle by altering the entry in S phase. Particularly, in proliferating

cells, Gsx2 expression blocks the cell cycle progression, whereas Ebf1 promotes it (Garcia-Dominguez, 2003; Garel et al., 1999; Méndez-Gómez & Vicario-Abejón, 2012).

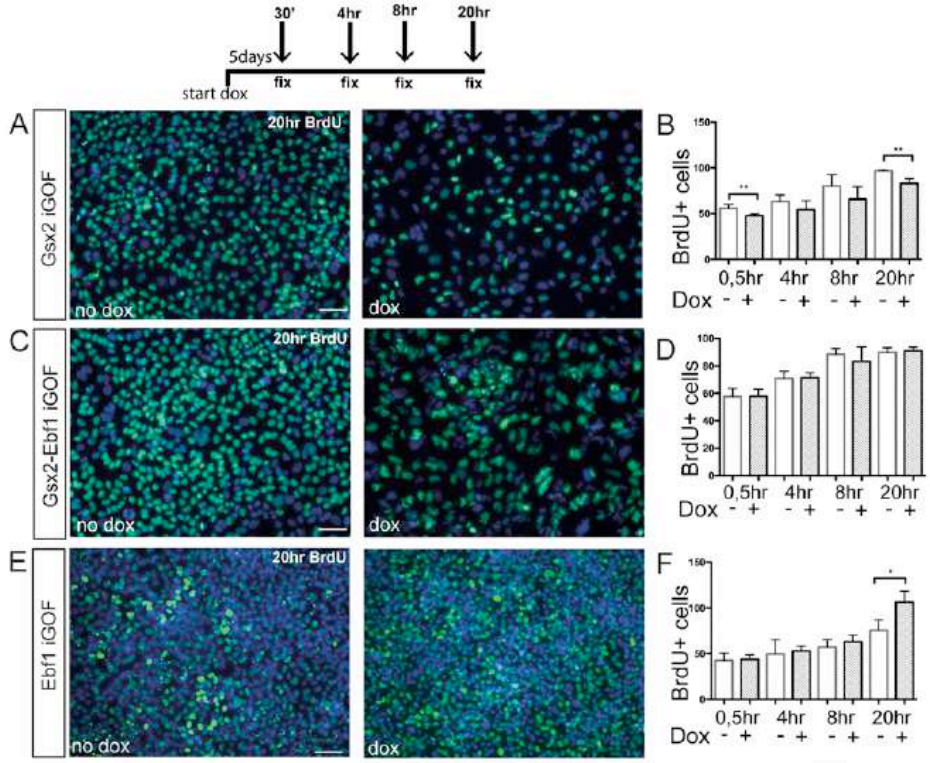

Figure 52: Cumulative BrdU assay. (Panel A, C, E) Immunofluorescence of BrdU incorporation (green) after 20 hrs in the three hES iGOF cell lines in Dox and no Dox condition (scale bar=50 μm); (Panel B, D, F) quantification of BrdU incorporation (n=3 independent experiments, data are represented as means ± SD; two-tailed t test analysis. *p < 0.05, **p< 0.01).

To test whether the overexpression of Gsx2 and Ebf1 regulated the cell cycle state also in hES-derived neural progenitor cells, we administered doxycycline from day 20 to day 30 of the Delli Carri protocol and cell cycle kinetics were analysed by a BrdU/IddU double labelling paradigm. Both BrdU and iododeoxyuridineare (IddU) are halogenated thymidine analogues and are incorporated into DNA synthesized during S-phase. The sequential exposure of proliferating cells to IddU and subsequently BrdU allows us to differentiate between defined populations of cells, by using primary antibodies, that uniquely recognize the BrdU or IddU incorporation (for details see Material and Methods section). The relative sizes of these populations allow us to calculate the total cell cycle time (Tc) and the length of S-phase (Ts) of the proliferating pool. For the application of this assay we followed the Martynoga et al., protocol, published in 2005 (diagram in Figure 53, Panel G).

At day 0 of differentiation, without doxycycline induction, we found that the Tc of the different iGOF lines was of 19.4 ± 4.4 hours. Next at day 30 of differentiation, the Tc of the hES-derived neural progenitors was assessed (Figure 53, Panel A–F), and we found results in agreement with the BrdU cumulative analysis shown in Figure 52, Panel A-F: estimation of control cell (no

doxycycline) Tc was 12 ± 1 hours, whereas the Gsx2 overexpressing cells showed a Tc of 24 ± 4 hours (Figure 53, Panel H). This indicates that the effect of Gsx2 overexpression on cell cycle is exerted by regulating its length. Next, we analysed the contribution of Ebf1 on the cell cycle by measuring Tc in Gsx2–Ebf1 iGOF cells, finding a value of 7 ± 1 hours, suggesting that Ebf1 could override a Gsx2-mediated increase of cell-cycle length (Figure 53, Panel H). Ebf1 iGOF line showed a cell cycle duration similar to the double Gsx2–Ebf1 iGOF (Figure 53, Panel E–F-H). All together these data indicate that in neuronal progenitors, only Gsx2 increases the cell cycle length. In fact, the cell line with only Ebf1 and the line with the combination of the two TFs has the same cell cycle length as the control cells.

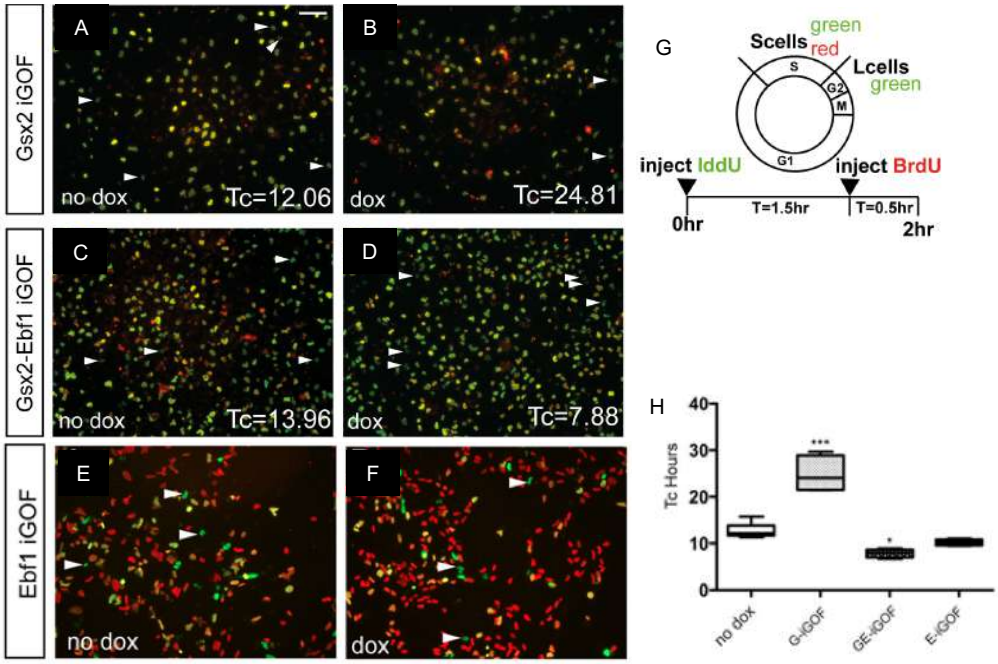

Figure 53: Calculation of cell cycle kinetics. (Panel A, B, C, D, E, F, G) Immunofluorescence of BrdU incorporation (red) and IddU incorporation (green) after 2 hours from the injection in the three hES iGOF cell lines in Dox and no Dox condition (scale bar=50 μm); (Panel H) quantification of cell cycle length (the whiskers of the graph show the largest and smallest values; ***$p < 0.0005$, *$p < 0.05$).

To rule out the possibility that Gsx2 iGOF cells were undergoing differentiation (and thus incorporating less BrdU), we analysed MAP2 expression at day 30. This marker was chosen as it represents maturing neurons and is expressed in our differentiating cultures until day 80. Gsx2 iGOF showed a marked reduction of $MAP2^{+}$ cells (Figure 54), in agreement with the previous cell cycle analysis data and further suggesting that Gsx2 overexpressing cells do not exit the cell cycle.

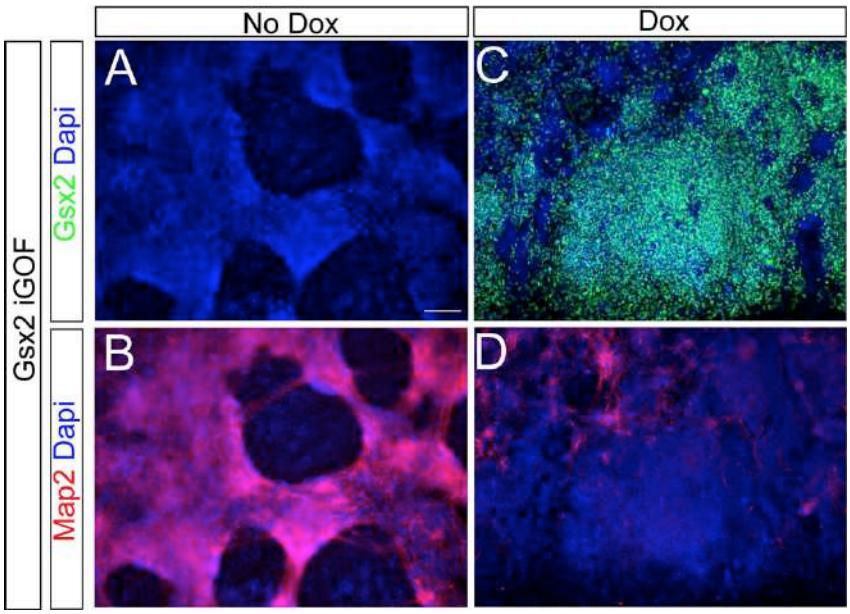

Figure 54: GSX2 and MAP2 expression at day 30 in Gsx2 iGOF cell line (scale bar=100 µm).

To confirm the effect of Gsx2 and Ebf1 on cell cycle kinetics, we analysed the expression of Ki67 and BrdU incorporation in differentiating iGOF lines. To do so, doxycycline was administered from day 20 until day 30 of differentiation, as reported diagram G in Figure 55, BrdU was administered for 2 hours at day 25 of neuronal maturation. The cells were then fixed at day 30 and analysed for BrdU incorporation and Ki67 expression. The cell cycle index was calculated by dividing the total number of $BrdU^{+}/Ki67^{-}$ cells by the total number of $BrdU^{+}$ cells. This number identifies the cells that became post-mitotic between after 25, which corresponds to the beginning of the maturation phase of the protocol. As showed in Figure 55 panel A-F, the three cell lines showed different phenotypes. Gsx2 overexpressing cells were more likely to remain in the cell cycle (50.2 ± 29.7% reduction of cell cycle exit over non-induced cells, Figure 55, Panel H); induced Gsx2-Ebf1 iGOF cells exited the cell cycle (150 ± 28% increase over non-induced cells, Figure 55, Panel H). Ebf1 iGOF overexpressing cells were 113 ± 7% more likely to exit the cell cycle (Figure 55, Panel H).

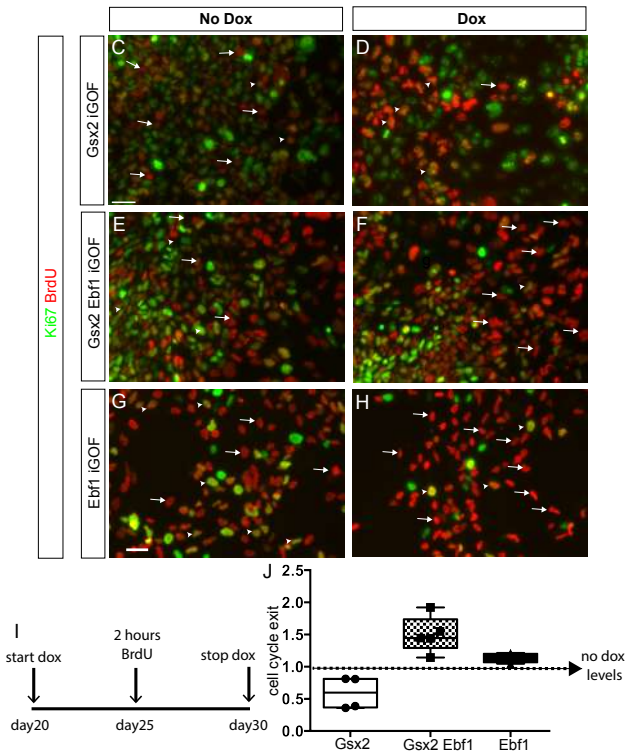

Figure 55: Immunofluorescence of Ki67 and BrdU at day 30 in the three iGOF cell lines. Gsx2 and Ebf1 differentially regulate cell-cycle exit and promote striatal differentiation. (Panel A–F) Representative images of cell-cycle exit studies. Arrows point to $BrdU^+/Ki67^-$ cells, that exited cell cycle; arrowheads point to $BrdU^+/Ki67^+$ cells, still proliferating (scale bar=75 μm); (Panel G) Schematic representation cell-cycle exit assay, by administering for 2 hours BrdU at day 25 of neuronal maturation in the temporal window of doxycycline treatment, from day 20 until day 30; (Panel H) Quantification of cell-cycle exit in Gsx2, Gsx2–Ebf1, and Ebf1 lines after 10 days of doxycycline treatment compared with basal conditions (no doxycycline, dotted line). Box shows the median and the 25th and 75th percentiles. The whiskers of the graph show the largest and smallest values (data are represented as means ± SD, n=3, t-test $^{**}p < 0.005$).

Together, these results were in line with the hypothesis of Gsx2 retaining neural progenitor cells in an undifferentiated state, while Ebf1 induces cell-cycle exit and progenitor maturation.

In conclusion, these data reflect the role of these two TFs *in vivo*, in fact in VZ Gsx2 maintains the neural progenitors in un-differentiated state, promoting their quiescent state (Méndez-Gómez & Vicario-Abejón, 2012); whereas Ebf1 promotes the maturation of neural precursors in the MZ (Garcia-Dominguez, 2003; Garel et al., 1999)

3.4. Evaluating the effects of TFs overexpression in MSN identity acquisition

To determine the striatal differentiation potential of hES cells overexpressing Gsx2 and Gsx2-Ebf1 between days 20 to 30, we conducted long-term differentiation experiments and analyzed the cells at day 80. We studied the expression of two key markers for mature striatal neurons, DARPP32 and CTIP2, along with MAP2 expression.

We quantified the number of generated striatal MSNs by analysing the area occupied by $CTIP2^+/DARPP32^+$ cells per field. Interestingly, we found a significantly higher efficiency of

CTIP2$^+$/DARPP32$^+$ neuron generation in the doxycycline-induced iGOF Gsx2–Ebf1 line only, compared with non-induced cells (38.8 ± 13.7% and 3.8 ± 3.1% respectively, Figure 56, E). Overexpression of Gsx2 and Ebf1 increased by more than five-fold the numbers of differentiated MSNs compared to normal hES H9 cells (7.13 ± 4.52%).

Finally, we studied if the Gsx2–Ebf1 combination could confer functional electrophysiological properties to the differentiated neurons. For this analysis, we took advantage of collaboration with Prof. Gerardo Biella at University of Pavia. Although passive membrane properties did not change significantly between doxycycline-treated and untreated cells (data not shown), we found interesting results studying sodium currents. In particular, Na^+ current density was significantly higher Gsx2–Ebf1 overexpressing cells compared to doxycycline untreated cells (from 30.7 ± 6.6 pA/pF in control cells to 76.1 ± 10.1 pA/pF in Gsx2–Ebf1 overexpressing cells; Figure 56, F). This data suggested that the neurons obtained from the overexpression of Gsx2-Ebf1 were more able to initiate and propagate action potentials.

As control, we verified the CTIP2 and DARPP32 expression in the other two iGOF lines, Gsx2 and Ebf1 alone cell lines, and we confirmed that only with the combination of the two TFs we had an increase in MSNs efficiency (Figure 57, data not quantified).

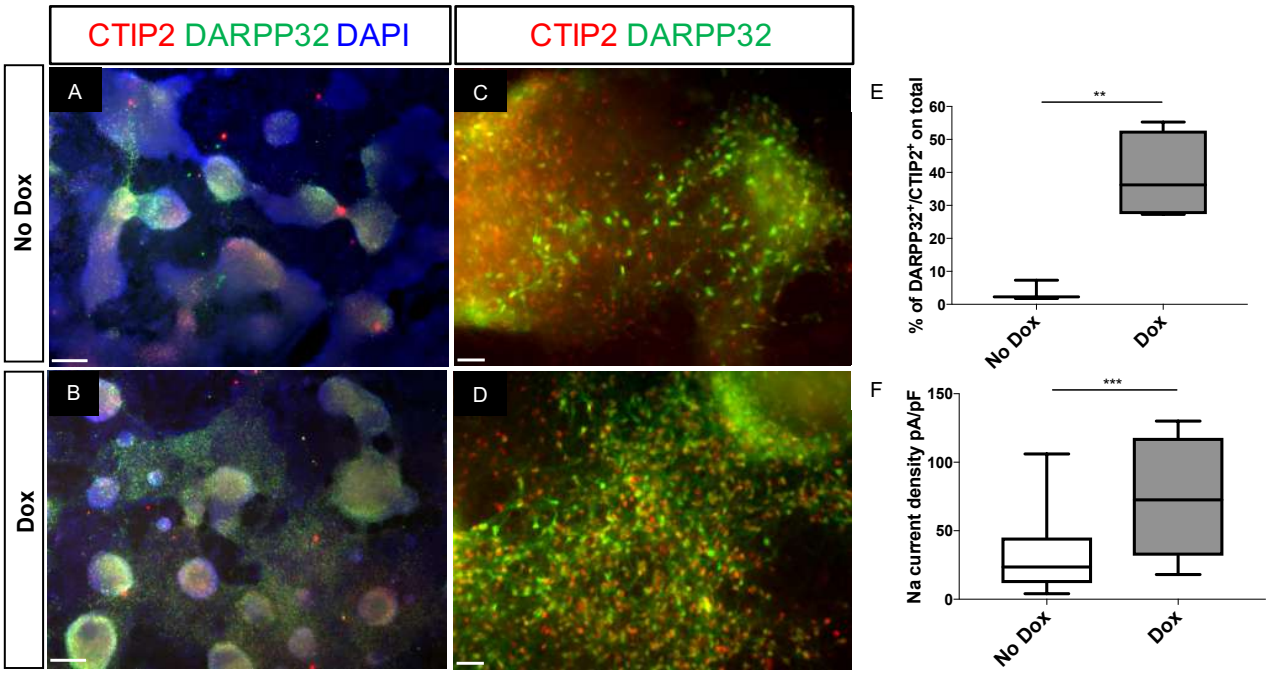

Figure 56: Immunodetection in Gsx2-Ebf1 iGOF cell line at day 80. (Panel A, B, C, D) Staining for DARPP32 and CTIP2 (scale bar=75 µm in A and B; and 250 µm in C and D); (Panel E) Quantification of DARPP32$^+$/CTIP2$^+$ cells on the Dapi positive area (data are represented as means ± SD, t test, **p < 0.005); (Panel F) Measurements of the Na^+ current density (data are represented as means ± SD, t test, ***p < 0.001).

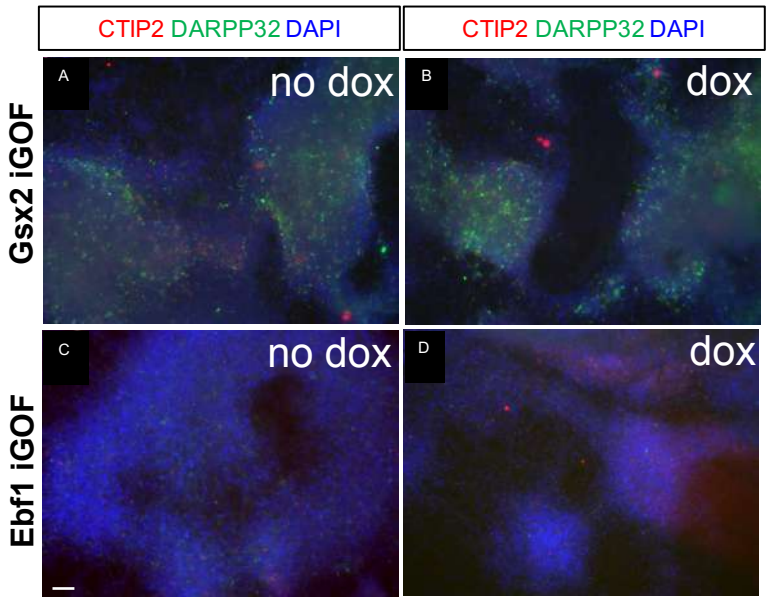

Figure 57: Immunodetection in Gsx2 and Ebf1 iGOF cell lines at day 80. (Panel A) Staining for DARPP32 and CTIP2 at day 80 without Doxycycline and (Panel B) after Doxycycline treatment in Gsx2 iGOF cell line; (Panel C) Immunofluorescence of DARPP32 and CTIP2 at day 80 without Doxycycline and (Panel D) after Doxycycline treatment in Ebf1 iGOF cell line (scale bar=100 μm)

In summary, these experiments showed that only the Gsx2-Ebf1 overexpression facilitate striatal maturation in hES cells *in vitro*.

To confirm the data obtained in the Gsx2-Ebf1 iGOF cell line, we decided to test a non-integrating system for the ectopic expression of these TFs.

3.5. Modified mRNA as non-integrating strategy for TF expression: preliminary results

The described iGOF system is based on a random integration approach, which bears risks of mutagenesis in the treated cells. In order to progress towards a possible therapeutic translation of this approach, we have considered using a non-integrating virus-free system for the overexpression of Gsx2–Ebf1 based on Modified mRNAs (mmRNAs) (Elango et al., 2005; Uzri & Gehrke, 2009), which are a new non-integrating strategy for reprogramming cell fate based on administration of synthetic mRNAs modified to overcome innate antiviral responses.

The cDNA of a gene of interest, optimized with regard to human codon usage, is cloned into a basic vector system containing the T7 promotor and a 5' and 3' UTR. RNA is generated in an animal component–free production process by T7-based transcription and subsequent 5' capping and 3' polyadenylation. Optionally, Ψ-UTP- and 5-mCTP-modified nucleotides are introduced to reduce innate immune responses against RNA in downstream applications. RNA is DNase treated, sterile filtered, and lyophilized (Figure 58).

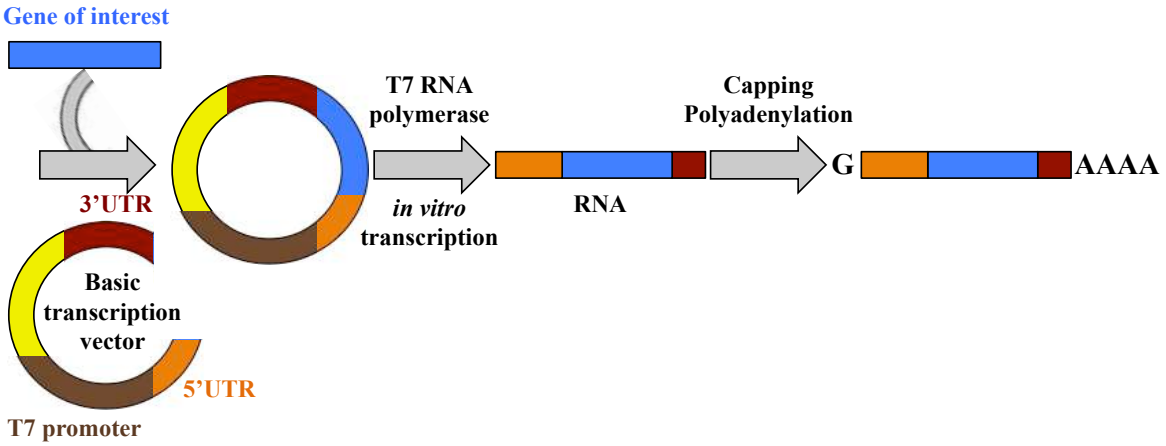

Figure 58: Design of the vector contained gene of interest under control of T7 promoter.

To promote efficient translation and boost RNA half-life in the cytoplasm, a 5' guanine cap is incorporated by inclusion of a synthetic cap analogue during the transcription *in vitro*. The open reading frame (ORF) of the gene of interest is flanked by a 5' untranslated region (UTR) containing a Kozak translational initiation signal and an alpha-globin 3' UTR terminating with an oligo(dT) sequence for template addition of a polyA tail. Cytosolic delivery of mmRNA into mammalian cells can be achieved via electroporation or by complexing the RNA with a cationic vehicle to facilitate uptake by endocytosis. Published results indicate that a repetitive transfection regimen would be required to sustain high levels of ectopic expression for short-lived proteins over an extended period of time (Warren et al., 2010) (Figure 59).

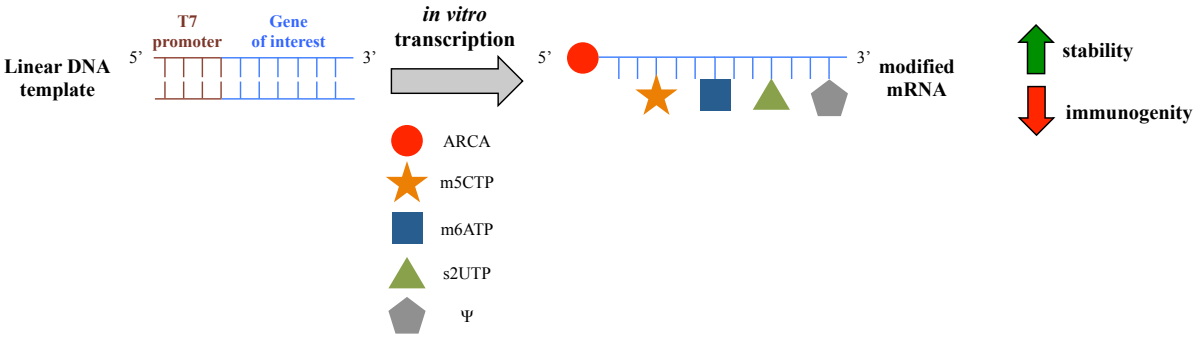

Figure 59: Pharmacokinetic properties of synthetic mRNA are improved by nucleotide analogue incorporation during *in vitro* RNA synthesis.

Modified mRNAs encoding for GFP were transfected in neural progenitors of hES H9 at day 20 (as described in Figure 60), and we tested two different reagents and protocols for the transfection, the StemMACS™ mRNA (Miltenyi Biotec) and *Trans*IT®-mRNA (Mirus Company). For the measurement of the transfection efficiency, we fixed the cells treated with 100ng and 200ng after 24 and 48 hours. The 200ng of GFP mmRNA transfected with Miltenyi

protocol at 48 hours post transfection showed the highest expression of GFP (31 ± 6.05%) (Figure 61).

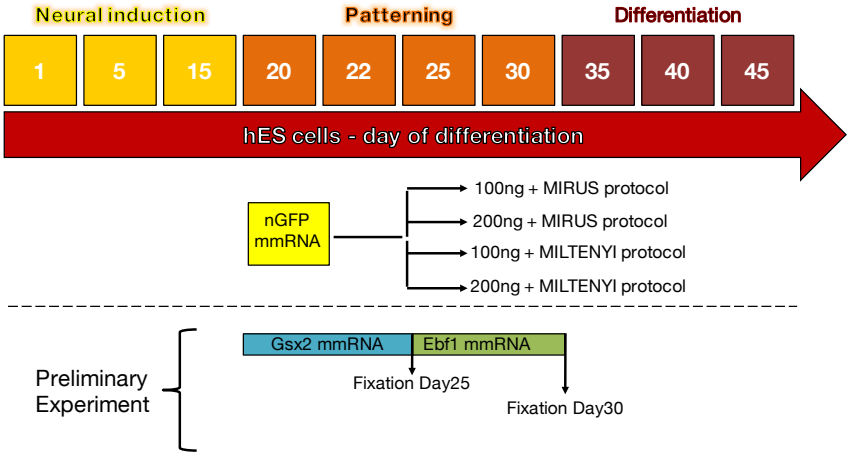

Figure 60: Experimental design for setting and using of mmRNA.

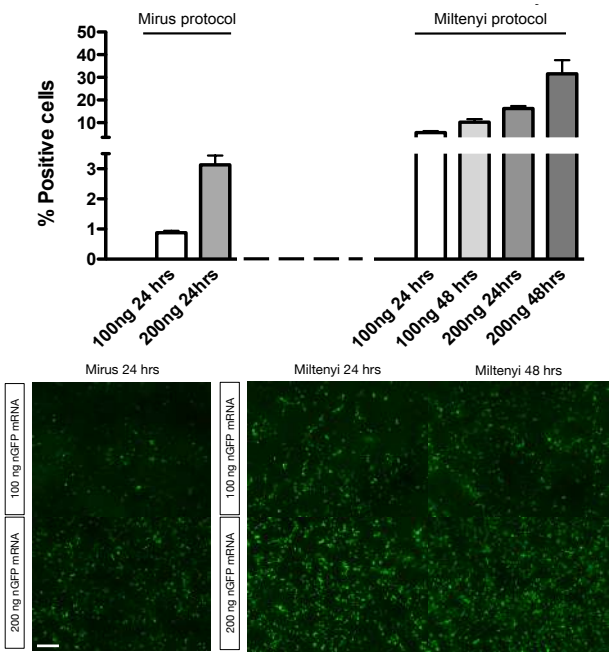

Figure 61: (bottom) Testing different protocols and concentration of mmRNA transfection (scale bar=50 µm) on hES H9 and (top) quantification (data are represented as means ± SEM).

After this set up, we applied the same mmRNA concentration and transfection protocol to transfect MSN progenitors from day 20 until day 25 hES H9 with mmRNA for Gsx2 followed by mmRNA transfection for Ebf1, from day 25 until day 30 (experimental details in Figure 60). As we could observe in Figure 62, we obtained 32.73 ± 6.15% $Gsx2^+$ cells and 32.73 ± 6.15% $Ebf1^+$ cells.

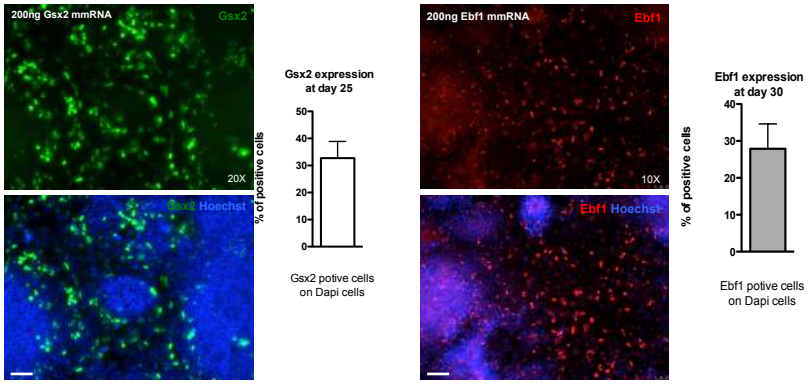

Figure 62: Transfection efficiency for Gsx2 and Ebf1 mmRNA during differentiation of hES H9 (scale bar=100 µm and 50 µm) and quantification (data are represented as means ± SEM).

In a preliminary experiment, we also observed a down regulation in PAX6 expression after Gsx2 mmRNA transfection at day 25. The transfected cells showed 15.73 ± 2.18% $PAX6^{+}$ compared to 49.57 ± 5.19% in the un-transfected cells (Figure 63). This data confirms the effect of Gsx2 expression on the down-regulation of PAX6, the same observed in the iGOF cell line. This first observation corroborates the idea that this non-integrating system is a viable alternative to the overexpression system.

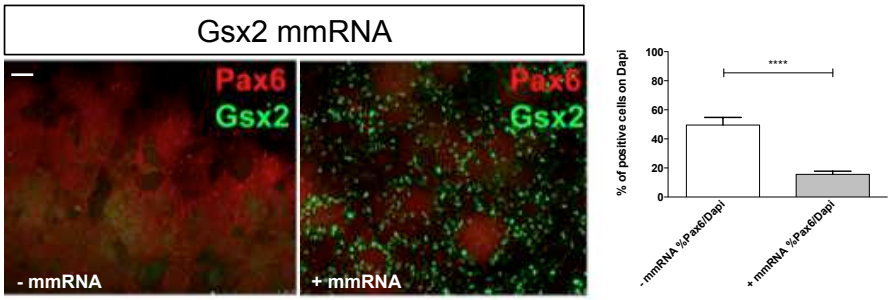

Figure 63: Gsx2 mmRNA transfection effect on Pax6 expression (scale bar=50 µm) and quantification (n=1 experiment, with 25 images analyzed; data are represented as means ± SEM, t-test ****p<0.0001).

These preliminary data showed that mmRNAs are well expressed in hES cells and hES cells-derived neural progenitors (Figure 63).

The application of mmRNA solves the problem of the integration used in the iGOF system, which modified the genome of the cells. In this system, in fact, we didn't know the number of copy of nucleofected plasmids that carried the TFs integrated in the cell genome.

Aiming at the development of an ectopic expression system compatible with the GMP procedures necessary for the cell replacement approach, the mmRNA approach represents a promising method to increase the number of authentic MSNs without genome alteration.

3.6. Evaluation of survival and maturation of iGOF (Gsx and Ebf1 overexpressors)-derived MSNs after transplantation

To evaluate the potential for cell replacement therapies of the striatal progenitors and neurons obtained *in vitro* we focused on the evaluation of the ability of these cells to survive and mature in the resident tissue *in vivo*. First of all, we worked on setting up cell transplantation condition with the aim to observe a good survival and maturation of the transplanted cells. Preliminary experiments performed in my lab had shown a good survival of neural progenitors transplanted at day 20 of the Delli Carri protocol. According to these evidences, colleagues in the lab have performed several transplantations following the same paradigm and we evaluated the capacity of these neurons to mature in the resident tissue. Then, they applied the new-improved transplantation approach on the Gsx2-Ebf1 iGOF cell line, to evaluate their capacity to mature in the striatum of the host.

Intrastriatal injection of Quinolinic Acid (QA) in rats produces an axon-sparing lesions similar to those observed in HD. QA was a potent excitant of neurons in the brain, by acting as an agonist at the N-methyl-D-aspartate (NMDA) sensitive population glutamate receptors, therefore causes selective neuronal lesions. Injection of QA in the striatum generally spares GABAergic interneurons and affected only MSNs, which are able to up take and metabolize the QA. For this reason, this is a good reproduction of neuropathology of HD than other excitotoxins (Beal et al., 1991; Schwarcz et al., 1986). Transplantation of human cells into experimental animals may elicit an immune rejection. Athymic nude rats, immunodeficient due to the lack of a normal thymus, in combination of QA lesions provide a useful model for our cell transplantation studies.

This model allows us to verify if it is possible to repopulate a lesioned striatum with *in vitro*-differentiated MSNs. My goal has been to characterise the hES-derived MSN progenitors after *in vivo* transplantation in this animal model of HD. These experiments were performed in collaboration with Prof. Alessandro Vercelli at the Neuroscience Institute Cavalieri Ottolenghi (NICO) in Turin and Prof. Rosa Maria Moresco at San Raffaele University in Milan.

We decided to transplant cells after 20 days of *in vitro* differentiation. This time point was selected based on previous experiments showing that cells differentiated until day 20 showed optimal survival 2 weeks after transplantation (Figure 64). Moreover, a small percentage of $Ki67^+$ cells was found demonstrating that the day 20 grafted neural progenitors promptly exited cell cycle, without forming overgrowths. With respect to Delli Carri et al., where the cells were transplanted at day 38 of differentiation we expect that grafting younger cells could increase their survival and integration in the striatum of the host.

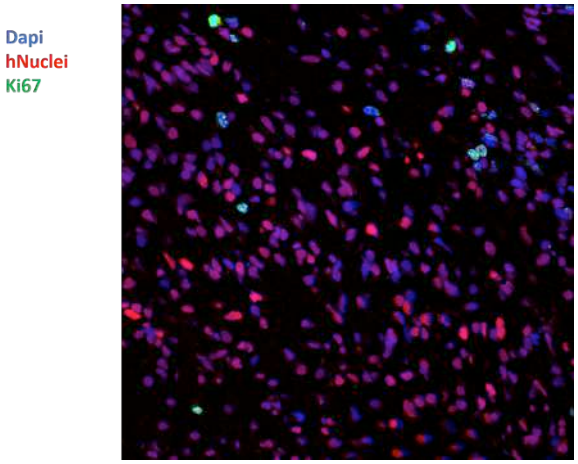

Figure 64: Section of rat striatum showing hNuclei$^+$ cells two weeks after transplantation. Cells have been grafted at day 20 of *in vitro* differentiation.

To characterize the hES H9-derived MSN progenitors after transplantation in QA-lesioned athymic rats, we followed the experimental protocol reported in Figure 65.

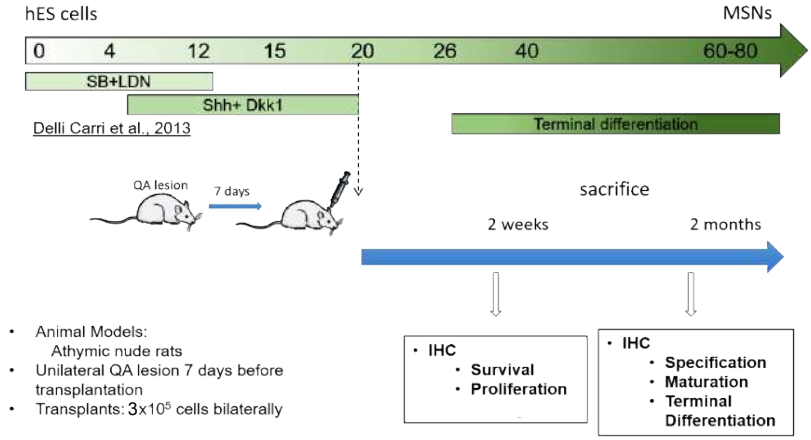

Figure 65: Experimental design of *in vitro* culture and transplantation procedure.

The lesion was produced by my colleagues through an unilateral striatal injection of 210 nmol of freshly made QA using the following stereotaxic coordinates: AP= +0.5, L= +/-2.8, V= 5.0. Seven days later we grafted 3x10^5 cells in both lesioned and non-lesioned striata.

20 animals were sorted into two groups of 10 animal each and sacrificed 2 weeks and 2 months after surgery. Good survival of the cells was evident at both time points as highlighted by hNuclei staining, which specifically recognizes human cells, in the post mortem striatal tissue.

To analyse the identity of the surviving cells at 2 weeks and 2 months after surgery we performed immunohistochemistry for NESTIN by using a human specific antibody and for the neuronal marker MAP2. We found that cells delivered to the lesioned hemisphere were able to integrate in the host tissue already 2 weeks from grafting (Figure 66).

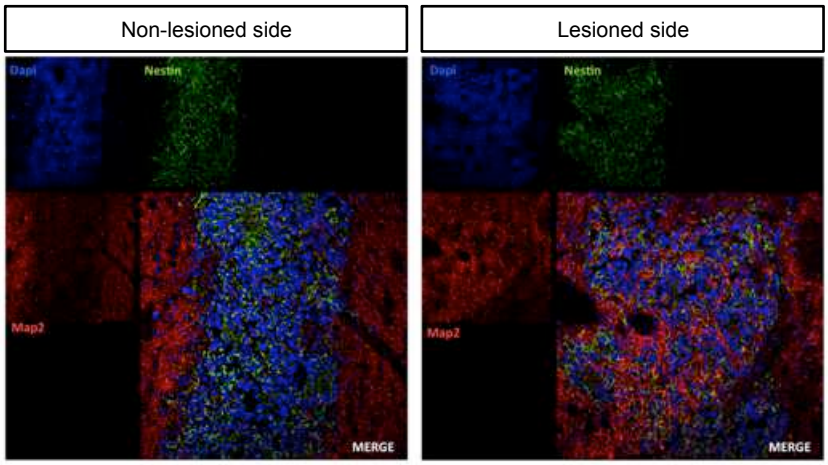

Figure 66: hNESTIN and MAP2 immunostaining on specimens of lesioned and non-lesioned striatum 2 weeks after surgery. A better integration of cells in the lesioned side is indicated by the higher MAP2 staining.

No expression of synaptic marker SYNAPSIN was found 2 weeks after surgery (Figure 67). This is not surprising at this early time point, after only two weeks after grafting, where transplanted cells are not expected to have already established direct cell-to-cell connections.

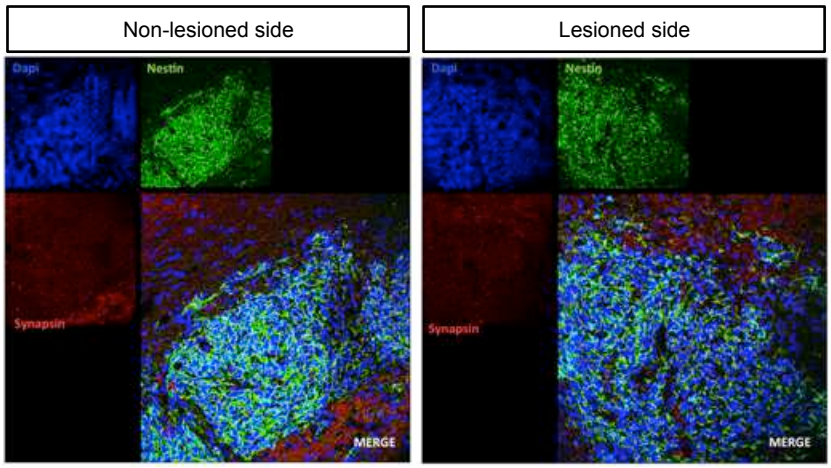

Figure 67: Immunohistochemistry of hNESTIN and SYNAPSIN in rat striatal tissue 2 weeks after grafting.

We then analysed whether the transplanted cells could generate mature MSNs by assessing CTIP2/DARPP32 co-expression in 3 sections spanning the rostro-caudal axis of the graft in both lesioned and non-lesioned sides 2 months after transplant in 10 animals (Figure 68). The frequency of CTIP2 and DARPP32 positive cells over hNuclei was determined by stereological approach. Figure 69 shows that 50% CTIP2^{+} cells, 3% of which were also DARPP32^{+}, were present 2 months after surgery.

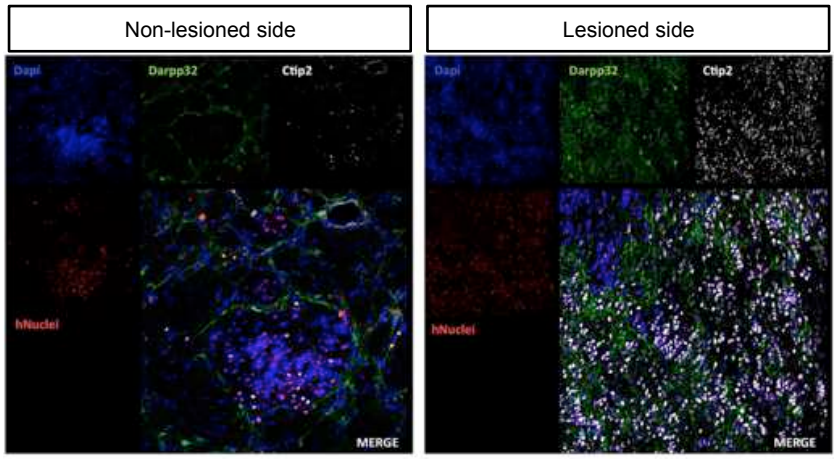

Figure 68: Immunohistochemistry for hNuclei, CTIP2, DARPP32 in rat striatal tissue 2 months after transplant.

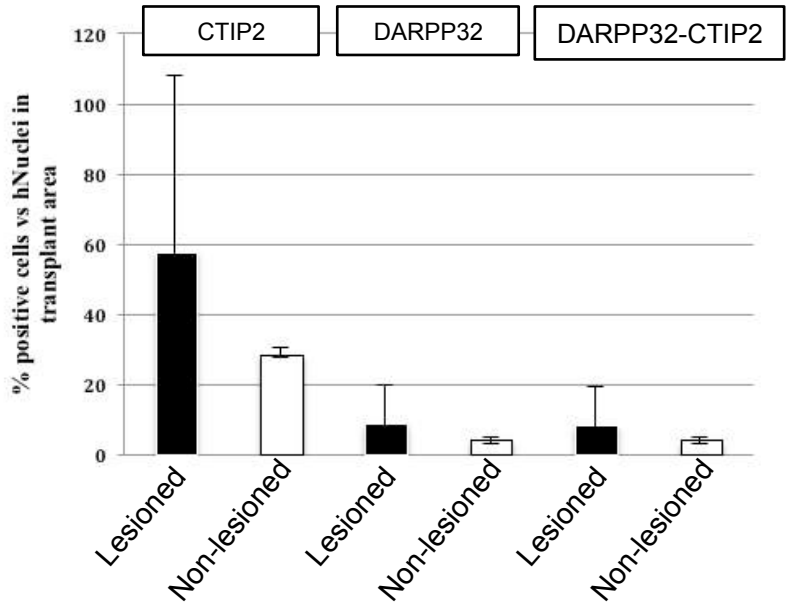

Figure 69: Stereological quantification in lesioned and non-lesioned side in the grafts 2 months after transplant of CTIP2, DARPP32, and DARPP32-CTIP2 co-expressing positive cells.

Figure 70 shows the widespread presence of surviving cells 2 months after transplant in the entire section of the brain of one representative animal. We therefore decided to look into more detail at the ability of these cells to extend processes throughout the brain by evaluating co-expression of hNCAM/hNESTIN in sections distal from the grafts. Figure 71 shows sporadic hNCAM positive fibres running through the corpus callosum 2 months after transplant.

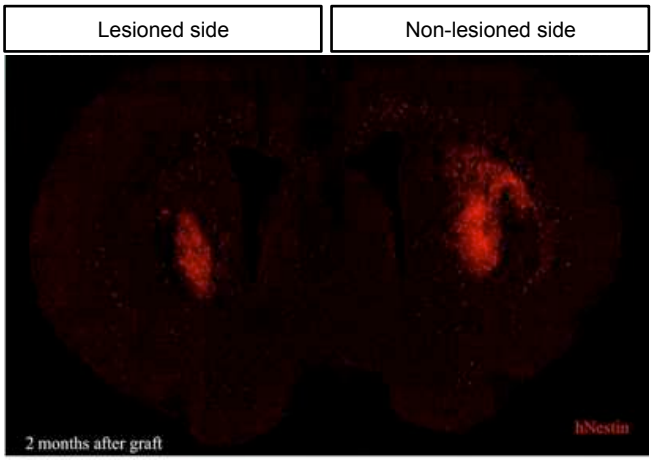

Figure 70: hNestin mosaic of the entire rat brain section, 2 months after surgery.

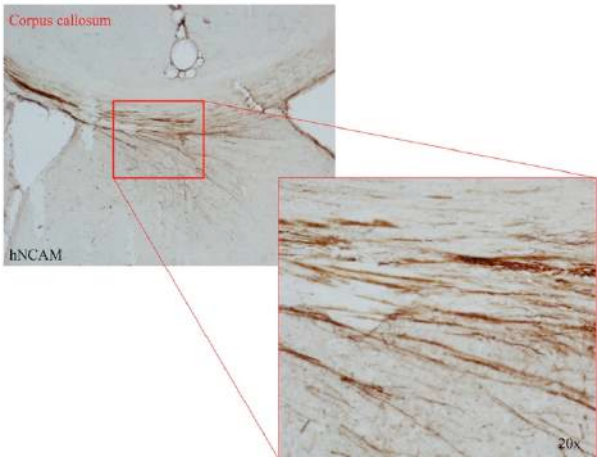

Figure 71: Immunohistochemistry of hNCAM positive fibers running through the corpus callosum and showing the ability of the graft to extend processes along long distances.

These preliminary observations suggest that hES-derived MSN progenitors derived according to the Delli Carri protocol can survive, mature and extend processes outside of the striatal nuclei. Day 20 immature neural progenitors were also able to differentiate and express mature striatal markers such as CTIP2 and DARPP32 without showing signs of overgrowth. We decided to adopt this experimental design to evaluate the survival and maturation capacity of differentiated Gsx2-Ebf1 iGOF cells *in vivo*.

To investigate long-term survival and differentiation of Gsx2-Ebf1 iGOF cells after transplantation in the striatum of QA-lesioned, athymic adult rats, the transplanted animals were followed up for two months and then sacrificed for immunohistochemical analysis to determine the striatal differentiation potential of hES cells overexpressing Gsx2–Ebf1 *in vivo* in term of $hNuclei^{+}$ MSNs detected in the striatum of the host.

Since cells at day 20 of the differentiation protocol are more suitable for transplantation, we decided to anticipate the induction of Gsx2 and Ebf1 to the temporal window day 15-20 of neuronal differentiation and cells at day 20 were used for transplantation in the QA lesioned rats (Figure 72, Panel A).

Two months after transplantation, we found hNuclei^{+} cells in the transplantation site (Figure 72, Panel B and C, the red cells), suggesting survival of the grafted cells (average of 53 ± 16% hNuclei^{+} cells on the total DAPI cells). To further investigate the co-expression of CTIP2 and DARPP32 in hNuclei^{+} cells, we performed a triple staining shown in Figure 72, Panel E and F. We quantified the cells that were hNuclei/CTIP2 double positive, and we found 23 ± 6% of cells expressing both markers (Figure 72, Panel D).

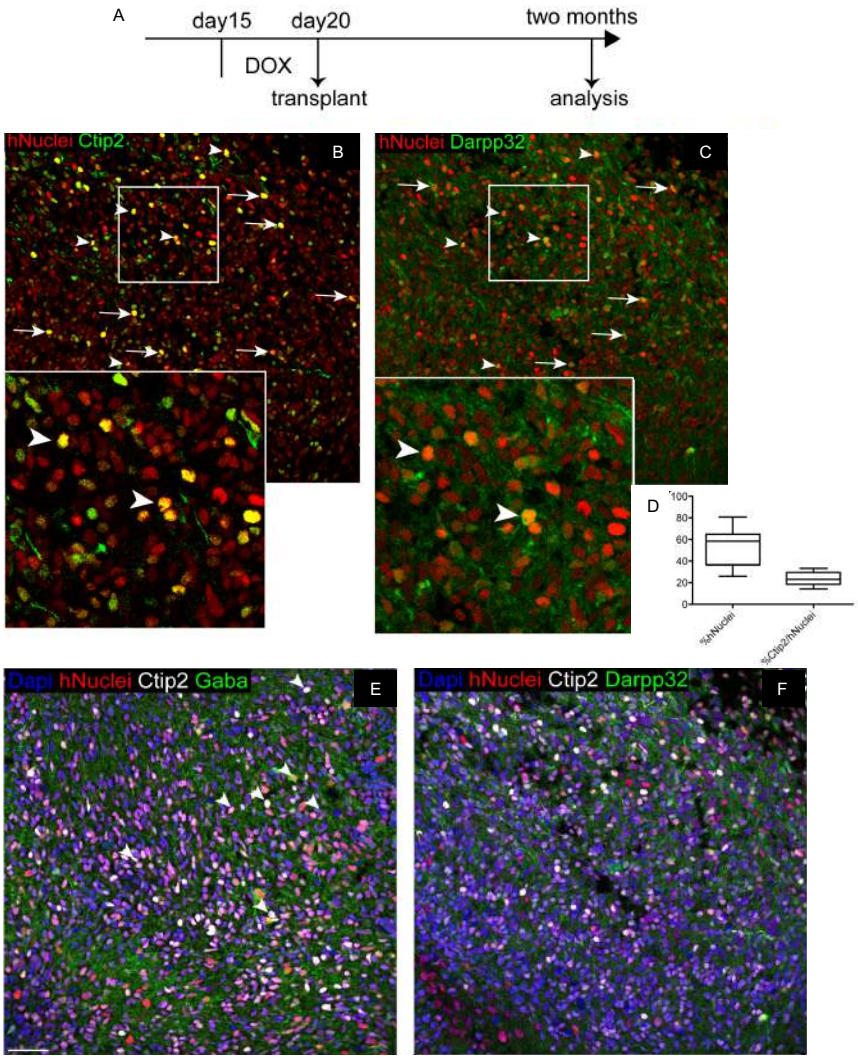

Figure 72: Immunohistochemistry of Gsx2-Ebf1 iGOF cell line 2 months after transplantation. (Panel A) Experimental design for hES cell-derived neural progenitor transplantation in QA-lesioned athymic rats. (Panel B, C, E, F) Immunohistochemistry for hNuclei^{+}, CTIP2, and DARPP32 or GABA cells two months after transplantation. Arrows point to grafted human cells expressing either CTIP2 or DARPP32 (scale bar=35 µm and scale bar=15 µm for insets); (Panel D) Quantification of human cells in the grafted site, hNuclei^{+} cells, and of CTIP2^{+} cells in the hNuclei^{+} population. Box shows the median and the 25th and 75th percentiles. The whiskers of the graph show the largest and smallest values.

Surprisingly, when we quantified the percentage of hNuclei$^+$ MSNs obtained from the transplantation of cells that did not receive doxycycline, we found the similar percentage of CTIP2 and DARPP32 positive cells in the graft (Figure 73, Panel A-B).

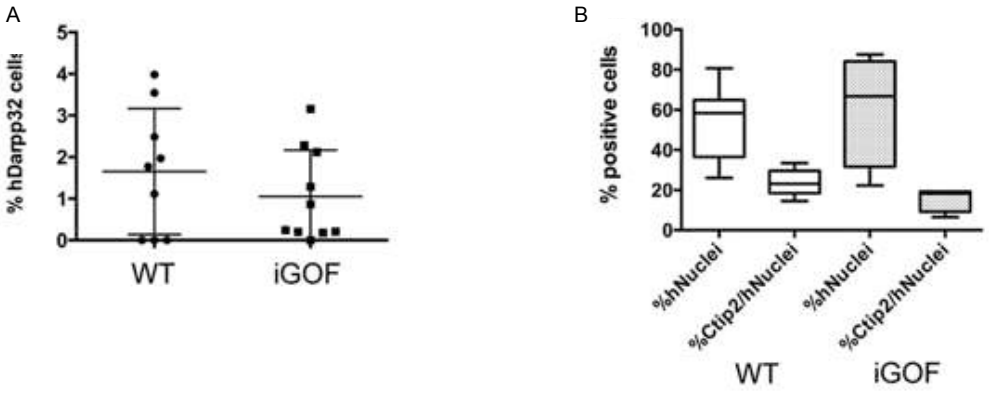

Figure 73: Quantification of percentage of hNuclei$^+$ MSNs cells obtained from the transplantation. (Panel A) Quantification of DARPP32 cells of human origin in the grafts, (Panel B) CTIP2 cells of human origin in the grafts in un-treated cells (indicated WT) and doxycycline treated (indicated iGOF) cells (data are represented as means ± SD).

All the data collected with the iGOF cell lines, published in Faedo et al., 2017 (Faedo et al., 2017), had shown the role of Gsx2 in restraining cell-cycle progression in neural progenitors, while the differentiation defect was rescue by Ebf1 expression. The co-recruitment of Gsx2 and Ebf1 caused a more efficient neuronal differentiation. Even if these two TFs are not expressed in the same region and time during human fetal brain development (Onorati et al., 2014), their combined expression in hES derived neural progenitors allowed to increase the neuronal differentiation, in term of authentic MSNs. However, the overexpressing cells after *in vivo* transplantation in QA athymic rat, did not show an increase in number of CTIP2$^+$/DARPP32$^+$ compared to un-treated cells. These results suggest that Gsx2–Ebf1 overexpression improves striatal differentiation *in vitro*, but it does not have an effect on the maturation of striatal progenitors *in vivo*.

Conclusions and Future Prospects

Conclusions and Future Prospects

This PhD thesis mainly aimed at two goals. First, to study the steps of *in vitro* differentiation from hPSC into MSN with the differentiation protocol published by Delli Carri et al., 2013 and validates its reproducibility across multiple cell lines. Second, to improve this protocol in order to obtain authentic MSNs that could be potentially used as disease modelling platform in pre-clinical studies for Huntington's Disease (HD).

All the four tested lines (H9 hES, Roslin hES, RUES2 hES and hiPS) showed canonical neural induction in terms of PAX6 and FOXG1 expression, and at day 25 we identified equal frequencies of ventral neural progenitor positive for GSX2 and ASCL1 markers. At day 35, the cells acquired a striatal precursor identity as indicated by co-labelling of NKX2.1, CTIP2 and ISLET1 markers. At the end of the differentiation (day 50), all the cell lines showed positivity for the MSN markers CTIP2, GABA and DARPP32 albeit with some variability. In conclusion, with these experiments we have demonstrated that the protocol previously established in the lab can be applied with good reproducibility to diverse hPSC lines.

The newly elaborated pipeline for image analysis allowed us to quantify several nuclear and cytoplasmic markers. This approach enabled us to quantify DARPP32 and CTIP2, and study the cell cycle dynamics during the differentiation protocol. For example, this analysis has highlighted that the expression of p27, both in H9 and RUES2 lines, remains static and showed no increase in expression from day 30 until the end of differentiation. This result correlates with the persistency of a $Ki67^{+}$ fraction in the same culture conditions. Conversely, our analysis showed that only a fraction of cells became p27 positive at day 30, with no increase until the end of the protocol (day 50: 7.13 ± 4.52%), suggesting that in these conditions only a part of the cells was instructed to transit to a post-mitotic phase. Despite general consistency, our data highlighted a different intrinsic ability of the hESC lines to mature in MSNs and exit from cell cycle. Specifically, RUES2 cells failed in generating DARPP32 positive neurons at the end of differentiation.

In this context and with the aim of improving the striatal differentiation protocol, we used H9 hES cells to study the effects of the forced expression of Gsx2 and Ebf1, transcription factors important for striatal neural progenitor specification and their maturation, respectively. We also implemented a non-integrating system based on modified mRNA for ectopic expression of the same TFs as a potential future strategy for cell replacement applications. Our data provide the proof of principle that TF expression *in vitro* can improve the efficiency of our differentiation

protocol. Notably, time-controlled expression of Gsx2 and Ebf1 during *in vitro* differentiation has allowed to significantly increase the overall efficiency of the procedure from 7.12 % to 38.8% of MSNs generated after 50 days of differentiation. This was also reflected in the cell cycle state of the cells. In particular after Gsx2 induction, we observed changes in neural progenitor's cell cycle. In fact, Gsx2 may keep ventral neural progenitor cells in an un-differentiated state, by promoting cell cycle to "pause", thus inducing a G_0-like state inhibiting neural maturation. This effect was rescued by Ebf1 expression and cells were able to mature and exit from the cell cycle. These findings suggest that monitoring the cell cycle state during differentiation combined with forcing it's exit by using compounds in specific time windows could be a good strategy to improve the percentage of post-mitotic neurons at the end of differentiation.

Other studies highlighted that the cell cycle state can influence the acquisition of a specific fate after application of different differentiation protocols (Dalton, 2013; Pauklin & Vallier, 2014). Pauklin and Vallier have demonstrated that hESCs in early G1 phase are more permissive to endoderm differentiation, while cells in late G1 are prone to switch from endodermal to neuroectodermal fate acquisition (Pauklin & Vallier, 2014). In light of these observations, we can speculate that the changes in cell cycle state in different cell lines could have a significant downstream effect during differentiation. This might explain the variability observed in DARPP32 expression in our four cell lines. In this case, the use of compounds able to modulate cell cycle progression and synchronisation may represent a promising approach to improve neural induction, cell fate acquisition and maturation.

As previously reported in Delli Carri et al., 2013, the data obtained after *in vivo* transplantation of hESCs differentiated *in vitro* confirmed a relatively poor efficiency of conversion of hESC into MSNs. We thought that transplanting cells at day 20 of the differentiation protocol instead that at day 38 as in Delli Carri, could help to promote their survival and integration in the striatum of the host. At day 20, in fact, the cells are in a neural progenitor state and are therefore more permissive and tolerant to transplant. Nonetheless, we obtained a small number of human MSNs in the striatum of QA lesioned rats, showing also in this case that the cells were not able to mature with high efficiency in the host brain. Low efficiency of conversion may be the result of different exposure to morphogens that cells face in *vivo.* As described, *in vitro* differentiation relies on 25 days of continuous exposure to SHH and WNT signalling inhibition that is prematurely terminated during the *in vivo* paradigm at the time of transplantation, shortening the window of exposure of the cells to SHH and WNT signalling inhibition by 5 days. This may

compromise *in vivo* the efficiency of conversion leading to the observed reduced frequency of MSNs.

Generation of authentic MSNs was not improved also when we tested grafting efficiency of hESC expressing Gsx2 and Ebf1. Transplantation of iGOF cells in QA-lesioned animals did not achieve an increase of *bona fide* MSNs in the graft 2 months after transplantation as expected according to the *in vitro* data showing a significant increase in the overall efficiency MSNs generation compared to un-transfected cells. Also in this case, discrepancies between the *in vitro* and *in vivo* paradigms could explain the obtained data. In order to perform the transplant at day 20 of differentiation, the cells received doxycycline from day 15 to day 20 while for the *in vitro* experiments we overexpressed Gsx2 and Ebf1 from day 20 until day 30. We therefore believe that low efficiency in the generation of MSNs *in vivo* may be due to the different doxycycline exposure window used to force expression of the TFs. In the next future, we will transplant iGOF cells at day 20 and sustain the transgenes expression by *in vivo* administration of doxycycline through drinkable water, based on the fact that this antibiotic is able to pass the blood-brain barrier, as shown in Torper et al., 2013 (Torper et al., 2013).

In summary, this thesis work highlights that the generation of precisely patterned neural cells from human Embryonic Stem cells (hESC) and pluripotent stem cells (hPSCs) is a crucial step to develop optimal cellular models to study neurodevelopment and to model neurodegenerative disease. This work provides a detailed characterization of authentic striatal medium spiny neurons (MSNs) by implementing a highly elaborate microscope image acquisition pipeline that enabled us to identify and quantify specific cell states and transitions occurring during our *in vitro* differentiation protocol (Delli Carri et al., 2013). In addition, we pinpointed Gsx2 and Ebf1 as two essential transcription factors during these shifts in identities and designed an overexpressing system to deliver these factors in a time controlled manner. This strategy has improved conversion into mature MSNs *in vitro* from 7% to 38%. However, further studies will be required to test whether *in vivo* transplantation of Gsx2-Ebf1 overexpressing cells in adult athymic QA-lesioned rats is a good strategy to increase generation efficiency of authentic MSNs. In this respect, the implementation of the mmRNA strategy will be useful as an alternative approach for the non-integrating ectopic expression of these TFs. Therefore, we are planning to optimize this system in GMP cell lines, in the prospective of cell replacement therapies.

Materials and Methods

Materials and Methods

ES cell culture. hES H9 cell line was cultured on Cultrex™ (12-18 mg/ml, Trevigen) with mTeSR (StemCell Technology) and medium was changed daily. Cells were splitted once a week with PBS plus EDTA 0.5 mM, without centrifugation and re-plated without the Rock inhibitor (Y-2763221, Cell Guidance System).

hES RUES2 parental cell line was cultured on Geltrex™ (120-180 ug/ml, Thermo Fisher Scientific) with mTeSR (StemCell Technology) and medium was changed daily. Cells were passaged enzymatically with twice a week by ReLESR (StemCell Technology).

hES Roslin cell lines (RC9 and RC17) was cultured on Cultrex™ (12-18 mg/ml, Trevigen) with StemPro™ hESC SFM (Thermo Fisher Scientific) and medium was changed daily. Cells were splitted once a week with PBS plus EDTA 0.5 mM and, after centrifugation, re-plated with Rock inhibitor (Y-2763221, Cell Guidance System).

hiPS cells were cultured on Cultrex™ (12-18 mg/ml, Trevigen) with mTeSR (StemCell Technology) and medium was changed daily. Cells were splitted twice a week with ReLESR (StemCell Technology) and, after centrifugation, re-plated with the Rock inhibitor (Y-2763221, Cell Guidance System).

Neuronal differentiation. hES and hiPS cells were plated for neuronal induction. Briefly, cells were plated at a density of 0.7×10^5 cells cm^2 on Cultrex™ (12-18 mg/ml, Trevigen) coated dishes in grow medium supplemented with 10 μM ROCK inhibitor (Y-2763221, Cell Guidance System). Cell cultures were expanded for three days until they were 70% confluent. The starting differentiation medium includes DMEM/F12 (Life Technologies) with N2 and B27 (Life Technologies), supplemented with 500 nM LDN193189 (Sigma) and 10 μM SB431542 (Tocris), which was used until re-plating. The medium was changed daily. Starting on day 5, 200 ng ml^{-1} SHHC-25II (R&D) and 100ng ml^{-1} DKK-1 (Peprotech) were added to the culture and maintained until day 25. After the appearance of rosettes (between day 10 and day 15), the entire cell population was detached using Accutase (Millipore) and re-plated at a cell density of 2.5×10^4 cells cm^2 on dishes coated with Cultrex™ (12-18 mg/ml, Trevigen) without grow factors. The cells were maintained in terminal differentiation medium, which was composed of N2 medium supplemented with B27 and 30ng ml^{-1} BDNF, until the end of differentiation.

Immunofluorescence. Cells were fixed in 4% (wt/vol) paraformaldehyde (PFA) for 15 minutes at room temperature (RT) and washed 3 times with phosphate-buffered saline (PBS). Cells were then permeabilized with PBS containing 0.5% Triton X-100 (Sigma) and blocked with 10% (vol/vol) normal goat serum (NGS; Vector) for 1 hour at room temperature (RT). Next, cells were incubated overnight at 4°C with different primary antibodies. In the Table 6 details for each antibody were reported.

Antibodies_Day0	Company	Code	Working dilution	Unmasking
Ki67	Abcam	AB15580	1:1000	
Oct3/4	Santa Cruz	SC-5279	1:100	
p27	Cell Signaling	BK3698S	1:1000	
Sox2	Millipore	AB5603	1:200	

Antibodies_Day15	Company	Code	Working dilution	Unmasking
Foxg1	Diatech	M227	1:1000	for human cells: EDTA 60°C 10min
Ki67	Abcam	AB15580	1:1000	
p27	Cell Signaling	BK3698S	1:1000	
Pax6	Covance (BioLegend)	901301	1:2500	

Antibodies_Day25	Company	Code	Working dilution	Unmasking
βIII-Tubulin	Promega	T8660	1:2500	
Ascl1	BD	556604	1:1000	
Ctip2	Abcam	AB18465	1:1000	
Ebf1	Santa Cruz	SC-137065	1:1000	
Gsx2	Millipore	ABN162	1:250	for human cells: EDTA 60°C 10min
Islet1	DHSB	39.4D5-S	1:1000	
Ki67	Abcam	AB15580	1:1000	
Map2	BD	556320	1:1000	
Nkx2.1	Abcam	AB76013	1:1000	
p27	Cell Signaling	BK3698S	1:1000	
Pax6	Covance (BioLegend)	901301	1:2500	
Tbr1	Abcam	AB23345	1:1000	
Tbr2	Abcam	AB31940	1:1000	

Antibodies_Day50	Company	Code	Working dilution	Unmasking
βIII-Tubulin	Promega	T8660	1:2500	
Ctip2	Abcam	AB18465	1:1000	
Darpp-32	Abcam	AB40801	1:250	
Ebf1	Santa Cruz	SC-137065	1:1000	
GABA	Sigma	A2052	1:500	
GAD67	Millipore	MAB5406	1:2500	
Islet1	DHSB	39.4D5-S	1:1000	
Ki67	Abcam	AB15580	1:1000	
Map2	BD	556320	1:1000	
Nkx2.1	Abcam	AB76013	1:1000	
p27	Cell Signaling	BK3698S	1:1000	
Pax6	Covance (BioLegend)	901301	1:2500	
Tbr1	Abcam	AB23345	1:1000	
Tbr2	Abcam	AB31940	1:1000	

Table 5: Antibodies used to better characterize striatal differentiation protocol at different time points.

After 3 washes in PBS 0.1% Triton X-100 (Sigma), appropriate secondary antibodies conjugated to Alexa fluorophores 488, 568, 546 and 647 (Molecular Probes, Invitrogen) were diluted 1:500 in blocking solution and mixed with Hoechst 33258 (5 μg ml^{-1}; Molecular Probes, Invitrogen) to counterstain the nuclei. Images were acquired with a Leica DMI 6000B microscope (5x, 10x and 20x objectives), analyzed with LAS-AF imaging software, and then processed using Adobe Photoshop, only to adjust contrast for optimal RGB rendering.

For the quantification, the images were acquired by Leica TCS SP5 confocal microscope (40x objective, zoom 1.7). Confocal images were acquired at a resolution of 1024 X 1024 dpi and 200 Hz speed in 12 bits, and each focal plane was 10 μm thick. We acquired three z stacks for each focal plane and 9 different fields for each analyzed well.

Laser intensity, gain, and offset were maintained constant in each analysis and each time point. After acquisition, for the quantification analysis on the images were applied the Median Filter, a nonlinear filter, with Kernel size of a 3 x 3 pixel matrix to remove noise and background.
Histological specimens of transplantations were examined using a Leica TCS SP5 confocal microscope. Confocal images were taken at a resolution of 1024 X 1024 dpi and 150 Hz speed, and each focal plane was 1 μm thick. Laser intensity, gain, and offset were maintained constant in each analysis. In collaboration with NICO institute in Turin, there were analyzed three animals for each condition.

Quantification with CellProfiler software. CellProfiler is a versatile, open-source software tool to quantify data from biological images. It is designed for modular, flexible, high-throughput analysis of images, measuring size, shape, intensity, and texture of every cell (or other object) in every image. For our purpose, all the images carrying the different immunocytochemical staining were analysed starting from a grayscale picture of the individual channels (blue, green and red – two colours staining). Images were filtered so that each channel was analysed for the appropriate marker Images of nuclear markers (DAPI, GSX2, CTIP2, ASCL1, PAX6, FOXG1) were processed with the following modules:

- "**ApplyThreshold**" to remove background using two-classes "Global" "Otsu" thresholding method
- "**IdentifyPrimaryObject**" in the size range of 5 to 15 pixels using "Global" or "Adaptive" thresholding strategy with 2-classes "Otsu" and "Automatic" smoothing method. "Laplacian of Gaussian" was used as method to distinguish clumped object and "Propagate" as method to divide clumped objects.

Images carrying staining for cytoplasmic markers such as Darpp32 were processed first using the EnhanceOrSuppressFeatures module using the operation "**Enhance**", feature "**Tubeness**" and a smoothing scale of 2.0.
Objects were then identified using the "**IdentifyPrimaryObject**" module with a typical object diameter of 5-20 pixels, "**Global**" thresholding strategy and MCT thresholding method using "**Intensity**" as method to distinguish clumped object and again "**Intensity**" as method to divide clumped objects.
To establish whether a cell is double positive for the two markers performed in the same staining or anyway to relate every object identified to a DAPI-positive object, we used the "**RelateObjects**" module. This module allows associating child objects with parent objects so

relating objects identified by one staining with the DAPI or with a second staining (double positive cells).

The frequency of cells positive for each marker was calculated using the "**CalculateMath**" module by dividing the number of parent object by the number of DAPI-identified objects.

The data were finally exported into spreadsheets using the "**ExportToSpreadsheet**" module.

An example of Pipeline for the triple nuclear staining DAPI, ASCL1 and GSX2 with all the module variable details is the following:

Pipeline "CellProfiler Pipeline: http://www.cellprofiler.org

Version:3
DateRevision:20140723173957
GitHash:6c2d896
ModuleCount:13
HasImagePlaneDetails:False

Images:*[module_num:1|svn_version:\'Unknown\'|variable_revision_number:2|show_window:False|notes:\x5B\'To begin creating your project, use the Images module to compile a list of files and/or folders that you want to analyze. You can also specify a set of rules to include only the desired files in your selected folders.\'\x5D|batch_state:array(\x5B\x5D, dtype=uint8)|enabled:True|wants_pause:False :Filter images?:Images only Select the rule criteria:and (file doesnot contain ""foxp2"")*

Metadata:*[module_num:2|svn_version:\'Unknown\'|variable_revision_number:4|show_window:False|notes:\x5B\'The Metadata module optionally allows you to extract information describing your images (i.e, metadata) which will be stored along with your measurements. This information can be contained in the file name and/or location, or in an external file.\'\x5D|batch_state:array(\x5B\x5D, dtype=uint8)|enabled:True|wants_pause:False]*

Extract metadata?:No
Metadata data type:Text
Metadata types:{}
Extraction method count:1
Metadata extraction method:Extract from image file headers
Metadata source:File name
Regular expression:^(?P<Plate>.)_(?P<Well>\x5BA-P\x5D\x5B0-9\x5D{2})_s(?P<Site>\x5B0-9\x5D)_w(?P<ChannelNumber>\x5B0-9\x5D)*
Regular expression:(?P<Date>\x5B0-9\x5D{4}_\x5B0-9\x5D{2}_\x5B0-9\x5D{2})$
Extract metadata from:All images
Select the filtering criteria:and (file does contain """")
Metadata file location:
Match file and image metadata:\x5B\x5D
Use case insensitive matching?:No

NamesAndTypes:*[module_num:3|svn_version:\'Unknown\'|variable_revision_number:5|show_window:False|notes:\x5B\'The NamesAndTypes module allows you to assign a meaningful name to each image by which other modules will refer to it.\', \'---\', \'Load the images by matching files in the folder against the unique text pattern for each stain \x3A d0.tif for nuclei, d1.tif for the PH3 image. The two images together comprise an image set.\'\x5D|batch_state:array(\x5B\x5D, dtype=uint8)|enabled:True|wants_pause:False]*

Assign a name to:Images matching rules
Select the image type:Grayscale image
Name to assign these images:DNA
Match metadata:\x5B\x5D
Image set matching method:Order
Set intensity range from:Image metadata
Assignments count:3
Single images count:0

Select the rule criteria:and (file does contain ""ch00"")
Name to assign these images:OrigRed
Name to assign these objects:Cell
Select the image type:Grayscale image
Set intensity range from:Image metadata
Retain outlines of loaded objects?:No
Name the outline image:LoadedObjects
Select the rule criteria:and (file does contain ""ch01"")
Name to assign these images:OrigGreen
Name to assign these objects:Nucleus
Select the image type:Grayscale image
Set intensity range from:Image metadata
Retain outlines of loaded objects?:No
Name the outline image:LoadedObjects
Select the rule criteria:and (file does contain ""ch02"")
Name to assign these images:OrigBlue
Name to assign these objects:Cytoplasm
Select the image type:Grayscale image
Set intensity range from:Image metadata
Retain outlines of loaded objects?:No
Name the outline image:LoadedOutlines

***Groups**:[module_num:4|svn_version:\'Unknown\'|variable_revision_number:2|show_window:False|notes:\x5B\'The Groups module optionally allows you to split your list of images into image subsets (groups) which will be processed independently of each other. Examples of groupings include screening batches, microtiter plates, time-lapse movies, etc.\'\x5D|batch_state:array(\x5B\x5D, dtype=uint8)|enabled:True|wants_pause:False]*
Do you want to group your images?:No
grouping metadata count:1
Metadata category:None

***ApplyThreshold:**[module_num:5|svn_version:\'Unknown\'|variable_revision_number:7|show_window:True|notes:\x5B\x5D|batch_state:array(\x5B\x5D, dtype=uint8)|enabled:True|wants_pause:False]*
Select the input image:OrigBlue
Name the output image:ThreshBlue
Select the output image type:Grayscale
Set pixels below or above the threshold to zero?:Below threshold
Subtract the threshold value from the remaining pixel intensities?:No
Number of pixels by which to expand the thresholding around those excluded bright pixels:0.0
Threshold setting version:1
Threshold strategy:Global
Thresholding method:Otsu
Select the smoothing method for thresholding:Manual
Threshold smoothing scale:1.0
Threshold correction factor:1.0
Lower and upper bounds on threshold:0.0,1.0
Approximate fraction of image covered by objects?:0.01
Manual threshold:0.0
Select the measurement to threshold with:None
Select binary image:None
Masking objects:None
Two-class or three-class thresholding?:Two classes
Minimize the weighted variance or the entropy?:Weighted variance
Assign pixels in the middle intensity class to the foreground or the background?:Foreground
Method to calculate adaptive window size:Image size Size of adaptive window:10

ApplyThreshold:*[module_num:6|svn_version:\'Unknown\'|variable_revision_number:7|show_window:True|notes:\x5B\x5D|batch_state:array(\x5B\x5D, dtype=uint8)|enabled:True|wants_pause:False]*

Select the input image:OrigGreen
Name the output image:ThreshGreen
Select the output image type:Grayscale
Set pixels below or above the threshold to zero?:Below threshold
Subtract the threshold value from the remaining pixel intensities?:No
Number of pixels by which to expand the thresholding around those excluded bright pixels:0.0
Threshold setting version:1
Threshold strategy:Global
Thresholding method:Otsu
Select the smoothing method for thresholding:Manual
Threshold smoothing scale:1.0
Threshold correction factor:1.0
Lower and upper bounds on threshold:0.0,1.0
Approximate fraction of image covered by objects?:0.01
Manual threshold:0.0
Select the measurement to threshold with:None
Select binary image:None
Masking objects:None
Two-class or three-class thresholding?:Two classes
Minimize the weighted variance or the entropy?:Weighted variance
Assign pixels in the middle intensity class to the foreground or the background?:Foreground
Method to calculate adaptive window size:Image size
Size of adaptive window:10

ApplyThreshold:*[module_num:7|svn_version:\'Unknown\'|variable_revision_number:7|show_window:True|notes:\x5B\x5D|batch_state:array(\x5B\x5D, dtype=uint8)|enabled:True|wants_pause:False]*

Select the input image:OrigRed
Name the output image:ThreshRed
Select the output image type:Grayscale
Set pixels below or above the threshold to zero?:Below threshold
Subtract the threshold value from the remaining pixel intensities?:No
Number of pixels by which to expand the thresholding around those excluded bright pixels:0.0
Threshold setting version:1
Threshold strategy:Global
Thresholding method:Otsu
Select the smoothing method for thresholding:Manual
Threshold smoothing scale:1.0
Threshold correction factor:1.0
Lower and upper bounds on threshold:0.0,1.0
Approximate fraction of image covered by objects?:0.01
Manual threshold:0.0
Select the measurement to threshold with:None
Select binary image:None
Masking objects:None
Two-class or three-class thresholding?:Two classes
Minimize the weighted variance or the entropy?:Weighted variance
Assign pixels in the middle intensity class to the foreground or the background?:Foreground
Method to calculate adaptive window size:Image size
Size of adaptive window:10

IdentifyPrimaryObjects:*[module_num:8|svn_version:\'Unknown\'|variable_revision_number:10|show_window:True|notes:\x5B\x5D|batch_state:array(\x5B\x5D, dtype=uint8)|enabled:True|wants_pause:False]*

Select the input image:ThreshBlue
Name the primary objects to be identified:Nuclei
Typical diameter of objects, in pixel units (Min,Max):5,15

Discard objects outside the diameter range?:Yes
Try to merge too small objects with nearby larger objects?:No
Discard objects touching the border of the image?:Yes
Method to distinguish clumped objects:Laplacian of Gaussian
Method to draw dividing lines between clumped objects:Propagate
Size of smoothing filter:10
Suppress local maxima that are closer than this minimum allowed distance:7.0
Speed up by using lower-resolution image to find local maxima?:Yes
Name the outline image:PrimaryDAPI
Fill holes in identified objects?:After both thresholding and declumping
Automatically calculate size of smoothing filter for declumping?:Yes
Automatically calculate minimum allowed distance between local maxima?:Yes
Retain outlines of the identified objects?:Yes
Automatically calculate the threshold using the Otsu method?:Yes
Enter Laplacian of Gaussian threshold:0.7
Automatically calculate the size of objects for the Laplacian of Gaussian filter?:Yes
Enter LoG filter diameter:5.0
Handling of objects if excessive number of objects identified:Continue
Maximum number of objects:500
Threshold setting version:1
Threshold strategy:Global
Thresholding method:Otsu
Select the smoothing method for thresholding:Automatic
Threshold smoothing scale:1.0
Threshold correction factor:1
Lower and upper bounds on threshold:0.0,1.0
Approximate fraction of image covered by objects?:0.05
Manual threshold:0.0
Select the measurement to threshold with:None
Select binary image:None
Masking objects:None
Two-class or three-class thresholding?:Two classes
Minimize the weighted variance or the entropy?:Weighted variance
Assign pixels in the middle intensity class to the foreground or the background?:Foreground
Method to calculate adaptive window size:Image size
Size of adaptive window:10

IdentifyPrimaryObjects*:[module_num:9|svn_version:\'Unknown\'|variable_revision_number:10|show_window:True|notes:\x5B\x5D|batch_state:array(\x5B\x5D, dtype=uint8)|enabled:True|wants_pause:False]*
Select the input image:ThreshRed
Name the primary objects to be identified:Ascl1
Typical diameter of objects, in pixel units (Min,Max):8,20
Discard objects outside the diameter range?:Yes
Try to merge too small objects with nearby larger objects?:No
Discard objects touching the border of the image?:Yes
Method to distinguish clumped objects:Laplacian of Gaussian
Method to draw dividing lines between clumped objects:Propagate
Size of smoothing filter:10
Suppress local maxima that are closer than this minimum allowed distance:7.0
Speed up by using lower-resolution image to find local maxima?:Yes
Name the outline image:PrimaryAscl1
Fill holes in identified objects?:After both thresholding and declumping
Automatically calculate size of smoothing filter for declumping?:Yes
Automatically calculate minimum allowed distance between local maxima?:Yes
Retain outlines of the identified objects?:Yes
Automatically calculate the threshold using the Otsu method?:No
Enter Laplacian of Gaussian threshold:0.1

Automatically calculate the size of objects for the Laplacian of Gaussian filter?:Yes
Enter LoG filter diameter:5.0
Handling of objects if excessive number of objects identified:Continue
Maximum number of objects:500
Threshold setting version:1
Threshold strategy:Adaptive
Thresholding method:Otsu
Select the smoothing method for thresholding:Automatic
Threshold smoothing scale:1.0
Threshold correction factor:1
Lower and upper bounds on threshold:0.0,1.0
Approximate fraction of image covered by objects?:0.05
Manual threshold:0.0
Select the measurement to threshold with:None
Select binary image:None
Masking objects:None
Two-class or three-class thresholding?:Two classes
Minimize the weighted variance or the entropy?:Weighted variance
Assign pixels in the middle intensity class to the foreground or the background?:Foreground
Method to calculate adaptive window size:Image size
Size of adaptive window:10

***IdentifyPrimaryObjects**:[module_num:10|svn_version:\'Unknown\'|variable_revision_number:10|show_window:True|notes:\x5B\x5D|batch_state:array(\x5B\x5D, dtype=uint8)|enabled:True|wants_pause:False]*
Select the input image:ThreshGreen
Name the primary objects to be identified:Gsx2
Typical diameter of objects, in pixel units (Min,Max):8,20
Discard objects outside the diameter range?:Yes
Try to merge too small objects with nearby larger objects?:No
Discard objects touching the border of the image?:Yes
Method to distinguish clumped objects:Laplacian of Gaussian
Method to draw dividing lines between clumped objects:Propagate
Size of smoothing filter:10
Suppress local maxima that are closer than this minimum allowed distance:7.0
Speed up by using lower-resolution image to find local maxima?:Yes
Name the outline image:PrimaryGsx2
Fill holes in identified objects?:After both thresholding and declumping
Automatically calculate size of smoothing filter for declumping?:Yes
Automatically calculate minimum allowed distance between local maxima?:Yes
Retain outlines of the identified objects?:Yes
Automatically calculate the threshold using the Otsu method?:No
Enter Laplacian of Gaussian threshold:0.1
Automatically calculate the size of objects for the Laplacian of Gaussian filter?:Yes
Enter LoG filter diameter:5.0
Handling of objects if excessive number of objects identified:Continue
Maximum number of objects:500
Threshold setting version:1
Threshold strategy:Adaptive
Thresholding method:Otsu
Select the smoothing method for thresholding:Automatic
Threshold smoothing scale:1.0
Threshold correction factor:1
Lower and upper bounds on threshold:0.0,1.0
Approximate fraction of image covered by objects?:0.05
Manual threshold:0.0
Select the measurement to threshold with:None
Select binary image:None

Masking objects:None
Two-class or three-class thresholding?:Two classes
Minimize the weighted variance or the entropy?:Weighted variance
Assign pixels in the middle intensity class to the foreground or the background?:Foreground
Method to calculate adaptive window size:Image size
Size of adaptive window:10

CalculateMath*:[module_num:11|svn_version:\'Unknown\'|variable_revision_number:2|show_window:True|notes:\x5B\x5D|batch_state:array(\x5B\x5D, dtype=uint8)|enabled:True|wants_pause:False]*
Name the output measurement:Ascl1vsDAPI
Operation:Divide
Select the numerator measurement type:Image
Select the numerator objects:Ascl1
Select the numerator measurement:Count_Ascl1
Multiply the above operand by:1.0
Raise the power of above operand by:1.0
Select the denominator measurement type:Image
Select the denominator objects:Nuclei
Select the denominator measurement:Count_Nuclei
Multiply the above operand by:1.0
Raise the power of above operand by:1.0
Take log10 of result?:No
Multiply the result by:100
Raise the power of result by:1.0
Add to the result:0.0
Constrain the result to a lower bound?:No
Enter the lower bound:0.0
Constrain the result to an upper bound?:No
Enter the upper bound:1.0

CalculateMath*:[module_num:12|svn_version:\'Unknown\'|variable_revision_number:2|show_window:True|notes:\x5B\'CalculateMath can also be used to obtain a per-image percentage of PH3-positive nuclei if ClassifyObjects is not practical to use for your assay\x3A Divide the PH3 nuclei count by the total nuclei count and multiply by 100. \'\x5D|batch_state:array(\x5B\x5D, dtype=uint8)|enabled:True|wants_pause:False]*
Name the output measurement:Gsx2vsDAPI
Operation:Divide
Select the numerator measurement type:Image
Select the numerator objects:Gsx2
Select the numerator measurement:Count_Gsx2
Multiply the above operand by:1
Raise the power of above operand by:1
Select the denominator measurement type:Image
Select the denominator objects:Nuclei
Select the denominator measurement:Count_Nuclei
Multiply the above operand by:1
Raise the power of above operand by:1
Take log10 of result?:No
Multiply the result by:100
Raise the power of result by:1
Add to the result:0
Constrain the result to a lower bound?:No
Enter the lower bound:0
Constrain the result to an upper bound?:No
Enter the upper bound:1

ExportToSpreadsheet:[module_num:13|svn_version:\'Unknown\'|variable_revision_number:11|show_window:True|notes:\x5B\'Export the per-image measurements to a comma-delimited file (.csv).\'\x5D|batch_state:array(\x5B\x5D, dtype=uint8)|enabled:True|wants_pause:False]
Select the column delimiter:Tab
Add image metadata columns to your object data file?:No
Limit output to a size that is allowed in Excel?:No
Select the measurements to export:Yes
Calculate the per-image mean values for object measurements?:No
Calculate the per-image median values for object measurements?:No
Calculate the per-image standard deviation values for object measurements?:No
Output file location:Default Input Folder sub-folder\x7CDocuments/CellProfiler Counts
Create a GenePattern GCT file?:No
Select source of sample row name:Metadata
Select the image to use as the identifier:None
Select the metadata to use as the identifier:None
Export all measurement types?:Yes
Press button to select measurements to export:Experiment\x7CModification_Timestamp,Experiment\x7CPipeline_Pipeline,Experiment\x7CRun_Timestamp,Experiment\x7CCellProfiler_Version
Representation of Nan/Inf:Null
Add a prefix to file names?:Yes
Filename prefix\x3A:Paola
Overwrite without warning?:Yes
Data to export:Image
Combine these object measurements with those of the previous object?:No
File name:Image.csv
Use the object name for the file name?:Yes

Generation of hES H9 inducible lines. For the generation of inducible hES cell lines, we first modified the commercially available pCMV-TetON-3G (Clontech) plasmid by removing the TetOn-3G cassette by digestion with EcoRI and HindIII (Biolabs). To create the inducible plasmid, we replaced the CRE cassette in a pCAG-CRE vector (Addgene) and inserted the gel-purified TetON-3G cassette, to generate a pCAG-TetON-3G vector. Then, we inserted in the pTRE3G-IRES responsive vector (Clontech) Gsx2 (in the first MCS) to create the pTRE3G-Gsx2 plasmid, Gsx2 (in the first MCS) together with Ebf1 (in the second MCS) to create the pTRE3G-Gsx2-IRES-Ebf1 plasmid, and Ebf1 alone (in the second MCS) to create the pTRE3G-IRES-Ebf1. Gsx2 cDNA was a gift from Kenneth Campbell (Cincinnati), Ebf1 cDNA was a gift from Giacomo Consalez (Milano).

hES (H9) cell line was cultured as described. 7 x10^6 cells were used for introducing the constructs by Nucleofection (Lonza) using a mouse ES cell nucleofection kit and electroporation protocol B16. 7µg of pCAG-TetON-3G in the first round and 7µg of pTRE-Gsx2 or pTRE-Gsx2-Ebf1 or pTRE-Ebf1 were used, together with 700ng of linear resistant marker (Puromycin). Cells were then plated in two Cultrex-coated 6 cm dishes with mTeSR (StemCell Technology) medium supplemented with Rock inhibitor (Y-2763221). After 72 hours antibiotics (Puromycin) were added to the medium for positive selection. Following

approximately 2 weeks in selection medium, hES cell colonies were carefully selected and expanded in Cultrex-coated 48-well plates. Clones were then expanded and tested for transgene expression after 48 hours of doxycycline treatment. During the first round, the clones were screened by transient transfections with a pTRE-Luciferase vector (Clontech), during the second round; the clones were screened by 48 hours doxycycline treatment and immunofluorescence analysis for Gsx2, Gsx2-Ebf1, and Ebf1.

Cell-Cycle Analysis with IdU and BrdU. For the assay based on IdU and BrdU administration, it was added IddU (Sigma) in the culture medium for 1 hours and 30 minutes followed by BrdU (Sigma) for 30 minutes. At the end of treatment with BrdU, the cells were fixed. For the double immunostaining for IdU and BrdU, a primary antibody mouse anti-BrdU/IdU was used, which recognizes both BrdU and IdU (clone B44, BD), and rat anti-BrdU (clone BU1/75, Abcam) which recognized only BrdU. To unmask BrdU and IdU staining after 4% PFA fixation, cells was treated with 0.2N HCl for 5 minutes at room temperature and then with 2N HCl for 20 minutes at 37°C. After 3 washes in PBS 0.1% Triton X-100 (Sigma), appropriate secondary antibodies conjugated to Alexa fluorophores 488, and 568 (Molecular Probes, Invitrogen) were diluted 1:500 in blocking solution and mixed with Hoechst 33258 (5 $\mu g\ ml^{-1}$; Molecular Probes, Invitrogen). For the estimation of cell cycle length, it was followed the paradigm described in Martynoga et al., 2005.

Cumulative BrdU Labelling. For the cumulative BrdU labelling, BrdU was added to the cell culture medium for different time windows in different wells. BrdU immunofluorescence is performed as described above for the cell-cycle analysis.

Study of Cell-Cycle Exit. As described above, hES iGOF cell lines were treated with doxycycline from day 20 to day 30 of neuronal differentiation. At day 25 cells were exposed to BrdU for 2 hours to label cells in the S-phase of the cell cycle. Neuronal differentiation was carried on until day 30, when cells were fixed and processed as described above for BrdU immunofluorescence. Cells were also stained for Ki67 to label all proliferating cells at day 30. Cell-cycle exit index was calculated by dividing the total number of $BrdU^+/Ki67^-$ cells by the total number of $BrdU^+$ cells.

Transplantations. For transplantation experiment we collaborated with professor Vercelli and his group at the Neuroscience Institute Cavalieri Ottolenghi (NICO) in Turin, and professor Moresco and her group at San Raffaele University in Milan.

Athymic NIH-FOXN1 nude rats (Charles River) of 200–250 g were lesioned with quinolinic acid (QA). For the transplantation of hES H9-derived cells, the QA lesion was induced by intrastriatal injection of 120 to 210 nmol of freshly prepared QA 7 days before cell transplantation following stereotaxic coordinates: AP= +0.5, L= +/-2.8, V= 5.0.

For the Gsx2–Ebf1 iGOF transplantation experiments the nude rats were lesioned 8 days before transplantation and the QA lesion was induced by intrastriatal injection of 210 nmol of freshly made QA in the right striatum using the following stereotaxic coordinates: AP, +0.6; L, ±2.8; V, 5.0. We injected 1 M PBS in the left striatum.

hESCs H9 and Gsx2-Ebf1 iGOF were differentiated following the protocol of Delli Carri et al., 2013, described above. The Gsx2-Ebf1 iGOF cells were treated with doxycycline from day 15 to day 20 of differentiation to induce Gsx2 and Ebf1 expression.

At day 20, both hES H9 and Gsx2-Ebf1 iGOF, the cells were detached with Accutase supplemented with N2 1:100 for 20–30 min at 37 °C. Cells were then resuspended to obtain a single cell suspension at a concentration of 50 x 10^3 cells per µL and then transplanted in complete medium by bilateral stereotaxic transplantation in lesioned adult athymic rats using the following coordinates: AP, +0.9; L, +3.1/–3.1; DV, 5.0. A total of 3 x 10^5 cells (6 µL) per injection site were delivered by a single injection. Two months after transplantation, the animals were killed, transcardially perfused, and the brains cryosectioned for immunohistochemical analyses. Animal experiments were carried out according to the National regulatory requirements and the Institutional Animal Care and Use Committee (IACUC).

mmRNA Transfections. For the preparation of mmRNA transfection mix we followed the manual of the StemMACS mRNA Reprogramming Kit (Miltenyi Biotec) using the StemMACS mRNA Transfection Reagent and StemMACS mRNA Transfection Buffer. We used 200 ng mmRNA of GSX2 and EBF1 (gently provided by Miltenyi Biotec) daily for 5 consecutive days. As a transfection control, 100ng and 200 ng of nuclear GFP (Miltenyi Biotec) were used for the preliminary experiments for the setting up of transfection condition and protocols. For the set up we also tested the *Trans*IT®-mRNA Reprogramming Kit (Mirus Company) using the *Trans*IT®-mRNA Transfection Reagent and *Trans*IT®-mRNA Transfection Buffer.

Statistical Analysis. Data represented in this thesis were analysed by PRISM software (GraphPad, version 6), for the statistical tests. Statistical significance was tested with the unpaired (nonparametric) t test as reported in each figure and legend. All results were expressed as means ± SEM for the images quantification and means ± SD for TF effect analysis.

The sample size was chosen based on our preliminary studies and on the variability across differentiations. Given that the long-term differentiation experiments (50 - 80 days) are susceptible to variability, we decided to perform five different biological experiments to address this issue. No data points were excluded from the reported analyses. Differentiation experiments were excluded when a poor neural induction was obtained (low Otx2, N-cadherin, and Pax6 expression). For the TFs analysis, the cell counting experiments were performed using specific software (CellProfiler or ITCN in ImageJ, partially automatic); therefore, they were performed blindly. The remaining cell counts were performed manually; no blinding was performed.

References

References

Agoston, D. V., Szemes, M., Dobi, A., Palkovits, M., Georgopoulos, K., Gyorgy, A., & Ring, M. A. (2007). Ikaros is expressed in developing striatal neurons and involved in enkephalinergic differentiation. *Journal of Neurochemistry*, *102*(6), 1805–1816. https://doi.org/10.1111/j.1471-4159.2007.04653.x

Alcamo, E. A., Chirivella, L., Dautzenberg, M., Dobreva, G., Fariñas, I., Grosschedl, R., & McConnell, S. K. (2008). Satb2 Regulates Callosal Projection Neuron Identity in the Developing Cerebral Cortex. *Neuron*, *57*(3), 364–377. https://doi.org/10.1016/j.neuron.2007.12.012

Altar, C. a, Cai, N., Bliven, T., Juhasz, M., Conner, J. M., Acheson, a L., Wiegand, S. J. (1997). Anterograde transport of brain-derived neurotrophic factor and its role in the brain. *Nature*, *389*(6653), 856–860. https://doi.org/10.1038/39885

Altmann, C. R., & Brivanlou, a H. (2001). Neural patterning in the vertebrate embryo. *International Review of Cytology*, *203*, 447–482. https://doi.org/10.1002/dvdy.20464

Anderson, S. A., Qiu, M., Bulfone, A., Eisenstat, D. D., Meneses, J., Pedersen, R., & Rubenstein, J. L. R. (1997). Mutations of the homeobox genes Dlx-1 and Dlx-2 disrupt the striatal subventricular zone and differentiation of late born striatal neurons. *Neuron*, *19*(1), 27–37. https://doi.org/10.1016/S0896-6273(00)80345-1

Arber, C., Precious, S. V., Cambray, S., Risner-Janiczek, J. R., Kelly, C., Noakes, Z., Li, M. (2015). Activin A directs striatal projection neuron differentiation of human pluripotent stem cells. *Development*, *142*(7), 1375–1386. https://doi.org/10.1242/dev.117093

Arlotta, P., Molyneaux, B. J., Jabaudon, D., Yoshida, Y., & Macklis, J. D. (2008). Ctip2 Controls the Differentiation of Medium Spiny Neurons and the Establishment of the Cellular Architecture of the Striatum. *Journal of Neuroscience*, *28*(3), 622–632. https://doi.org/10.1523/JNEUROSCI.2986-07.2008

Assoian, R. (2004). Stopping and Going with p27 kip1. *Developmental Cell*, 458–459. https://doi.org/10.1016/S1534-5807(04)00103-0

Aubry, L., Bugi, A., Lefort, N., Rousseau, F., Peschanski, M., & Perrier, A. L. (2008). Striatal progenitors derived from human ES cells mature into DARPP32 neurons in vitro and in quinolinic acid-lesioned rats. *Proceedings of the National Academy of Sciences of the United States of America*, *105*(43), 16707–12. https://doi.org/10.1073/pnas.0808488105

Bachoud-Levi, A. C., Deglon, N., Nguyen, J. P., Bloch, J., Bourdet, C., Winkel, L., Aebischer, P. (2000). Neuroprotective gene therapy for Huntington's disease using a polymer encapsulated BHK cell line engineered to secrete human CNTF. *Hum Gene Ther*, *11*(12), 1723–1729. https://doi.org/10.1089/10430340050111377

Bachoud-Lévi, A. C., Gaura, V., Brugières, P., Lefaucheur, J. P., Boissé, M. F., Maison, P., Peschanski, M. (2006). Effect of fetal neural transplants in patients with Huntington's disease 6 years after surgery: A long-term follow-up study. *Lancet Neurology*, *5*(4), 303–309. https://doi.org/10.1016/S1474-4422(06)70381-7

Barker, R. A., Mason, S. L., Harrower, T. P., Swain, R. A., Ho, A. K., Sahakian, B. J., Harper, R. (2013). The long-term safety and efficacy of bilateral transplantation of human fetal striatal tissue in patients with mild to moderate Huntington's disease. *Journal of Neurology, Neurosurgery & Psychiatry*, *84*(6), 657–665. https://doi.org/10.1136/jnnp-2012-302441

Bartolini, G., Ciceri, G., & Marín, O. (2013). Integration of GABAergic Interneurons into Cortical Cell Assemblies: Lessons from Embryos and Adults. *Neuron*, *79*(5), 849–864. https://doi.org/10.1016/j.neuron.2013.08.014

Bates, G. P., Dorsey, R., Gusella, J. F., Hayden, M. R., Kay, C., Leavitt, B. R., Tabrizi, S. J. (2015). Huntington disease. *Nature Reviews Disease Primers*, (April), 15005. https://doi.org/10.1038/nrdp.2015.5

Bayatti, N., Sarma, S., Shaw, C., Eyre, J. A., Vouyiouklis, D. A., Lindsay, S., & Clowry, G. J.

(2008). Progressive loss of PAX6, TBR2, NEUROD and TBR1 mRNA gradients correlates with translocation of EMX2 to the cortical plate during human cortical development. *European Journal of Neuroscience*, *28*(8), 1449–1456. https://doi.org/10.1111/j.1460-9568.2008.06475.x

Beal, M. F., Ferrante, R. J., Swartz, K. J., & Kowall, N. W. (1991). Chronic quinolinic acid lesions in rats closely resemble Huntington's disease. *The Journal of Neuroscience : The Official Journal of the Society for Neuroscience*, *11*(6), 1649–1659. https://doi.org/.

Behar, T., Ma, W., Hudson, L., & Barker, J. L. (1994). Analysis of the anatomical distribution of GAD67 mRNA encoding truncated glutamic acid decarboxylase proteins in the embryonic rat brain. *Developmental Brain Research*, *77*(1), 77–87. https://doi.org/10.1016/0165-3806(94)90215-1

Besson, A., Gurian-West, M., Chen, X., Kelly-Spratt, K. S., Kemp, C. J., & Roberts, J. M. (2006). A pathway in quiescent cells that controls p27Kip1 stability, subcellular localization, and tumor suppression. *Genes and Development*, *20*(1), 47–64. https://doi.org/10.1101/gad.1384406

Besson, A., Gurian-West, M., Schmidt, A., Hall, A., & Roberts, J. M. (2004). activation p27 Kip1 modulates cell migration through the regulation of RhoA activation. *Genes & Development*, *18*(8), 862–876. https://doi.org/10.1101/gad.1185504

Boehm, M., Yoshimoto, T., Crook, M. F., Nallamshetty, S., True, A., Nabel, G. J., & Nabel, E. G. (2002). A growth factor-dependent nuclear kinase phosphorylates p27(Kip1) and regulates cell cycle progression. *The EMBO Journal*, *21*(13), 3390–3401. https://doi.org/10.1093/emboj/cdf343

Briscoe, J., & Ericson, J. (2001). Specification of neuronal fates in the ventral neural tube. *Current Opinion in Neurobiology*, *11*(1), 43–49. https://doi.org/10.1016/S0959-4388(00)00172-0

Bulfone, a, Puelles, L., Porteus, M. H., Frohman, M. a, Martin, G. R., & Rubenstein, J. L. (1993). Spatially restricted expression of Dlx-1, Dlx-2 (Tes-1), Gbx-2, and Wnt-3 in the embryonic day 12.5 mouse forebrain defines potential transverse and longitudinal segmental boundaries. *The Journal of Neuroscience : The Official Journal of the Society for Neuroscience*, *13*(7), 3155–3172. https://doi.org/10.1523/jneurosci.2750-07.2007

Campbell, K., Olsson, M., & Björklund, A. (1995). Regional incorporation and site-specific differentiation of striatal precursors transplanted to the embryonic forebrain ventricle. *Neuron*, *15*(6), 1259–1273. https://doi.org/10.1016/0896-6273(95)90006-3

Canals, J. M. (2004). Brain-Derived Neurotrophic Factor Regulates the Onset and Severity of Motor Dysfunction Associated with Enkephalinergic Neuronal Degeneration in Huntington's Disease. *Journal of Neuroscience*, *24*(35), 7727–7739. https://doi.org/10.1523/JNEUROSCI.1197-04.2004

Casarosa, S., Fode, C., & Guillemot, F. (1999). Mash1 regulates neurogenesis in the ventral telencephalon. *Development (Cambridge, England)*, *126*, 525–534. https://doi.org/10.1371/journal.pcbi.0020117

Cattaneo, E., Rigamonti, D., Goffredo, D., Zuccato, C., & Sipione, S. (2001). Loss of normal huntingtin function : new developments in Huntington ' s disease research. *Trends in Neurosciences*, *24*(3), 182–188.

Chambers, S. M., Fasano, C. A., Papapetrou, E. P., Tomishima, M., Sadelain, M., & Studer, L. (2009). Highly efficient neural conversion of human ES and iPS cells by dual inhibition of SMAD signaling. *Nature Biotechnology*, *27*(3), 275–280. https://doi.org/10.1038/nbt.1529

Chiang, C., Litingtung, Y., Lee, E., Young, K. E., Corden, J. L., Westphal, H., & Beachy, P. A. (1996). Cyclopia and defective axial patterning in mice lacking Sonic hedgehog gene function. *Nature*, *383*(6599), 407–413. https://doi.org/10.1038/383407a0

Cobos, I., Shimamura, K., Rubenstein, J. L. R., Martínez, S., & Puelles, L. (2001). Fate Map of the Avian Anterior Forebrain at the Four-Somite Stage, Based on the Analysis of Quail–Chick Chimeras. *Developmental Biology*, *239*(1), 46–67. https://doi.org/10.1006/dbio.2001.0423

Copp, A. J., Greene, N. D. E., & Murdoch, J. N. (2003). The genetic basis of mammalian

neurulation. *Nature Reviews Genetics*, *4*(10), 784–793. https://doi.org/10.1038/nrg1181

Corbin, J. G., Gaiano, N., Machold, R. P., Langston, A., & Fishell, G. (2000). The Gsh2 homeodomain gene controls multiple aspects of telencephalic development. *Development (Cambridge, England)*, *127*(23), 5007–5020.

Cox, W. G., & Hemmati-Brivanlou, A. (1995). Caudalization of neural fate by tissue recombination and bFGF. *Development*, *121*, 4349–4358.

Crook, Z. R., & Housman, D. (2011). Huntington's Disease: Can Mice Lead the Way to Treatment? *Neuron*, *69*(3), 423–435. https://doi.org/10.1016/j.neuron.2010.12.035

Crossley, P. H., Martinez, S., Ohkubo, Y., & Rubenstein, J. L. R. (2001). Coordinate expression of Fgf8, Otx2, Bmp4, and Shh in the rostral prosencephalon during development of the telencephalic and optic vesicles. *Neuroscience*, *108*(2), 183–206. https://doi.org/10.1016/S0306-4522(01)00411-0

Cudkowicz, M., & Kowall, N. W. (1990). Degeneration of pyramidal projection neurons in Huntingtons-disease cortex. *Annals of Neurology*, *27*(2), 200–204. https://doi.org/10.1002/ana.410270217

Cunningham, J. J., Levine, E. M., Zindy, F., Goloubeva, O., Roussel, M. F., & Smeyne, R. J. (2002). The Cyclin-Dependent Kinase Inhibitors p19Ink4d and p27Kip1 Are Coexpressed in Select Retinal Cells and Act Cooperatively to Control Cell Cycle Exit. *Molecular and Cellular Neuroscience*, *19*(3), 359–374. https://doi.org/10.1006/mcne.2001.1090

Dalton, S. (2013). G1 compartmentalization and cell fate coordination. *Cell*, *155*(1), 13–14. https://doi.org/10.1016/j.cell.2013.09.015

Danjo, T., Eiraku, M., Muguruma, K., Watanabe, K., Kawada, M., Yanagawa, Y., Sasai, Y. (2011). Subregional Specification of Embryonic Stem Cell-Derived Ventral Telencephalic Tissues by Timed and Combinatory Treatment with Extrinsic Signals. *Journal of Neuroscience*, *31*(5), 1919–1933. https://doi.org/10.1523/JNEUROSCI.5128-10.2011

Deacon, T. W., Pakzaban, P., & Isacson, O. (1994). The lateral ganglionic eminence is the origin of cells committed to striatal phenotypes: neural transplantation and developmental evidence. *Brain Research*, *668*(1–2), 211–219. https://doi.org/10.1016/0006-8993(94)90526-6

Delli Carri, A., Onorati, M., Lelos, M. J., Castiglioni, V., Faedo, A., Menon, R., Cattaneo, E. (2013). Developmentally coordinated extrinsic signals drive human pluripotent stem cell differentiation toward authentic DARPP-32+ medium-sized spiny neurons. *Development*, *140*(2), 301–312. https://doi.org/10.1242/dev.084608

Deng, Y. P., Albin, R. L., Penney, J. B., Young, A. B., Anderson, K. D., & Reiner, A. (2004). Differential loss of striatal projection systems in Huntington's disease: A quantitative immunohistochemical study. *Journal of Chemical Neuroanatomy*, *27*(3), 143–164. https://doi.org/10.1016/j.jchemneu.2004.02.005

Doetsch, F., Verdugo, J. M.-G., Caille, I., Alvarez-Buylla, A., Chao, M. V, & Casaccia-Bonnefil, P. (2002). Lack of the cell-cycle inhibitor p27Kip1 results in selective increase of transit-amplifying cells for adult neurogenesis. *The Journal of Neuroscience : The Official Journal of the Society for Neuroscience*, *22*(6), 2255–64. https://doi.org/22/6/2255

Doniach, T. (1993). Planar and vertical induction of anteroposterior pattern during the development of the amphibian central nervous system. *Journal of Neurobiology*, *24*(10), 1256–1275. https://doi.org/10.1002/neu.480241003

Ehrlich, M. E. (2012). Huntington's Disease and the Striatal Medium Spiny Neuron: Cell-Autonomous and Non-Cell-Autonomous Mechanisms of Disease. *Neurotherapeutics*, *9*(2), 270–284. https://doi.org/10.1007/s13311-012-0112-2

Eisenstat, D. D., Liu, J. K., Mione, M., Zhong, W., Yu, G., Anderson, S. A., Rubenstein, J. L. R. (1999). DLX-1, DLX-2, and DLX-5 expression define distinct stages of basal forebrain differentiation. *Journal of Comparative Neurology*, *414*(2), 217–237. https://doi.org/10.1002/(SICI)1096-9861(19991115)414:2<217::AID-CNE6>3.0.CO;2-I

Elango, N., Elango, S., Shivshankar, P., & Katz, M. S. (2005). Optimized transfection of mRNA

transcribed from a d(A/T)100tail-containing vector. *Biochemical and Biophysical Research Communications*, *330*(3), 958–966. https://doi.org/10.1016/j.bbrc.2005.03.067

Elias, L. A. B., Potter, G. B., & Kriegstein, A. R. (2009). NIH Public Access, *59*(5), 679–682. https://doi.org/10.1016/j.neuron.2008.08.017.A

Evans, A. E., Kelly, C. M., Precious, S. V., & Rosser, A. E. (2012). Molecular Regulation of Striatal Development: A Review. *Anatomy Research International*, *2012*, 1–14. https://doi.org/10.1155/2012/106529

Faedo, A., Laporta, A., Segnali, A., Galimberti, M., Besusso, D., Cesana, E., Cattaneo, E. (2017). Differentiation of human telencephalic progenitor cells into MSNs by inducible expression of Gsx2 and Ebf1. *Proceedings of the National Academy of Sciences of the United States of America*, *114*(7). https://doi.org/10.1073/pnas.1611473114

Feinberg, T. E., & Mallatt, J. (2013). The evolutionary and genetic origins of consciousness in the cambrian period over 500 million years ago. *Frontiers in Psychology*, *4*(OCT), 1–27. https://doi.org/10.3389/fpsyg.2013.00667

Fero, M. L., Rivkin, M., Tasch, M., Porter, P., Carow, C. E., Firpo, E., Roberts, J. M. (1996). A syndrome of multiorgan hyperplasia with features of gigantism, tumorigenesis, and female sterility in p27Kip1-deficient Mice. *Cell*, *85*(5), 733–744. https://doi.org/10.1016/S0092-8674(00)81239-8

Fjodorova, M., Noakes, Z., & Li, M. (2015). How to make striatal projection neurons. *Neurogenesis*, *2*(1), 1–6. https://doi.org/10.1080/23262133.2015.1100227

Fukuchi-Shimogori, T. (2001). Neocortex Patterning by the Secreted Signaling Molecule FGF8. *Science*, *294*(5544), 1071–1074. https://doi.org/10.1126/science.1064252

Furuta, Y., & Hogan, B. L. M. (1998). BMP4 is essential for lens induction in the mouse embryo. *Genes and Development*, *12*(23), 3764–3775. https://doi.org/10.1101/gad.12.23.3764

Fusco, F. R., Zuccato, C., Tartari, M., Martorana, A., De March, Z., Giampà, C., Bernardi, G. (2003). Co-localization of brain-derived neurotrophic factor (BDNF) and wild-type huntingtin in normal and quinolinic acid-lesioned rat brain. *European Journal of Neuroscience*, *18*(5), 1093–1102. https://doi.org/10.1046/j.1460-9568.2003.02844.x

Galderisi, U., Jori, F. P., & Giordano, A. (2003). Cell cycle regulation and neural differentiation. *Oncogene*, *22*(33), 5208–5219. https://doi.org/10.1038/sj.onc.1206558

Garcia-Calero, E., Bahamonde, O., & Martinez, S. (2013). Differences in number and distribution of striatal calbindin medium spiny neurons between a vocal-learner (Melopsittacus undulatus) and a non-vocal learner bird (Colinus virginianus). *Frontiers in Neuroanatomy*, *7*(December), 46. https://doi.org/10.3389/fnana.2013.00046

Garcia-Dominguez, M. (2003). Ebf gene function is required for coupling neuronal differentiation and cell cycle exit. *Development*, *130*(24), 6013–6025. https://doi.org/10.1242/dev.00840

Garel, S., Marín, F., Grosschedl, R., & Charnay, P. (1999). Ebf1 controls early cell differentiation in the embryonic striatum. *Development (Cambridge, England)*, *126*, 5285–5294. https://doi.org/5285-5294

Gauthier, L. R., Charrin, B. C., Borrell-Pagès, M., Dompierre, J. P., Rangone, H., Cordelières, F. P., Saudou, F. (2004). Huntingtin controls neurotrophic support and survival of neurons by enhancing BDNF vesicular transport along microtubules. *Cell*, *118*(1), 127–138. https://doi.org/10.1016/j.cell.2004.06.018

Gerfen, C. R. (2000). Molecular effects of dopamine on striatal-projection pathways. *Trends in Neurosciences*, *23*, S64–S70. https://doi.org/10.1016/S1471-1931(00)00019-7

Gerfen, C. R., Engber, T. M., Mahan, L. C., Susel, Z., Chase, T. N., Monsma, F. J., & Sibley, D. R. (1990). D1 and D2 dopamine receptor regulated gene expression of striatonigral and striatopallidal neurons. *Science*, *250*(1986), 1429–1432. https://doi.org/10.1126/science.2147780

Ghanem, N., Jarinova, O., Amores, A., Long, Q., Hatch, G., Park, B. K., … Ekker, M. (2003). Regulatory roles of conserved intergenic domains in vertebrate Dlx bigene clusters. *Genome*

Research, *13*(4), 533–543. https://doi.org/10.1101/gr.716103

Goto, A., Niki, T., Moriyama, S., Funata, N., Moriyama, H., Nishimura, Y., … Fukayama, M. (2004). Immunohistochemical study of Skp2 and Jab1, two key molecules in the degradation of P27, in lung adenocarcinoma. *Pathology International*, *54*(9), 675–681. https://doi.org/10.1111/j.1440-1827.2004.01679.x

Greenberg, Z., Ramshaw, H., & Schwarz, Q. (2015). Time Windows of Interneuron Development: Implications to Our Understanding of the Aetiology and Treatment of Schizophrenia. *Neuroscience 2015, Vol. 2, Pages 294-321*, *2*(September), 294–321. https://doi.org/10.3934/Neuroscience.2015.4.294

Greene, N. D. E., Stanier, P., & Copp, A. J. (2009). Genetics of human neural tube defects. *Human Molecular Genetics*, *18*(R2). https://doi.org/10.1093/hmg/ddp347

Guillemot, F. (2005). Cellular and molecular control of neurogenesis in the mammalian telencephalon. *Current Opinion in Cell Biology*, *17*(6), 639–647. https://doi.org/10.1016/j.ceb.2005.09.006

Guillemot, F., Lo, L.-C., Johnson, J. E., Auerbach, A., Anderson, D. J., & Joyner, A. L. (1993). Mammalian achaete-scute homolog 1 is required for the early develoment of olfactory and autonomic neurons. *Cell*, *75*, 463–476.

Han, I., YiMel, Y., Kordower, J. H., Brady, S. T., & Morfini, G. A. (2010). Differential vulnerability of neurons in Huntington's disease. *J Neurochem*, *113*(5), 1073–1091. https://doi.org/10.1111/j.1471-4159.2010.06672.x.Differential

Hébert, J. M., & Fishell, G. (2008). NIH Public Access. *Nature Reviews Neuroscience*, *9*(9), 678–685. https://doi.org/10.1038/nrn2463.The

Hébert, J. M., & McConnell, S. K. (2000). Targeting of cre to the Foxg1 (BF-1) Locus Mediates loxP Recombination in the Telencephalon and Other Developing Head Structures. *Developmental Biology*, *222*(2), 296–306. https://doi.org/10.1006/dbio.2000.9732

Hedreen, J. C., Peyser, C. E., Folstein, S. E., & Ross, C. A. (1991). Neuronal loss in layers V and VI of cerebral cortex in Huntington's disease. *Neuroscience Letters*, *133*(2), 257–261. https://doi.org/10.1016/0304-3940(91)90583-F

Hemmati-Brivanlou, a, & Melton, D. (1997). Vertebrate neural induction. *Annual Review of Neuroscience*, *20*, 43–60. https://doi.org/10.1146/annurev.neuro.20.1.43

Herkenham, M., Edley, S. M., & Stuart, J. (1984). Cell clusters in the nucleus accumbens of the rat, and the mosaic relationship of opiate receptors, acetylcholinesterase and subcortical afferent terminations. *Neuroscience*, *11*(3), 561–593. https://doi.org/10.1016/0306-4522(84)90045-9

Hisaoka, T., Nakamura, Y., Senba, E., & Morikawa, Y. (2010). The forkhead transcription factors, Foxp1 and Foxp2, identify different subpopulations of projection neurons in the mouse cerebral cortex. *Neuroscience*, *166*(2), 551–563. https://doi.org/10.1016/j.neuroscience.2009.12.055

Hoch, R. V., Lindtner, S., Price, J. D., & Rubenstein, J. L. R. (2015). OTX2 Transcription Factor Controls Regional Patterning within the Medial Ganglionic Eminence and Regional Identity of the Septum. *Cell Reports*, *12*(3), 482–494. https://doi.org/10.1016/j.celrep.2015.06.043

Hogan, B. L., Robertson, E. J., Hynes, M., Qiu, M., Shimamura, K., Sussel, L., Rubenstein, J. L. R. (1995). Control of anteroposterior and dorsoventral domains of Nkx-6.1 gene expression relative to other Nkx genes during vertebrate CNS development. *Mechanisms of Development*, *72*(1), 71–83. https://doi.org/10.1016/S0925-4773(98)00018-5

Hoshaw, B. A., Malberg, J. E., & Lucki, I. (2005). Central administration of IGF-I and BDNF leads to long-lasting antidepressant-like effects. *Brain Research*, *1037*(1–2), 204–208. https://doi.org/10.1016/j.brainres.2005.01.007

Houart, C., Caneparo, L., Heisenberg, C. P., Barth, K. A., Take-Uchi, M., & Wilson, S. W. (2002). Establishment of the telencephalon during gastrulation by local antagonism of Wnt signaling. *Neuron*, *35*(2), 255–265. https://doi.org/10.1016/S0896-6273(02)00751-1

Inoue, T., Nakamura, S., & Osumi, N. (2000). Fate Mapping of the Mouse Prosencephalic Neural

Plate. *Developmental Biology*, *219*(2), 373–383. https://doi.org/10.1006/dbio.2000.9616

Jain, M., Armstrong, R. J. E., Barker, R. A., & Rosser, A. E. (2001). Cellular and molecular aspects of striatal development. *Brain Research Bulletin*, *55*(4), 533–540. https://doi.org/10.1016/S0361-9230(01)00555-X

Jessell, T. M. (2000). Neuronal specification in the spinal cord: inductive signals and transcriptional codes. *Nature Reviews Genetics*, *1*(1), 20–29. https://doi.org/10.1038/35049541

Kanatani, S., Yozu, M., Tabata, H., & Nakajima, K. (2008). COUP-TFII Is Preferentially Expressed in the Caudal Ganglionic Eminence and Is Involved in the Caudal Migratory Stream. *Journal of Neuroscience*, *28*(50), 13582–13591. https://doi.org/10.1523/JNEUROSCI.2132-08.2008

Kawaguchi, Y., Wilson, C. J., Augood, S. J., & Emson, P. C. (1995). Striatal Interneurons - Chemical, Physiological and Morphological Characterization. *Trends in Neurosciences*, *18*(12), 527–535. https://doi.org/10.1016/0166-2236(95)98374-8

Kepecs, A., & Fishell, G. (2014). Interneuron cell types are fit to function. *Nature*, *505*(7483), 318–326. https://doi.org/10.1038/nature12983

Kim, a S., Anderson, S. a, Rubenstein, J. L., Lowenstein, D. H., & Pleasure, S. J. (2001). Pax-6 regulates expression of SFRP-2 and Wnt-7b in the developing CNS. *The Journal of Neuroscience : The Official Journal of the Society for Neuroscience*, *21*(5), RC132. https://doi.org/20015023 [pii]

Kreitzer, A. C. (2009). Physiology and Pharmacology of Striatal Neurons. *Annual Review of Neuroscience*, *32*(1), 127–147. https://doi.org/10.1146/annurev.neuro.051508.135422

Krushel, L. A., Connolly, J. A., & van der Kooy, D. (1989). Pattern formation in the mammalian forebrain: patch neurons from the rat striatum selectively reassociate in vitro. *Developmental Brain Research*, *47*(1), 137–142. https://doi.org/10.1016/0165-3806(89)90116-8

Krushel, L. A., Fishell, G., & van der Kooy, D. (1995). Pattern Formation in the Mammalian Forebrain: Striatal Patch and Matrix Neurons Intermix Prior to Compartment Formation. *European Journal of Neuroscience*, *7*(6), 1210–1219. https://doi.org/10.1111/j.1460-9568.1995.tb01111.x

Lamb, T. M., & Harland, R. M. (1995). Fibroblast growth factor is a direct neural inducer, which combined with noggin generates anterior-posterior neural pattern. *Development (Cambridge, England)*, *121*(1995), 3627–3636. https://doi.org/10.1158/1078-0432.CCR-10-2050

Lanciego, J. L., Luquin, N., & Obeso, J. A. (2012). Functional neuroanatomy of the basal ganglia. *Cold Spring Harbor Perspectives in Medicine*, *2*(12), 1–20. https://doi.org/10.1101/cshperspect.a009621

Lee, J.-H., Nikolict, M., Baptista, C. A., Eseng Lai, L.-H. T., & Massaguei, A. J. (1996). The brain-specific activator p35 allows Cdk5 to escape inhibition by p27Kipl in neurons. *Nature*, *93*(April), 3259–3263.

Li, H., Zeitler, P. S., Valerius, M. T., Small, K., & Potter, S. S. (1996). Gsh-1, an orphan Hox gene, is required for normal pituitary development. *The EMBO Journal*, *15*(4), 714–24.

Lin, P.-Y., & Tseng, P.-T. (2015). Decreased glial cell line-derived neurotrophic factor levels in patients with depression: A meta-analytic study. *Journal of Psychiatric Research*, *63*, 20–27. https://doi.org/10.1016/j.jpsychires.2015.02.004

Liu, J. K., Ghattas, I., Shiying, L., Sandy, C., and J Rubenstein, J. L. R. (1997). Dlx Genes Encode DNA-Binding Proteins That Are Expressed in an Overlapping And Sequential Pattern During Basal Ganglia Differentiation. *Developmental Dynamics*, *512*, 498–512.

Lo, L. C., Johnson, J. E., Wuenschell, C. W., Saito, T., & Anderson, D. J. (1991). Mammalian achaete-scute homolog 1 is transiently expressed by spatially restricted subsets of early neuroepithelial and neural crest cells. *Genes and Development*, *5*(9), 1524–1537. https://doi.org/10.1101/gad.5.9.1524

Lobo, M. K., Yeh, C., & Yang, X. W. (2008). Pivotal role of early B-cell factor 1 in development of striatonigral medium spiny neurons in the matrix compartment. *Journal of Neuroscience Research*, *86*(10), 2134–2146. https://doi.org/10.1002/jnr.21666

Long, J. E., Garel, S., Alvarez-Dolado, M., Yoshikawa, K., Osumi, N., Alvarez-Buylla, A., & Rubenstein, J. L. R. (2007). Dlx-Dependent and -Independent Regulation of Olfactory Bulb Interneuron Differentiation. *Journal of Neuroscience*, *27*(12), 3230–3243. https://doi.org/10.1523/JNEUROSCI.5265-06.2007

Long, J. E., Swan, C., Liang, W. S., Cobos, I., Potter, G. B., & Rubenstein, J. L. R. (2009). Dlx1&2 and Mash1 transcription factors control striatal patterning and differentiation through parallel and overlapping pathways. *Journal of Comparative Neurology*, *512*(4), 556–572. https://doi.org/10.1002/cne.21854

Lumsden, A., & Krumlauf, R. (1996). Patterning the Vertebrate Neuraxis. *Science*, *274*(5290), 1109–1115. https://doi.org/10.1126/science.274.5290.1109

Lupo, G., Harris, W. A., & Lewis, K. E. (2006). Mechanisms of ventral patterning in the vertebrate nervous system. *Nature Reviews. Neuroscience*, *7*(2), 103–114. https://doi.org/10.1038/nrn1843

Ma, L., Hu, B., Liu, Y., Vermilyea, S. C., Liu, H., Gao, L., Zhang, S. C. (2012). Human embryonic stem cell-derived GABA neurons correct locomotion deficits in quinolinic acid-lesioned mice. *Cell Stem Cell*, *10*(4), 455–464. https://doi.org/10.1016/j.stem.2012.01.021

Manuel, M., & Price, D. J. (2005). Role of Pax6 in forebrain regionalization. *Brain Research Bulletin*, *66*(4–6), 387–393. https://doi.org/10.1016/j.brainresbull.2005.02.006

Marin, O., Anderson, S. a, & Rubenstein, J. L. (2000). Origin and molecular specification of striatal interneurons. *The Journal of Neuroscience : The Official Journal of the Society for Neuroscience*, *20*(16), 6063–6076. https://doi.org/10934256

Martín-Ibáñez, R., Crespo, E., Urbán, N., Sergent-Tanguy, S., Herranz, C., Jaumot, M., Canals, J. M. (2010). Ikaros-1 couples cell cycle arrest of late striatal precursors with neurogenesis of enkephalinergic neurons. *Journal of Comparative Neurology*, *518*(3), 329–351. https://doi.org/10.1002/cne.22215

Mattis, V. B., Tom, C., Akimov, S., Saeedian, J., ??stergaard, M. E., Southwell, A. L., Svendsen, C. N. (2015). HD iPSC-derived neural progenitors accumulate in culture and are susceptible to BDNF withdrawal due to glutamate toxicity. *Human Molecular Genetics*, *24*(11), 3257–3271. https://doi.org/10.1093/hmg/ddv080

McAllister, S. S., Becker-Hapak, M., Pintucci, G., Pagano, M., & Dowdy, S. F. (2003). Novel p27(kip1) C-terminal scatter domain mediates Rac-dependent cell migration independent of cell cycle arrest functions. *Molecular and Cellular Biology*, *23*(1), 216–28. https://doi.org/10.1128/MCB.23.1.216

Méndez-Gómez, H. R., & Vicario-Abejón, C. (2012). The homeobox gene Gsx2 regulates the self-renewal and differentiation of neural stem cells and the cell fate of postnatal progenitors. *PLoS ONE*, *7*(1). https://doi.org/10.1371/journal.pone.0029799

Molyneaux, B. J., Arlotta, P., Menezes, J. R. L., & Macklis, J. D. (2007). Neuronal subtype specification in the cerebral cortex. *Nature Reviews Neuroscience*, *8*(6), 427–437. https://doi.org/10.1038/nrn2151

Muzio, L., DiBenedetto, B., Stoykova, A., Boncinelli, E., Gruss, P., & Mallamaci, A. (2002). Conversion of cerebral cortex into basal ganglia in Emx2(-/-) Pax6(Sey/Sey) double-mutant mice. *Nature Neuroscience*, *5*(12), 737–745. https://doi.org/10.1038/nn892

Nery, S., Fishell, G., & Corbin, J. G. (2002). The caudal ganglionic eminence is a source of distinct cortical and subcortical cell populations. *Nature Neuroscience*, *5*(12), 1279–1287. https://doi.org/10.1038/nn971

Nguyen, L., Besson, A., Heng, J. I., Schuurmans, C., Teboul, L., Parras, C., Guillemot, F. (2006). Differentiation and Migration in the Cerebral Cortex. *Genes and Development*, 1511–1524. https://doi.org/10.1101/gad.377106.Cyclin-dependent

Nicoleau, C., Varela, C., Bonnefond, C., Maury, Y., Bugi, A., Aubry, L., Perrier, A. L. (2013). Embryonic stem cells neural differentiation qualifies the role of Wnt/Catenin signals in human telencephalic specification and regionalization. *Stem Cells*, *31*(9), 1763–1774.

https://doi.org/10.1002/stem.1462

Nural, H. F., & Mastick, G. S. (2004). Pax6 guides a relay of pioneer longitudinal axons in the embryonic mouse forebrain. *Journal of Comparative Neurology*, *479*(4), 399–409. https://doi.org/10.1002/cne.20317

Ohkubo, Y., Chiang, C., & Rubenstein, J. L. R. (2002). Coordinate regulation and synergistic actions of BMP4, SHH and FGF8 in the rostral prosencephalon regulate morphogenesis of the telencephalic and optic vesicles. *Neuroscience*, *111*(1), 1–17. https://doi.org/10.1016/S0306-4522(01)00616-9

Onorati, M., Castiglioni, V., Biasci, D., Cesana, E., Menon, R., Vuono, R., Cattaneo, E. (2014). Molecular and functional definition of the developing human striatum. *Nature Neuroscience*, *17*(12), 1804–1815. https://doi.org/10.1038/nn.3860

Panganiban, G., & Rubenstein, J. L. R. (2002). Developmental functions of the Distal-less/Dlx homeobox genes. *Development (Cambridge, England)*, *129*(19), 4371–86. https://doi.org/10.1016/s0361-9230(01)00770-5

Pauklin, S., & Vallier, L. (2014). The cell-cycle state of stem cells determines cell fate propensity (Cell (2013) 155 (135-147)). *Cell*, *156*(6), 1338. https://doi.org/10.1016/j.cell.2014.02.044

Pearson, J. C., Lemons, D., & McGinnis, W. (2005). Modulating Hox gene functions during animal body patterning. *Nature Reviews Genetics*, *6*(12), 893–904. https://doi.org/10.1038/nrg1726

Petryniak, M. A., Potter, G. B., Rowitch, D. H., & Rubenstein, J. L. R. (2007). Dlx1 and Dlx2 Control Neuronal versus Oligodendroglial Cell Fate Acquisition in the Developing Forebrain. *Neuron*, *55*(3), 417–433. https://doi.org/10.1016/j.neuron.2007.06.036

Pombero, A., & Martinez, S. (2009). Telencephalic morphogenesis during the process of neurulation: An experimental study using quail-chick chimeras. *Journal of Comparative Neurology*, *512*(6), 784–797. https://doi.org/10.1002/cne.21933

Puelles, L., Kuwana, E., Puelles, E., Bulfone, A., Shimamura, K., Keleher, J., Rubenstein, J. L. R. (2000). Pallial and subpallial derivatives in the embryonic chick and mouse telencephalon, traced by the expression of the genes Dlx-2, Emx-1, Nkx-2.1, Pax-6, and Tbr-1. *Journal of Comparative Neurology*, *424*(3), 409–438. https://doi.org/10.1002/1096-9861(20000828)424:3<409::AID-CNE3>3.0.CO;2-7

Puelles, L., & Rubenstein, J. L. R. (1993). Expression patterns of homeobox and other putatuve regulatory genes in the embryonic mouse forebrain suggest a neuromeric organization. *Trends Neurosci.*, *16*(11), 472–479.

Reddington, A. E., Rosser, A. E., & Dunnett, S. B. (2014). Differentiation of pluripotent stem cells into striatal projection neurons: a pure MSN fate may not be sufficient. *Frontiers in Cellular Neuroscience*, *8*(December), 398. https://doi.org/10.3389/fncel.2014.00398

Reiner, A., Albin, R. L., Anderson, K. D., D'Amato, C. J., Penney, J. B., & Young, A. B. (1988). Differential loss of striatal projection neurons in Huntington disease. *Proceedings of the National Academy of Sciences*, *85*(15), 5733–5737. https://doi.org/10.1073/pnas.85.15.5733

Reynisdóttir, I., & Massagué, J. (1997). The subcellular locations of pl5(Ink4b) and p27(Kip1) coordinate their inhibitory interactions with cdk4 and cdk2. *Genes and Development*, *11*(4), 492–503. https://doi.org/10.1101/gad.11.4.492

Rink, E., & Wullimann, M. F. (2002). Connections of the ventral telencephalon and tyrosine hydroxylase distribution in the zebrafish brain (Danio rerio) lead to identification of an ascending dopaminergic system in a teleost. *Brain Research Bulletin*, *57*(3–4), 385–387. https://doi.org/10.1016/S0361-9230(01)00696-7

Rosas, H. D., Hevelone, N. D., Zaleta, A. K., Greve, D. N., Salat, D. H., & Fischl, B. (2005). Regional cortical thinning in preclinical Huntington disease and its relationship to cognition. *Neurology*, *65*(5), 745–747. https://doi.org/10.1212/01.wnl.0000174432.87383.87

Ross, C. A., & Tabrizi, S. J. (2011). Huntington ' s disease : from molecular pathogenesis to clinical treatment. *The Lancet Neurology*, *10*(1), 83–98. https://doi.org/10.1016/S1474-4422(10)70245-3

Rowitch, D. H., & Kriegstein, A. R. (2010). Developmental genetics of vertebrate glial–cell specification. *Nature*, *468*(7321), 214–222. https://doi.org/10.1038/nature09611

Rubenstein, J. L., Martinez, S., Shimamura, K., & Puelles, L. (1994). The embryonic vertebrate forebrain: the prosomeric model. *Science (New York, N.Y.)*, *266*(5185), 578–80. https://doi.org/10.1126/science.7939711

Rubenstein, J. L. R., Shimamura, K., Martinez, S., Puelles, L., Kohtz, J. D., Baker, D. P., Cattaneo, E. (1998). Pattern formation in the striatum: devlopmental changes in the distribution of striatonigral projections. *Nature Reviews Neuroscience*, *2*(1), 239–255. https://doi.org/10.1101/cshperspect.a009621

Ruiz, M., & Déglon, N. (2012). Viral-mediated overexpression of mutant huntingtin to model HD in various species. *Neurobiology of Disease*, *48*(2), 202–211. https://doi.org/10.1016/j.nbd.2011.08.023

Ruiz I Altaba, A., Nguyên, V., & Palma, V. (2003). The emergent design of the neural tube: Prepattern, SHH morphogen and GLI code. *Current Opinion in Genetics and Development*, *13*(5), 513–521. https://doi.org/10.1016/j.gde.2003.08.005

Sakaue-Sawano, A., Kurokawa, H., Morimura, T., Hanyu, A., Hama, H., Osawa, H., … Miyawaki, A. (2008). Visualizing Spatiotemporal Dynamics of Multicellular Cell-Cycle Progression. *Cell*, *132*(3), 487–498. https://doi.org/10.1016/j.cell.2007.12.033

Sanes, D. H., Reh, T. A., & Harris, W. A. (William A. (2006). *Development of the nervous system*.

Schoenwolf, G. C., & Nichols, D. H. (1984). Histological and ultrastructural studies on the origin of caudal neural crest cells in mouse embryos. *J Comp Neurol*, *222*(4), 496–505. https://doi.org/10.1002/cne.902220404

Schoenwolf, G. C., & Smith, J. L. (1990). Mechanisms of neurulation: traditional viewpoint and recent advances. *Development (Cambridge, England)*, *109*(2), 243–270. Retrieved from http://www.ncbi.nlm.nih.gov/pubmed/2205465

Schwarcz, R., Whetsell, W., & Mangano, R. (1986). Quinolinic Acid: An Endogenous Metabolite That Produces Axon-Sparing Lesions in Rat Brain. *Science*, *219*(50).

Sherr, C. J., & Roberts, J. M. (1995). Inhibitors of mammalian cyclin-dependent kinases. *Genes & Development*, 1149–1163. https://doi.org/10.1101/gad.9.10.1149

Shimamura, K., Hartigan, D. J., Martinez, S., Puelles, L., & Rubenstein, J. L. (1995). Longitudinal organization of the anterior neural plate and neural tube. *Development*, *121*(12), 3923–3933. https://doi.org/8575293

Shimamura, K., Rubenstein, J. L., Shimamura J L, K. A. U. R., Shimamura, K., & Rubenstein, J. L. (1997). Inductive interactions direct early regionalization of the mouse forebrain. *Development (Cambridge, England)*, *124*(14), 2709–2718. https://doi.org/10.1016/0092-8674(93)90249-p

Simeone, A., Avantaggiatoa, V., Cristina, M., Mavilio, F., Arrac, C., Cotellid, F., Acamporaa, D. (1995). Retinoic acid induces stage-specific antero-posterior transformation of rostra1 central nervous system. *Mechanisms of Development*, *51*, 83–98.

Song, D. D., & Harlan, R. E. (1994). Genesis and migration patterns of neurons forming the patch and matrix compartments of the rat striatum. *Developmental Brain Research*, *83*(2), 233–245. https://doi.org/10.1016/0165-3806(94)00144-8

Stenman, J., Toresson, H., & Campbell, K. (2003). Identification of two distinct progenitor populations in the lateral ganglionic eminence: implications for striatal and olfactory bulb neurogenesis. *The Journal of Neuroscience : The Official Journal of the Society for Neuroscience*, *23*(1), 167–174. https://doi.org/23/1/167 [pii]

Sueiro, C., Carrera, I., Molist, P., Rodríguez-Moldes, I., & Anadón, R. (2004). Distribution and development of glutamic acid decarboxylase immunoreactivity in the spinal cord of the dogfish Scyliorhinus canicula (elasmobranchs). *The Journal of Comparative Neurology*, *478*(April), 189–206. https://doi.org/10.1002/cne.20285

Sugars, K. L., & Rubinsztein, D. C. (2003). Transcriptional abnormalities in Huntington disease. *Trends in Genetics*, *19*(5), 233–238. https://doi.org/10.1016/S0168-9525(03)00074-X

Sussel, L., Marin, O., Kimura, S., & Rubenstein, J. L. (1999). Loss of Nkx2.1 homeobox gene function results in a ventral to dorsal molecular respecification within the basal telencephalon: evidence for a transformation of the pallidum into the striatum. *Development*, *126*(15), 3359–3370. https://doi.org/10393115

Szczêsny, E., OElusarczyk, J., Glombik, K., Budziszewska, B., Kubera, M., Lasoñz, W., & Basta-Kaim, A. (2013). Possible contribution of IGF-1 to depressive disorder. *Pharmacological Reports*, *65*(6), 1622–1631. https://doi.org/10.1016/S1734-1140(13)71523-8

Szucsik, J. C., Witte, D. P., Li, H., Pixley, S. K., Small, K. M., & Potter, S. S. (1997). Altered Forebrain and Hindbrain Development in Mice Mutant for theGsh-2Homeobox Gene. *Developmental Biology*, *191*(2), 230–242. https://doi.org/10.1006/dbio.1997.8733

Takahashi, H., & Liu, F. C. (2006). Genetic patterning of the mammalian telencephalon by morphogenetic molecules and transcription factors. *Birth Defects Research Part C - Embryo Today: Reviews*, *78*(3), 256–266. https://doi.org/10.1002/bdrc.20077

Tao, W., & Lai, E. (1992). Telencephalon-restricted expression of bf-1, a new member of the hnf-3 fork head gene family, in the developing rat brain. *Neuron*, *8*, 957–966.

Tomoda, K., Kubota, Y., & Kato, J. (1999). Degradation of the cyclin-dependent-kinase inhibitor p27Kip1 is instigated by Jab1. *Nature*, *398*(6723), 160–165. https://doi.org/10.1038/18230

Toresson, H., & Campbell, K. (2001). A role for Gsh1 in the developing striatum and olfactory bulb of Gsh2 mutant mice. *Development (Cambridge, England)*, *128*(23), 4769–4780.

Toresson, H., Potter, S. S., & Campbell, K. (2000). Genetic control of dorsal-ventral identity in the telencephalon: opposing roles for Pax6 and Gsh2. *Development (Cambridge, England)*, *127*(20), 4361–4371.

Torper, O., Pfisterer, U., Wolf, D. A., Pereira, M., Lau, S., Jakobsson, J., Parmar, M. (2013). Generation of induced neurons via direct conversion in vivo. *Proceedings of the National Academy of Sciences*, *110*(17), 7038–7043. https://doi.org/10.1073/pnas.1303829110

Uzri, D., & Gehrke, L. (2009). Nucleotide Sequences and Modifications That Determine RIG-I/RNA Binding and Signaling Activities. *Journal of Virology*, *83*(9), 4174–4184. https://doi.org/10.1128/JVI.02449-08

Valerius, M. T., Li, H., Stock, J. L., Weinstein, M., Kaur, S., Singh, G., & Potter, S. S. (1995). Gsh-1: a novel murine homeobox gene expressed in the central nervous system. *Developmental Dynamics : An Official Publication of the American Association of Anatomists*, *203*(3), 337–351. https://doi.org/10.1002/aja.1002030306

van der Kooy, D., & Fishell, G. (1987). Neuronal birthdate underlies the development of striatal compartments. *Brain Research*, *401*(1), 155–161. https://doi.org/10.1016/0006-8993(87)91176-0

Vieira, C., Pombero, A., García-Lopez, R., Gimeno, L., Echevarria, D., & Martínez, S. (2010). Molecular mechanisms controlling brain development: An overview of neuroepithelial secondary organizers. *International Journal of Developmental Biology*, *54*(1), 7–20. https://doi.org/10.1387/ijdb.092853cv

Waclaw, R. R., Wang, B., Pei, Z., Ehrman, L. A., & Campbell, K. (2009a). Distinct Temporal Requirements for the Homeobox Gene Gsx2 in Specifying Striatal and Olfactory Bulb Neuronal Fates. *Neuron*, *63*(4), 451–465. https://doi.org/10.1016/j.neuron.2009.07.015

Waclaw, R. R., Wang, B., Pei, Z., Ehrman, L. A., & Campbell, K. (2009b). Distinct Temporal Requirements for the Homeobox Gene Gsx2 in Specifying Striatal and Olfactory Bulb Neuronal Fates. *Neuron*, *63*(4), 451–465. https://doi.org/10.1016/j.neuron.2009.07.015

Wang, H. F., & Liu, F. C. (2001). Developmental restriction of the LIM homeodomain transcription factor Islet-1 expression to cholinergic neurons in the rat striatum. *Neuroscience*, *103*(4), 999–1016. https://doi.org/10.1016/S0306-4522(00)00590-X

Warren, L., Manos, P. D., Ahfeldt, T., Loh, Y. H., Li, H., Lau, F., Rossi, D. J. (2010). Highly efficient reprogramming to pluripotency and directed differentiation of human cells with synthetic modified mRNA. *Cell Stem Cell*, *7*(5), 618–630.

https://doi.org/10.1016/j.stem.2010.08.012

Wichterle, H., Turnbull, D. H., Nery, S., Fishell, G., & Alvarez-Buylla, A. (2001). In utero fate mapping reveals distinct migratory pathways and fates of neurons born in the mammalian basal forebrain. *Development (Cambridge, England)*, *128*(19), 3759–3771.

Wilson, L., & Maden, M. (2005). The mechanisms of dorsoventral patterning in the vertebrate neural tube. *Developmental Biology*, *282*(1), 1–13. https://doi.org/10.1016/j.ydbio.2005.02.027

Wilson, P. G., & Stice, S. S. (2006). Development and differentiation of neural rosettes derived from human embryonic stem cells. *Stem Cell Reviews*, *2*(1), 67–77. https://doi.org/10.1007/s12015-006-0011-1

Yuen, T. J., Silbereis, J. C., Griveau, A., Chang, S. M., Daneman, R., Fancy, S. P. J., Rowitch, D. H. (2014). Oligodendrocyte-encoded HIF function couples postnatal myelination and white matter angiogenesis. *Cell*, *158*(2), 383–396. https://doi.org/10.1016/j.cell.2014.04.052

Yun, K., Fischman, S., Johnson, J., Hrabe de Angelis, M., Weinmaster, G., & Rubenstein, J. L. R. (2002). Modulation of the notch signaling by Mash1 and Dlx1/2 regulates sequential specification and differentiation of progenitor cell types in the subcortical telencephalon. *Development (Cambridge, England)*, *129*(21), 5029–5040.

Yun, K., Garel, S., Fischman, S., & Rubenstein, J. L. R. (2003). Patterning of the lateral ganglionic eminence by the Gsh1 and Gsh2 homeobox genes regulates striatal and olfactory bulb histogenesis and the growth of axons through the basal ganglia. *Journal of Comparative Neurology*, *461*(2), 151–165. https://doi.org/10.1002/cne.10685

Yun, K., Potter, S., & Rubenstein, J. L. (2001). Gsh2 and Pax6 play complementary roles in dorsoventral patterning of the mammalian telencephalon. *Development (Cambridge, England)*, *128*(2), 193–205. https://doi.org/10.1242/DEV.00328

Zezula, J., Casaccia-Bonnefil, P., Ezhevsky, S. A., Osterhout, D. J., Levine, J. M., Dowdy, S. F., Koff, A. (2001). P21cip1 is required for the differentiation of oligodendrocytes independently of cell cycle withdrawal. *EMBO Reports*, *2*(1), 27–34. https://doi.org/10.1093/embo-reports/kve008

Zhang, X., Huang, C. T., Chen, J., Pankratz, M. T., Xi, J., Li, J., Zhang, S. C. (2010). Pax6 is a human neuroectoderm cell fate determinant. *Cell Stem Cell*, *7*(1), 90–100. https://doi.org/10.1016/j.stem.2010.04.017

Zimmerman, L. B., De Jesús-Escobar, J. M., & Harland, R. M. (1996). The Spemann organizer signal noggin binds and inactivates bone morphogenetic protein 4. *Cell*, *86*(4), 599–606. https://doi.org/10.1016/S0092-8674(00)80133-6

Zuccato, C., & Cattaneo, E. (2007). Role of brain-derived neurotrophic factor in Huntington's disease. *Progress in Neurobiology*, *81*(5–6), 294–330. https://doi.org/10.1016/j.pneurobio.2007.01.003

Differentiation of human telencephalic progenitor cells into MSNs by inducible expression of Gsx2 and Ebf1

Andrea Faedo[a,b,1,2], Angela Laporta[a,b], Alice Segnali[a,b,3], Maura Galimberti[a,b], Dario Besusso[a,b], Elisabetta Cesana[c], Sara Belloli[d,e], Rosa Maria Moresco[d,e], Marta Tropiano[f,g], Elisa Fucà[f,g], Stefan Wild[h], Andreas Bosio[h], Alessandro E. Vercelli[f,g], Gerardo Biella[c], and Elena Cattaneo[a,b,2]

[a]Laboratory of Stem Cell Biology and Pharmacology of Neurodegenerative Diseases, Department of Biosciences, University of Milan, 20122 Milan, Italy; [b]Istituto Nazionale Genetica Molecolare (INGM) Romeo ed Enrica Invernizzi, Milan 20122, Italy; [c]Department of Biology and Biotechnology, University of Pavia, 27100 Pavia, Italy; [d]Institute of Molecular Bioimaging and Physiology, National Research Council (IBFM-CNR), San Raffaele Scientific Institute, University of Milan Bicocca, 20132 Milan, Italy; [e]Department of Medicine and Surgery, University of Milan Bicocca, 20126 Milan, Italy; [f]Department of Neuroscience, Neuroscience Institute Cavalieri Ottolenghi, 10043 Torino, Italy; [g]Department of Neuroscience, National Institute of Neuroscience, 10043 Torino, Italy; and [h]Miltenyi Biotec GmbH, 51429 Bergisch Gladbach, Germany

Edited by Anders Bjorklund, Lund University, Lund, Sweden, and approved November 29, 2016 (received for review July 13, 2016)

Medium spiny neurons (MSNs) are a key population in the basal ganglia network, and their degeneration causes a severe neurodegenerative disorder, Huntington's disease. Understanding how ventral neuroepithelial progenitors differentiate into MSNs is critical for regenerative medicine to develop specific differentiation protocols using human pluripotent stem cells. Studies performed in murine models have identified some transcriptional determinants, including GS Homeobox 2 (Gsx2) and Early B-cell factor 1 (Ebf1). Here, we have generated human embryonic stem (hES) cell lines inducible for these transcription factors, with the aims of (*i*) studying their biological role in human neural progenitors and (*ii*) incorporating TF conditional expression in a developmental-based protocol for generating MSNs from hES cells. Using this approach, we found that Gsx2 delays cell-cycle exit and reduces Pax6 expression, whereas Ebf1 promotes neuronal differentiation. Moreover, we found that Gsx2 and Ebf1 combined overexpression in hES cells achieves high yields of MSNs, expressing Darpp32 and Ctip2, in vitro as well in vivo after transplantation. We show that hES-derived striatal progenitors can be transplanted in animal models and can differentiate and integrate into the host, extending fibers over a long distance.

MSNs | Gsx2 | Ebf1 | hES cells | HD

The striatum is the largest component of the basal ganglia, it is the hub of converging excitatory connections from the cortex and thalamus, and it originates the direct and indirect pathways, which are distinct basal ganglia circuits involved in motor control (1). In humans, the degeneration of the principal striatal neuronal population, the medium spiny neurons (MSNs), causes a severe neurodegenerative condition, Huntington's disease (HD). A main goal in the field is the study of the mechanisms underlying neuronal specification and degeneration. A large number of studies performed in model organisms, such as the mouse model organism, have provided fundamental insights into brain development, shedding light on genes, signaling pathways, and general rules of brain formation. It is not incidental to point out that obvious species-specific differences exist in many aspects between mice and humans (gestation, morphology, and gene expression regulation in time and space). Thus, additional model systems are needed to uncover specific functions of a gene in human development (2, 3). This task is also driven by the need to investigate neurological diseases, such as HD, in a model that more closely resembles human biology.

Here, we decided to take advantage of human embryonic stem (hES) cells to develop a model to study the roles of selected transcription factors (TFs) in human striatal development and as a strategy to increase recovery of authentic MSNs for transplantation purposes. During brain development, a set of TFs are expressed in different regions and times and cooperate to establish a dorsal–ventral and medial–lateral positional identity in progenitor cells and to specify neuronal terminal differentiation. In particular, in the developing telencephalon, two TFs play a key role in contributing to the formation of the striatum: the GS Homeobox 2 (Gsx2) and Early B-cell factor 1 (Ebf1).

Gsx2 is expressed in the ventral ventricular zone (VZ) of the telencephalon, where it is involved in maintaining the identity of early striatal progenitors, and it is required for promoting a striatal fate (4–8). Recently, two studies have reported about the role of Gsx2 in mouse neural stem cells, showing that Gsx2 regulates progenitor proliferation and differentiation (9, 10). Nonetheless, these studies focused on Gsx2 function in mouse neurospheres and in adult neural stem cells models that could bear different signatures with respect to human embryonic ventral progenitors. Ebf1 is a helix–loop–helix TF that has been shown to control cell differentiation in the murine embryonic striatum (11–13), but it has never been studied in a human model system of striatal development.

We have previously demonstrated that human ventral telencephalic progenitors can be generated from hES cells by using a Shh treatment coupled with Wnt inhibition (14, 15). These progenitors eventually differentiate into mature, electrophysiologically active neurons. However, the protocol yielded cultures containing Darpp32$^+$–Ctip2$^+$ cells never exceeding 10–15%. We therefore wished to establish a hES cell-based inducible gain-of-function (iGOF) system whereby TFs expressed in the developing striatum can be harnessed to improve MSN differentiation and to study

Significance

We established human embryonic stem (hES) cell-inducible lines to express specific transcription factors [GS Homeobox 2 (Gsx2) and Early B-cell factor 1 (Ebf1)] to improve medium spiny neuron (MSN) differentiation and to study human striatal development in vitro. We also used a nonintegrating system, by utilizing modified mRNAs to transiently overexpress Gsx2 and Ebf1 in a different hES cell line. These data can help to improve the differentiation protocols that aim to produce high-quality cell preparation suitable for cell transplantation in animal models of Huntington's disease. Finally, we show that hES-derived striatal progenitors can be transplanted in the striatum of animal models and can differentiate and integrate into the host, extending fibers over a long distance (including the substantia nigra, a striatal target).

Author contributions: A.F. and E. Cattaneo designed research; A.F., A.L., A.S., M.G., E. Cesana, S.B., M.T., and E.F. performed research; S.W. and A.B. contributed new reagents/analytic tools; A.F., D.B., R.M.M., A.E.V., G.B., and E. Cattaneo analyzed data; and A.F. wrote the paper.

The authors declare no conflict of interest.

This article is a PNAS Direct Submission.

[1]Present address: Axxam S.p.A. Cell Biology Unit, Bresso, 20091 Milan, Italy.

[2]To whom correspondence may be addressed. Email: andrea.faedo@unimi.it or elena.cattaneo@unimi.it.

[3]Present address: Istituto Neurologico Carlo Besta, 20133 Milan, Italy.

This article contains supporting information online at www.pnas.org/lookup/suppl/doi:10.1073/pnas.1611473114/-/DCSupplemental.

human striatal development. We uncovered roles for Gsx2 and Ebf1 during human striatal specification and differentiation, in particular in cell-cycle regulation. Moreover, we report that a specific temporal window of Gsx2 and Ebf1 overexpression in hES cells achieves high yields of MSNs in vitro, expressing Darpp32 and Ctip2, and that these cells can be found in vivo after transplantation. We show that these hES-derived striatal progenitors can be transplanted in animal models and can differentiate and integrate into the host, extending fibers over a long distance.

Results

Generation of Inducible hES Cell Lines. To shed light on the transcriptional program that drives human striatal differentiation, we decided to develop an inducible overexpression system in hES H9 cells. To this goal, we modified a commercially available TetON construct (Clontech) by moving the TetON cassette into a chicken beta-actin promoter with CMV enhancer-based plasmid (pCAG) (*Methods*) to avoid silencing effects (16). This construct was introduced by nucleofection (Fig. S1*A*) in hES H9 cells (p40–p50) along with a linear construct carrying a gene encoding for puromycin resistance. After selection, several stable hES cell clones were picked, amplified, and tested for inducibility by using a pTRE-Luciferase construct. We selected four clones that showed no basal Luciferase activity and high induction after 48 h of doxycycline treatment. We amplified and characterized the clones C4 and B6 that showed the highest Luciferase expression after transient transfection (Fig. S1*A*, chart). They responded promptly to differentiation stimuli similarly to the original H9 cells (Fig. S1 *K–N*). Next, we constructed three conditional vectors with the pTRE promoter, regulating Gsx2 (pTRE-Gsx2), Gsx2 alongside with Ebf1 by means of an IRES2 sequence (pTRE-Gsx2-Ebf1), and Ebf1 alone (pTRE-Ebf1). Using these three constructs, we carried out nucleofections in the hES-inducible clones (Fig. S1*A′*). After selection, several stable hES cell clones were picked, amplified, and tested for Gsx2, Gsx2–Ebf1, and Ebf1 expression. Four Gsx2, one Gsx2–Ebf1, and two Ebf1 overexpressing clones were chosen for the next experiments. We quantified Gsx2, Gsx2–Ebf1, and Ebf1 overexpression in the inducible hES cell clones after 72 h of doxycycline treatment (Fig. S1 *B–J*). Quantification of $Gsx2^+$ cells after 72 h of doxycycline induction in Gsx2 iGOF showed 55 ± 3% expression (Fig. S1*D*). Quantification of $Gsx2^+$ and $Ebf1^+$ cells in Gsx2–Ebf1 iGOF showed 51 ± 19% and 48 ± 22% expression, respectively (Fig. S1*G*), with virtually all of the cells coexpressing Gsx2 and Ebf1 (Fig. S1 *F′* and F′′). Finally, quantification of $Ebf1^+$ cells in Ebf1 iGOF showed 60 ± 8% expression (Fig. S1*J*). We next used Western Blot analysis to perform a second quantification experiment during neuronal differentiation, at day30, after 10 d of doxycycline treatment (Fig. S1*O*) in the three iGOF lines. Western Blot quantification (Fig. S1*P*) showed up-regulation of Gsx2 (12-fold in Gsx2–Ebf1 and 124-fold in Gsx2 iGOF) and Ebf1 (243-fold in Gsx2–Ebf1 and 267-fold in Ebf1 iGOF) in the three lines compared with basal culture conditions (no doxycycline).

Gsx2 and Ebf1 Regulation of Patterning Genes. The patterning activity of Gsx2 during ventral telencephalic development has been extensively studied in mouse models (4–7, 17). However, no

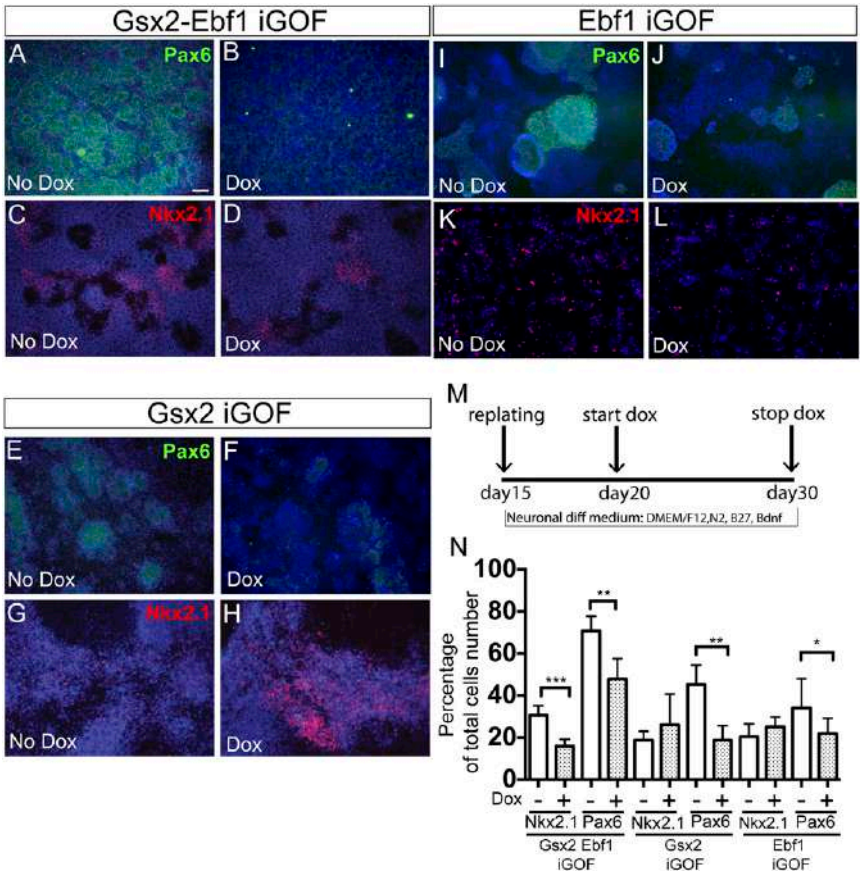

Fig. 1. Gsx2 and Ebf1 roles during patterning of telencephalic progenitors. (*A–D*) Gsx2–Ebf1 iGOF line down-regulates Pax6 and Nkx2.1 expression during the day 20–30 developmental window. Instead, Gsx2 and Ebf1 single lines down-regulated only Pax6 (*E–L*). Representative immunofluorescence images for Pax6 (green) and Nkx2.1 (red) expression. (Scale bar, 100 μm.) (*M*) Schema illustrating the experimental design. (*N*) Quantification analysis for Pax6 and Nkx2.1 expressing cells; $n = 3$ biological replicates. For Pax6 analysis, $n = 8$ (no dox) and $n = 10$ (dox). $^*P < 0.05$, $^{**}P < 0.01$, $^{***}P < 0.003$ two-tailed t test analysis. Data are presented as means ± SD.

information is available about its roles during human development. To determine the effects of Gsx2 and Ebf1 overexpression in human neural progenitors, we used a specific protocol that we previously showed to have the potential to generate, first, ventral telencephalic progenitors and, then, mature MSNs after 80 d in vitro (14, 15). However, the protocol yields cultures containing Darpp32$^+$/Ctip2$^+$ cells never exceeding 10–15%. We therefore wished to implement this protocol by establishing a hES cell-based iGOF system whereby TFs expressed in the developing striatum can be used to increase MSN yield. Thus, we decided to overexpress Gsx2, Gsx2–Ebf1, and Ebf1 in different temporal windows during hES neural differentiation: day 10–15, day 15–20, and day 20–30. To test this TF-mediated specification, we first analyzed regional patterning in the hES-derived neural progenitors. We found that Gsx2, Gsx2–Ebf1, and Ebf1 iGOF down-regulated Pax6, a dorsal cortical marker, at day 30 (Fig. 1 *A*, *B*, *E*, *F*, *I*, and *J*, and quantification in Fig. 1N) and at day15 (Fig. S2 *A–D*), corresponding to the end of the doxycycline treatments. Because Pax6 is also an important early neuroectodermal marker in humans (3), we sought to determine if Gsx2 overexpression could compromise the process of neural induction in hES cells. To test this possibility, Gsx2 expression was induced during the day 10–15 time window, the earliest period used in this study. Importantly, Gsx2 activation did not down-regulate Otx2 and *N*-Cadherin (two early neural plate markers) expression at day15, the end of the doxycycline treatment (Fig. S2 *E–H*), suggesting that the cells correctly went through neural induction.

Next, we performed immunostaining for Nkx2.1, a marker expressed in proliferative cells of the MGE, in striatal interneurons and in Ctip2$^+$ cells of the mature striatum (and in the hypothalamus). Because at this time point (day 30) most cells are still proliferating and we do not usually detect Ctip2 expression, the down-regulation of Nkx2.1 that we found in the double Gsx2–Ebf1 iGOF line (Fig. 1 *C*, *D*, *G*, *H*, *K*, and *L*, and quantification in Fig. 1N) suggests a suppression of an MGE fate.

Next, to move forward a transient and nonintegrating system, we generated a modified mRNA (mmRNA) for *Gsx2*. We transfected this mmRNA into H9 hES-derived neural progenitor cells from day 20 to day 25 of differentiation using the same protocol used for the iGOF lines. As shown in Fig. S2 *I–K*, Gsx2 overexpressing cells reduced Pax6 expression similarly to that found in the Gsx2 iGOF line (threefold decrease in both overexpressing systems).

Together, the data indicate that in hES cells that are undergoing neuronal conversion, Gsx2 and Ebf1 overexpression suppresses the dorsal marker Pax6 and the MGE marker Nkx2.1 while maintaining typical neuroepithelial markers (Otx2, *N*-Cadherin).

Given the in vivo expression of Gsx2 in progenitor cells and Ebf1 in early postmitotic neurons, we next investigated if and how Gsx2 and Ebf1 overexpression modified cell proliferation.

Gsx2 and Ebf1 Regulate Cell-Cycle Kinetics. Regulation of cell proliferation in the developing telencephalon is a tightly regulated process, and it is essential to produce the correct number of postmitotic neurons. To examine the effects of Gsx2 and Ebf1 overexpression in human progenitor cells, we first performed a cumulative BrdU analysis in the hES cell lines inducible for Gsx2 and Gsx2–Ebf1. After treating the cells with doxycycline for 5 d, we administered BrdU for 30 min and 4, 8, and 20 h. We found that the Gsx2 iGOF line showed a reduced BrdU incorporation compared with the untreated cells (Fig. 2*A* and quantification in Fig. 2*B*). In contrast, the Gsx2–Ebf1 double inducible line showed a similar BrdU incorporation propensity compared with the control line, suggesting that cell-cycle alteration by Gsx2 was rescued by Ebf1 (Fig. 2 *C* and *D*). Finally, we performed the same analysis also in the Ebf1 iGOF line, finding that at 20 h there was a significant increase in BrdU incorporation compared with the control line, the opposite phenotype found in Gsx2 iGOF cells (Fig. 2 *E* and *F*). These data suggested an involvement of Gsx2 and Ebf1 in cell-cycle regulation.

To test this hypothesis also in hES-derived neural progenitor cells (the biological context that more closely resembles the developing embryonic human brain), we administered doxycycline from day 20 to day 30 of the neuronal differentiation protocol and analyzed cell-cycle kinetics by a BrdU/IddU double labeling paradigm (18, 19) (see *Methods* for details and Fig. 2*K* for experimental design). We first tested this method in our hES cell lines, in basal conditions (no doxycycline), with culture conditions permitting pluripotency, finding a cell-cycle time (Tc) of 19.4 ± 4.4 h, comparable to previous published data (20). Next, we analyzed the Tc of day 30 hES-derived neural progenitor cells (Fig. 2 *G–L*), and we found results in agreement with the BrdU cumulative analysis performed in Fig. 2 *A–E*. Estimation of control cell (no doxycycline) Tc was 12 ± 1 h, whereas the Gsx2 overexpressing cells showed a Tc of 24 ± 4 h. Next, we analyzed the contribution of Ebf1 by measuring Tc in Gsx2–Ebf1 iGOF cells, finding a value of 7 ± 1 h, suggesting that Ebf1 could override a Gsx2-mediated increase of cell-cycle length. In agreement with these findings, when we examined the single Ebf1 iGOF line, we found that this line showed a cell cycle similar to the double Gsx2–Ebf1 iGOF (Fig. S3 *A–C*).

To rule out the possibility that Gsx2 iGOF cells were undergoing differentiation (and thus incorporating less BrdU), we analyzed Map2 expression at day30, the same time point used for the previous analysis. Gsx2 iGOF showed a marked reduction of Map2$^+$ cells (Fig. S3 *D–G*), in agreement with the previous cell-cycle analysis data and further suggesting that Gsx2$^+$ cells could not exit the cell cycle. Moreover, we investigated this Gsx2-mediated cell-cycle regulation also in another two hES inducible clones (G18 and G17; Fig. S3 *H–M*), finding similar results.

Together, these results suggest that Gsx2 regulates cell-cycle progression in human neural progenitor cells.

Gsx2 Constitutive Overexpression Modifies Proliferative Characteristics and Differentiation Potential of hES-Derived Neuroepithelial Stem Cells. To test if this Gsx2-driven cell-cycle regulation is telencephalic-dependent or represents a general role, we decided to test its overexpression in long-term self-renewing neuroepithelial stem (LT-NES) cells. LT-NES cells represent an excellent model for studying human neuroepithelial cell biology (21). They are hES cell-derived neural progenitors with an anterior hindbrain identity. Here, we decided to take advantage of this cell population and its regional identity to gain insights into the cell-cycle regulation by Gsx2.

We generated an LT-NES cell line overexpressing Gsx2 by nucleofection of a pCAG-Gsx2-IRES-Puromicyn vector and isolation of stable, positive clones. We characterized different clones, finding identical phenotypes across the different lines. A control cell line was also generated by using a pCAG-EGFP-IRES-Puromycin vector, and we found identical self-renewal capacity and differentiation potential compared with the unmodified cell line.

First, we decided to analyze the effects of Gsx2 overexpression during proliferation of LT-NES cells by means of BrdU studies. We first performed a BrdU pulse of 2 h, and we found a decrease in BrdU incorporation in LT-NES cells overexpressing Gsx2 (LT-NES-Gsx2), compared with the control cell line (form 36.3 ± 5.1% to 26.8 ± 5.9%, $P < 0.005$; Fig. S4 *A–C*). A similar proliferative defect was found after BrdU pulses of 4 and 24 h (Fig. S4*C*). We reasoned that this decrease in BrdU incorporation could be linked to an increase in cell differentiation or to an increase in cell-cycle length, which leads to a reduction in the number of times the cells pass through the S phase, thus reducing BrdU incorporation. Thus, we performed differentiation experiments and cell-cycle length studies to distinguish between these two possibilities.

First, we differentiated the cells for 10 d, and we analyzed the expression of the early neuronal marker βIII-Tubulin. We found that the number of newly formed neurons was decreased in LT-NES-Gsx2 compared with the control cell line (form 28.9 ± 7.8% to 15.1 ± 1.8%, $P < 0.05$; Fig. S4 *D–F*), in agreement with the results previously found in the Gsx2 iGOF hES line (Fig. S3 *D–G*). A

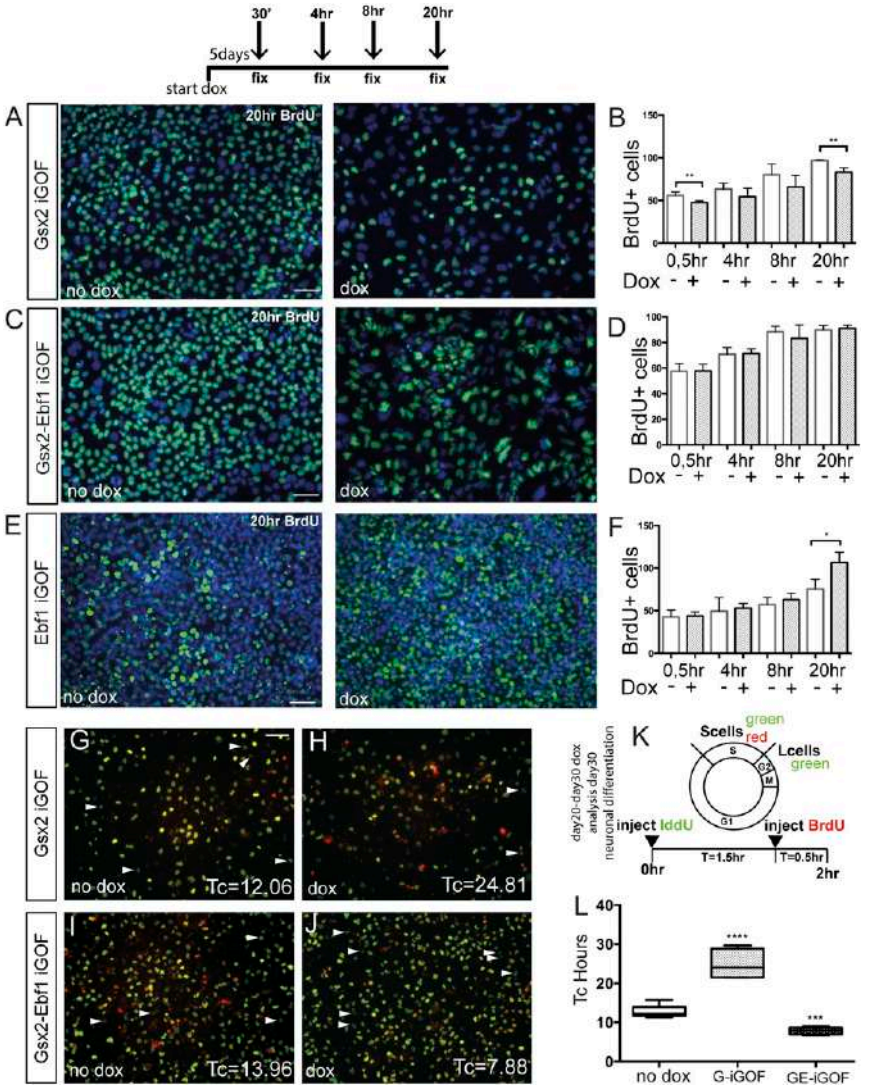

Fig. 2. Gsx2 and Ebf1 modulate cell-cycle kinetics. (*A*, *C*, and *E*) Representative images of a BrdU cumulative labeling experiment in Gsx2 (*A*), Gsx2–Ebf1 (*C*), and Ebf1 (*E*) iGOF lines in culture condition allowing pluripotency. BrdU was added to the culture media at 0.5, 4, 8, and 20 h. (*B*, *D*, and *F*) Quantification of $BrdU^+$ cells at the different time points. Data are represented as means ± SD; two-tailed *t* test analysis. $*P < 0.05$, $**P < 0.01$. (Scale bar, 75 μm.) (*G–J*) Representative images of neuronal progenitor cell-cycle length analysis using BrdU/IdU colabeling. Day 30 hES cell-derived neural progenitors, treated for 10 d with doxycycline, were exposed to IdU at T 0 h and with BrdU at T 1.5 h (see experimental design in *K*). Arrowheads point to cells that left the S-phase at T 1.5 h (L_{cells}, green only cells), whereas yellow cells are still in the S-phase at T 2 h. (Scale bar, 75 μm.) (*L*) Quantification of T_c estimation from BrdU/IdU analysis of Gsx2 and Gsx2–Ebf1 iGOF. Box shows the median and the 25th and 75th percentiles. The whiskers of the graph show the largest and smallest values. $***P < 0.0005$, $****P < 0.0001$.

similar result was found when studying the expression of a more mature neuronal marker such as Map2 (Fig. S4 *J* and *K*). Moreover, even when it was possible to detect βIII-Tubulin expression in LT-NES-Gsx2 cells (at early passages), more mature and lineage-specific markers, such as GABA, were absent (Fig. S4 *L* and *M*), further suggesting that Gsx2 overexpression impairs neuronal differentiation and maturation. Next, we asked if the decrease in BrdU incorporation was caused by a cell-cycle disregulation. To this goal, we performed an analysis of cell-cycle characteristics using the BrdU/IddU double labeling paradigm to estimate the cell-cycle length in the two cell populations, the LT-NES-Gsx2 and LT-NES-EGFP cells. We found that Gsx2 overexpression caused a significant increase in total cell-cycle length (T_c) compared with the control cell line (Fig. S4 *G–I*). This increase was even more pronounced after a few passages (Fig. S4*I*, see increment between p5 and p10, from 26.88 ± 1.84 h to 135.30 ± 33.79 h, $P < 0.005$), suggesting that Gsx2 overexpression has a cumulative effect during time. The control cell line, during the same time period, did not show a statistically significant increase in T_c (from 6.9 ± 0.1 to 9.5 ± 3, $P > 0.1$; Fig. S4*I*).

In conclusion, these data demonstrated that a constitutive Gsx2 overexpression was detrimental for proper neuronal differentiation and maturation, even in a nontelencephalic compartment, corroborating the results obtained in the hES inducible lines. Thus, to summarize the results shown in Fig. 2 and Fig. S4, Gsx2 has a major role in regulating proliferation, by lengthening the cell cycle in a context-independent manner.

Ebf1 Promotes Neuronal Differentiation and Maturation. The foregoing data demonstrate that Gsx2 has important roles in regulating cell-cycle progression, whereas Ebf1 expression probably enhances differentiation. To investigate the specific role of Ebf1 in human neural progenitor cells, we first studied the Ebf1 iGOF line. After overexpressing Ebf1 (by doxycycline treatment) in the day 20–30 temporal window of hES neuronal differentiation, we compared βIII-Tubulin expression with control (no doxycycline)

cells. Ebf1 overexpression resulted in a significant increase in the number of βIII-Tubulin$^+$ cells (Fig. S5 *A–D*, quantification in Fig. S5*C*). Next, to further test the Ebf1 role in increasing neuronal differentiation, we transfected an mmRNA for *Ebf1* (Miltenyi Biotec) in unmodified H9 hES-derived neural progenitor cells (exposed to the same protocol used for the iGOF lines). First, we tested transfection efficiency by staining for Ebf1 after 2 consecutive days of mmRNA delivery, finding a transfection efficiency of 32 ± 5% (Fig. S5 *E* and *F*). Next, we investigated βIII-Tubulin expression after 5 consecutive days of transfections (day 30). We found 17 ± 3% of cells expressing βIII-Tubulin compared with 11 ± 1% of untreated cells (Fig. S5 *G* and *H*, and quantification in Fig. S5*I*, $P < 0.01$, $n = 3$, unpaired *t* test). We then investigated if Ebf1 overexpression had an effect on neurite length or complexity. Interestingly, by using NeurphologyJ analysis (22), we found an increase of attachment points (Fig. S5 *J–L*) on neuronal soma (from 3.5 ± 0.1% to 4.7 ± 0.7% in transfected cells, normalized over total soma number, $P < 0.05$, $n = 3$, unpaired *t* test). These data strongly suggest that Ebf1 has a role as a neuronal differentiation player during hES differentiation.

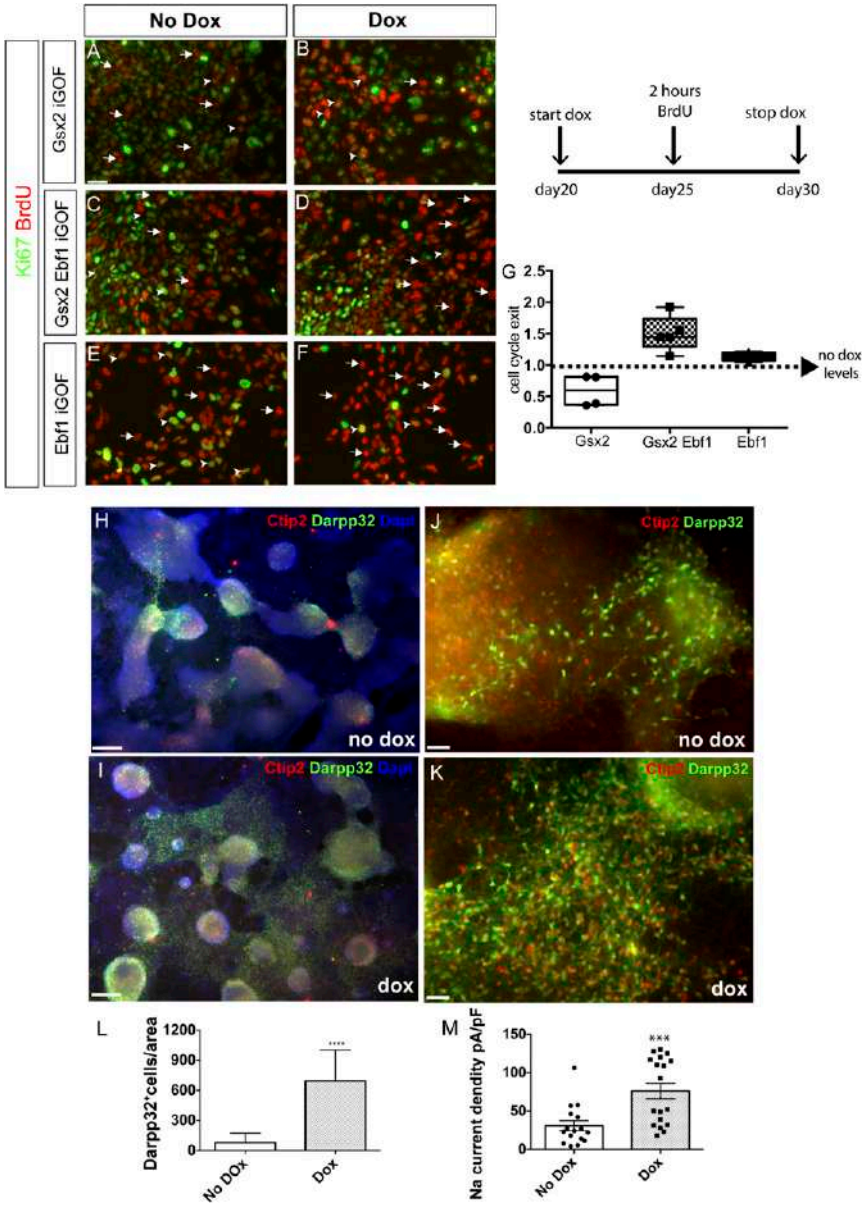

Fig. 3. Gsx2 and Ebf1 differentially regulate cell-cycle exit and promote striatal differentiation. (*A–F*) Representative images of cell-cycle exit studies following the experimental design depicted in *Top Right*. Arrows point to BrdU$^+$Ki67$^-$ cells (that exited cell cycle); arrowheads point to BrdU$^+$Ki67$^+$ cells (still proliferating). (Scale bar, 75 μm.) (*G*) Quantification of cell-cycle exit in Gsx2, Gsx2–Ebf1, and Ebf1 lines after 10 d of doxycycline treatments compared with basal conditions (no doxycycline, dotted line). Box shows the median and the 25th and 75th percentiles. The whiskers of the graph show the largest and smallest values. $^{**}P < 0.005$. (*H–K*) Representative images of neuronal monolayers generated from the Gsx2–Ebf1 iGOF line: immunofluorescence for Ctip2 (red) and Darpp32 (green) at day 80 of striatal differentiation, in day 20–30 doxycycline-treated (*I* and *K*) and nontreated cells (*H* and *J*). *H* and *I*, 5× magnification; *J* and *K*, 20× magnification. (*L*) Quantification of Darpp32$^+$ cells by automated cell counts of 10× fields normalized to the area occupied by nuclear counterstaining. The images in the figure represent reproducible results from four out of five differentiation experiments reaching day 80. [Scale bar, 250 μm (*J* and *K*) and 75 μm (*H* and *I*).] $^{****}P < 0.0001$. (*M*) Sodium current density of neuronal monolayer cultures at day 100 of differentiation in control and doxycycline-treated conditions. Data are represented as means ± SD. Individual round and squared dots represent individual recorded cells. Sodium current density was significantly higher ($^{***}P < 0.001$) in Gsx2–Ebf1 overexpressing cells.

Gsx2 and Ebf1 Overexpression Differentially Regulates Early Neuronal Differentiation. Taking into account the different proliferative responses of hES-derived neural progenitors to Gsx2 and Ebf1 overexpression and the increased neurogenesis after Ebf1 overexpression, we decided to investigate the tendency of Ebf1 and Gsx2–Ebf1 iGOF lines toward differentiation. First, we monitored neuronal differentiation during the differentiation process, finding better neuronal morphology in the two lines after doxycycline treatment. To quantify this differentiation propensity, we performed cell-cycle exit studies, by administering for 2 h BrdU at day 25 of neuronal maturation in a day 20–30 temporal window of doxycycline treatment. The cells were then fixed at day 30 and analyzed for BrdU and Ki67 expression (see schema in Fig. 3). Cell-cycle exit index was calculated by dividing the total number of $BrdU^+$ $Ki67^-$ cells by the total number of $BrdU^+$ cells. As shown in Fig. 3 *A*–*F* and quantified in Fig. 3*G*, the three cell lines showed different phenotypes. Gsx2 overexpressing cells were more likely to remain in the cell cycle (50.2 ± 29.7% reduction of cell-cycle exit over no-doxycycline cells; no doxycycline levels were arbitrarily set to 100; $P < 0.005$, $n = 3$; Fig. 3 *A* and *B*, quantification in Fig. 3G), in agreement with the data presented in Fig. S3 *D*–*G*. Ebf1 incorporation caused increased differentiation output in Gsx2–Ebf1 iGOF line (150 ± 28% increase in cell-cycle exit over no-doxycycline cells; no doxycycline levels were arbitrarily set to 100; $P < 0.05$, $n = 3$; Fig. 3 *C* and *D*, quantification in Fig. 3*G*). Finally, Ebf1 single iGOF overexpressing cells were 113 ± 7% more likely to exit the cell cycle (no doxycycline levels were arbitrarily set to 100%; $P < 0.05$, $n = 3$; Fig. 3 *E* and *F*, chart in Fig. 3*G*).

Again, these results were in line with the hypothesis of Gsx2 retaining neural progenitor cells in an undifferentiated state and Ebf1 controlling cell-cycle exit and progenitor maturation.

Gsx2–Ebf1 Overexpression Induces MSN Differentiation from hES Cells. To determine the striatal differentiation potential of hES cells overexpressing Gsx2–Ebf1 in the day 20–30 developmental window, we conducted long-term differentiation experiments and analyzed the cells at day 60 and day 80.

First, we evaluated the number of cells expressing the striatal neuronal markers Isl1 and Ctip2 at day 60 of differentiation. Isl1+ cells increased from 4.4 ± 0.9% in control cells (no doxycycline) to 25 ± 5% in Gsx2–Ebf1 overexpressing cells ($P < 0.00005$, $n = 3$; Fig. S6 *C* and *D*). $Ctip2^+$ cells increased from 8.5 ± 2.3% in control cells (no doxycycline) to 20 ± 3.9% in Gsx2–Ebf1 overexpressing cells ($P < 0.0005$, $n = 3$; Fig. S6 *E* and *F*). To further validate these findings using a different system and to move toward a non-integrating system, we also performed transfection experiments in the RC17 hES cell line using mmRNAs for Gsx2 and Ebf1. Following the experimental strategy shown in Fig. S6*B*, $Isl1^+$ cells increased from 6.2 ± 2.2% in nontransfected cells to 17.2 ± 3.2% in cells transfected sequentially with Gsx2 and Ebf1 (Fig. S6 *G* and *H*). At day 60 of differentiation, Ctip2+ cells increased from 20.10 ± 7.4% in nontransfected cells to 42.9 ± 7.5% in cells transfected sequentially with Gsx2 and Ebf1 (Fig. S6 *I* and *J*).

Next, we analyzed the neuronal population at day 80 of differentiation by studying Darpp32 and Ctip2 expression. Initially, we quantified the generated striatal neurons by expressing the density of $Ctip2^+$/$Darpp32^+$ area per arbitrary surface area (Fig. 3 *H* and *I*), finding a higher efficiency of $Darpp32^+$/$Ctip2^+$ neuron generation in the iGOF line compared with the control line (from 3.8 ± 3.1% to 38.8 ± 13.7%). Then we focused on the number of $Darpp32^+$ cells by performing automating soma cell counting (by using the NeurphologyJ ImageJ plugin; see *Methods* for quantification details), and we found a higher number of $Darpp32^+$ cells per unit area in the iGOF line than in control cells (from 79.5 ± 26.3 in basal condition to 693 ± 76 in iGOF; number of cells per area; see *Methods* for quantification details, $n = 3$; Fig. 3 *J* and *K*, quantification in Fig. 3*L*; $n = 3$).

Finally, we studied if the Gsx2–Ebf1 combination could confer functional electrophysiological properties to the differentiated neurons. Although passive properties did not change significantly between doxycycline-treated and nontreated cells, we found interesting results studying sodium currents. In particular, Na^+ current density was significantly higher in doxycycline-treated cells (from 30.7 ± 6.6 pA/pF in control cells to 76.1 ± 10.1 pA/pF in Gsx2–Ebf1 overexpressing cells, $P < 0.001$; Fig. 3*M*).

Gsx2–Ebf1 iGOF Cells Survive and Differentiate in Vivo After Transplantation. Next, we wanted to assess long-term survival and differentiation of Gsx2–Ebf1 iGOF cells after transplantation in the striatum of QA-lesioned, athymic adult rats. The transplanted animals were followed up to 2 mo and then killed for immunohistochemical analysis. To this goal, we decided to induce Gsx2 and Ebf1 expression from day 15–20 of neuronal differentiation and perform the transplant at day 20 (Fig. 4*A*). This time point was chosen according to previous studies performed in our laboratory, showing an increase in cell survival when cells were transplanted at day 20 compared with day 30. Two months after transplantation, we found many human $nuclei^+$ cells in the transplanted site (Fig. 4 *B* and *C*, red cells), suggesting optimal survival (average of 53 ± 16% human $nuclei^+$ cells; Fig. 4*D*). We then analyzed the expression of markers of mature striatal neurons: Ctip2, GABA, and Darpp32. Interestingly, Ctip2 and GABA were largely present in the lesioned transplanted site (human $nuclei^+$ cells) (Fig. 4*B*, arrowheads point to examples of $Ctip2^+$/$hNuclei^+$ cells). In addition, immunostaining for Darpp32 and Ctip2 showed similar results (Fig. 4*C*), with these two striatal markers expressed in the site of transplantation. To further investigate the coexpression of Ctip2 and Darpp32 in human $nuclei^+$ cells, we analyzed the immunostaining for Ctip2/human nuclei (Fig. 4*C*') and Darpp32/human nuclei (Fig. 4*C*") on the same section shown in Fig. 4C. *Insets* in Fig. 4 C' and C" show representative human $nuclei^+$ cells expressing both Ctip2 and Darpp32 markers. We quantified the cells that were human nuclei/Ctip2 double-positive, and we found 23 ± 6% of cells expressing both markers. When we quantified control (No Dox) cells, we found similar results (Fig. S7 *C* and *D* for Darpp32 and Ctip2 quantifications, respectively). Future studies will need to address the role of the in vivo environment in differentiating hES cells. These results suggest that Gsx2–Ebf1 iGOF cells were able to differentiate into striatal neurons in vivo as in vitro.

Long-Distance Axonal Outgrowth and Local Circuitry Integration of hES-Derived Striatal Neurons After Transplantation. We next performed a histological analysis of long-distance, target-specific outgrowth by using a human-specific antibody for NCAM (hNCAM). When grafted to the lesioned striatum, both WT and iGOF cells showed hNCAM-rich grafts (Fig. 4 *E* and *E*' as well as *F* and *F*' and Fig. S7 *A* and *B* for low-magnification pictures showing graft size). These grafts were able to extend axons to the substantia nigra (Fig. 4 *G* and *G*' as well as *H* and *H*'), a specific striatal target. We also quantified fiber length (*Methods*) in iGOF and control cells (Fig. S7*E*), finding similar results. Moreover, we could also observe the presence of human cells expressing the neurotransmitter GABA (Fig. 4 *I* and *J*). Lastly, these hES-derived progenitors were also able to differentiate into local circuitry interneurons, as shown by the presence of human cells expressing Calbindin (Fig. 4*K*), Calretinin (Fig. 4*L*), and Nkx2.1 (Fig. S7 *F* and *G*).

In summary, we provide evidence of an efficient integration in the host neuronal circuitry with human axonal extension to striatal-specific targets as the substantia Nigra.

Discussion

This study aimed to achieve two goals: (*i*) to study Gsx2 and Ebf1 function during human ventral telencephalic development, and (*ii*) to improve MSN differentiation from hES cells by transcriptional specification. In both efforts, we have succeeded in applying an iGOF system for forcing TF expression in defined temporal windows and in combining this approach with a morphogens-driven ventral telencephalic specification.

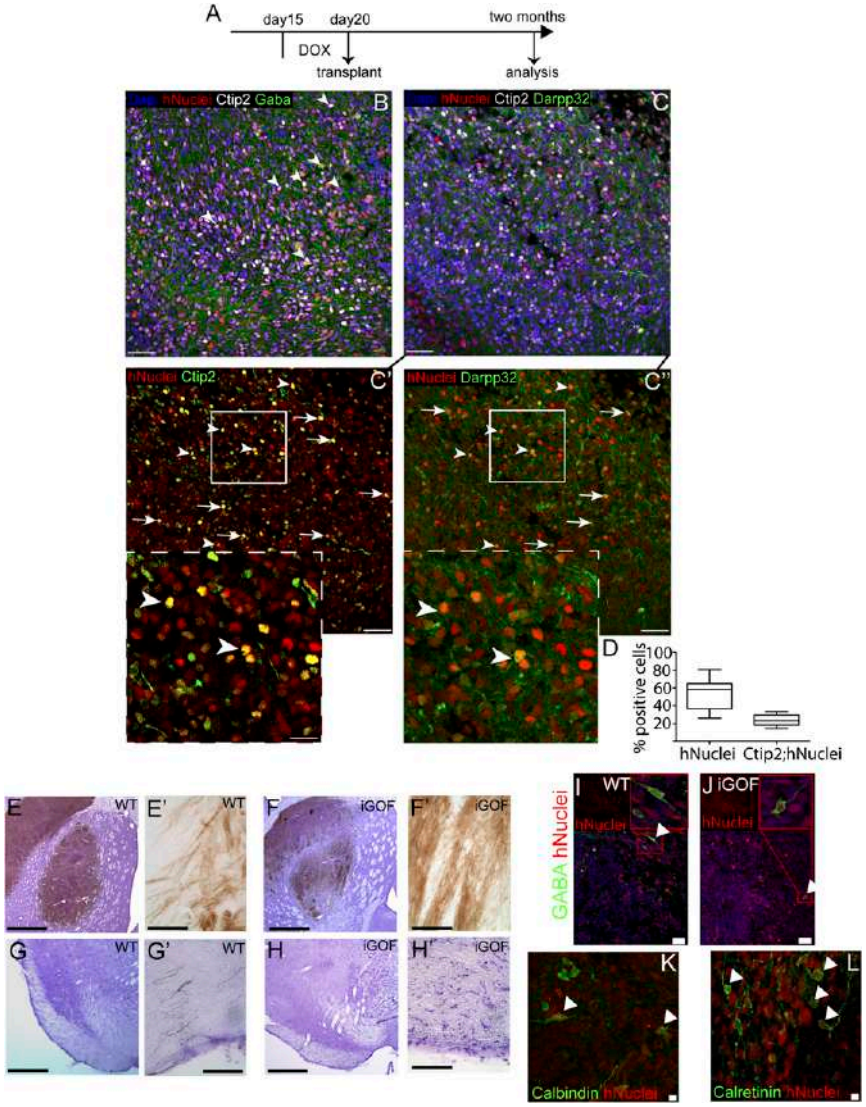

Fig. 4. Gsx2–Ebf1 overexpressing cells maturate in vivo into MSNs and extend axonal projections into distant targets. (*A*) Experimental design for hES cell-derived neural progenitor transplantation in QA-lesioned athymic rats, after 5 d of doxycycline treatment. (*B–C″*) Representative images of grafted cells 2 mo after transplantation, assayed for human nuclei marker and specific MSNs markers. *Insets* in *C′* and *C″* are magnifications of regions depicted in *C′* and *C″*. Arrowheads point to human cells expressing both Ctip2 and Darpp32. Arrows point to grafted human cells expressing either Ctip2 or Darpp32. [Scale bar, 35 μm (*B–C″*) and 15 μm (*Insets*).] (*D*) Quantification of human cells in the grafted site (hNuclei$^+$ cells) and of Ctip2$^+$ cells in the hNuclei$^+$ population. Box shows the median and the 25th and 75th percentiles. The whiskers of the graph show the largest and smallest values. [Scale bar, 75 μm (*B*, *C*, *C′*, and *C″*) and 30 μm (*Insets* in *C′* and *C″*).] (*E–H′*) DAB-developed sections stained for human NCAM antibody showing the neuronal outgrowth of intrastriatal transplants of hES-derived striatal progenitor cells. *E–H* and *G′* and *H′* were counterstained with Cresyl-Violet to show the surrounding tissue. (*I–J*) Examples of hNuclei$^+$GABA$^+$ cells found both in WT (*I*) and iGOF cells (*J*). [Scale bar, 250 μm (*E*, *F*, *G*, and *H*) and 25 μm (*E′*, *F′*, *G′*, and *H′*).] (*K* and *L*) Examples of hNuclei cells expressing the local interneurons markers Calbindin (*K*) and Calretinin (*L*). Calbindin$^+$ cells displayed a morphology reminiscent of the typical fusiform shape of human interneurons. Calretinin$^+$ cells exhibited ovoid somata, as expected for human striatal interneurons. [Scale bar, 25 μm (*I* and *J*) and 5 μm (*K* and *L*).]

In making progress toward the first aim, we have demonstrated a dual role for Gsx2 in embryonic human neural progenitors. First, it imparts a regional identity by directly or indirectly down-regulating Pax6 expression. We found this effect during different time windows of Gsx2 induction, suggesting a time-independent primary function for this TF. It is also important to note that Gsx2 iGOF cells responded properly to neural induction extrinsic signals as evidenced by the correct expression of early neural plate markers such as Otx2 and *N*-Cadherin. Second, Gsx2 has a major role in regulating proliferation, by lengthening the cell cycle in a context-independent manner: We found similar results in cells as different as LT-NES, self-renewing hES cells, and hES-derived neural progenitors. To begin with, we show that in LT-NES cells, a model of human neuroepithelial cells, constitutive Gsx2 overexpression caused a progressive increase in cell-cycle length during passages, leading to a proliferation block and to differentiation impairment.

Interestingly, Gsx2 time-restricted overexpression showed the same consequences on cell-cycle regulation, suggesting that this is a key Gsx2 role in neuronal progenitors. Moreover, because LT-NES cells have a ventral anterior hindbrain identity and hES-derived neural progenitors express more anterior markers, such as Otx2, this Gsx2 activity on cell-cycle regulation is context-independent and likely reflects a primary role. Interestingly, it is well accepted that during mouse development cell-cycle lengthening is correlated with enhanced neurogenesis (23). Our data about Gsx2-regulated cell-cycle lengthening are somehow in contrast, as we found a reduction in differentiation. It is probable that Gsx2 retains human neural progenitor cells in a condition that prevents excessive proliferation

and differentiation, with implications for the generation of the correct number of differentiated progeny during human development.

A recent paper has evidenced that in adult neural stem cells Gsx2 overexpression promotes the transition from quiescent to activated neural stem cells (9). Nonetheless, they also pointed out how a high level of Gsx2 blocks the lineage progression toward transit amplifying progenitors, a more differentiated cell population. Our findings obtained in human neural progenitors are in line with the suggestion that fine-tuned Gsx2 levels must be reached to promote neuronal differentiation. The ventral mouse and human telencephalon express at high-level Gsx2 in the VZ (4), including the LGE proliferative region, and these expression data likely reflect the roles played by this TF. Later during development, the Gsx2 expression is reduced in both the number of $Gsx2^+$ cells and the intensity levels (5), suggesting that its expression must be down-regulated over time to allow neuronal maturation.

Thus, our data point to a role for Gsx2 in restraining cell-cycle progression in neural progenitors while instructing a regional ventral phenotype. Of note, the differentiation defect observed in Gsx2 iGOF cells was rescue by Ebf1: the corecruitment of Gsx2 and Ebf1 caused a more efficient neuronal differentiation, while preserving the regional patterning activity of Gsx2, as shown by the Pax6 down-regulation. Interestingly, even if these two TFs are not expressed in the same region and time during development, their combination in hES cell-derived neural progenitors allowed a proper cell-cycle progression and neuronal differentiation, while maintaining a patterning activity (Pax6 down-regulation). We show here that Ebf1, by using iGOF lines or mmRNA transfections, can enhance neuronal differentiation in hES-derived neuronal populations, in terms of neuronal numbers and morphological characteristics.

In this work, we also identified a temporal window for an efficient iGOF transcriptional activation or mmRNAs transfections leading to improved human neural progenitor patterning and differentiation toward MSNs. In the last few years, the use of specific extrinsic signals in combination with the dual SMAD inhibition strategy resulted in the development of protocols for the derivation of many central and peripheral nervous system lineages from hES and iPS cells (24). Here we show that TFs with a different expression pattern and timing can be combined to efficiently differentiate hES H9 cells toward a striatal phenotype. This study has then provided a working system for combining extrinsic (morphogens) and intrinsic (TFs) players to manipulate hES or iPS cell fates. In particular, by combining a ventral-inducer like Gsx2 and a neuronal differentiation-effector as Ebf1 we could shift the differentiation outcome toward MSNs. Of interest for future studies in stem-cell therapies for HD, we show that, upon transplantation in HD rat models, Gsx2–Ebf1 iGOF cells can survive, differentiate, and express key striatal markers such as Ctip2 and Darpp32. Moreover, we show that striatal-patterned hES cells can project axons over long distances in the adult brain (of clinical importance), providing appropriate innervation of striatal GABA targets as the substantia nigra.

These findings in combination with the ability to use mmRNAs for nonintegrating transient gene expression might further pave the way for a rational modulation of cell fates, especially in clinical settings.

We also show that hES cells can be harnessed to model human embryonic development and neuronal differentiation by inducible expression of key developmental TFs. This technique allows mimicking and testing the temporal widows of TF activation during human embryonic development.

Methods

ES and LT-NES Cell Culture. The hES H9 cell line (Wicell) was cultured on Matrigel (BD, Becton Dickinson) or Matrix (Cell Guidance System). Pluripro (Cell Guidance System) medium was changed daily. Cells were passaged enzymatically with Accutase (Invitrogen) every 3 d. LT-NES cells were derived as described in ref. 21 and maintained in DMEM/F12 (Life Technologies) supplemented with N2 1:100 (Life Technologies), B27 1:1,000 (Life Technologies), and 10 ng/mL Fgf2 and Egf (Peprotech). LT-NES neuronal differentiation was triggered by removing Fgf2 and Egf from the medium. *Mycoplasma* contamination was checked every 3 mo.

Neuronal Differentiation. hES cells were plated for neuronal induction as described in ref. 25. Briefly, cells were plated at a density of 0.7×10^5 cells per cm^{-2} on Matrigel-coated dishes in Pluripro medium supplemented with 10 μM ROCK inhibitor (Y-27632[26], Sigma). Cell cultures were expanded for 3 d until they were nearly confluent. The starting differentiation medium included DMEM/F12 (Life Technologies) with N2 and B27 (Life Technologies), supplemented with 5 μM Dorsomorphin (Sigma) or 500 nM LDN 193189 (Sigma) and 10 μM SB431542 (Tocris), which were used until day 12. Every 2 d, the medium was replaced with new medium. Starting on day 5, 200 $ng{\cdot}mL^{-1}$ SHHC-25II (R&D) and 100 $ng{\cdot}mL^{-1}$ DKK-1 (Peprotech) were added to the culture and maintained for 3 wk. After the appearance of rosettes (around day 15), the entire cell population was detached using Accutase (Millipore) and replated at a cell density of 2.5×10^4 cells per cm^{-2} on dishes coated with Matrigel (BD, Becton Dickinson). The cells were maintained in terminal differentiation medium, which was composed of N2 medium supplemented with B27 and 30 $ng{\cdot}mL^{-1}$ BDNF, until the end of differentiation.

Generation of hES H9 Inducible Lines. To generate an inducible hES cell line, we first modified a pCMV-TetON-3G (Clontech) by removing the TetOn-3G cassette by digestion with EcoRI and HindIII (Biolabs). Then, we removed the CRE cassette of a pCAG-CRE vector (Addgene) and inserted the gel-purified TetON-3G cassette to generate a pCAG-TetON-3G vector. Next, we inserted in the pTRE3G-IRES responsive vector (Clontech) Gsx2 alone (in the first MCS), Gsx2 (in the first MCS) together with Ebf1 (in the second MCS), and Ebf1 alone (in the first MCS). Gsx2 cDNA was a gift from Kenneth Campbell, Cincinnati Children's Hospital Medical Center, Cincinnati, Ebf1 cDNA was a gift from Giacomo Consalez, Division of Neuroscience, San Raffaele Scientific Institute, Milan.

The hES H9 cell line was cultured as described. We used 8×10^6 cells for introducing the constructs by Nucleofection (Lonza) using a mouse ES cell nucleofection kit and electroporation protocol B16. We used 7 μg of pCAG-TetON-3G in the first round and 7 μg of pTRE-Gsx2 or pTRE-Gsx2-Ebf1 in the second round, together with 700 ng of linear resistant marker (Clontech, Puromycin during the first round and Hygromycin during the second round). Cells were then plated in two Matrigel-coated 6-cm dishes with Pluripro medium supplemented with Rock inhibitor (Y-27632[26]). After 72 h, antibiotics (Puromycin during the first round and Hygromycin during the second round) were added to the medium for positive selection. Following ∼2 wk in selection medium, hES cell colonies were carefully selected and expanded in Matrigel-coated 48-well plates. Clones were then expanded and tested for transgene expression after 48 h of doxycycline treatment. During the first round, the clones were screened by transient transfections with a pTRE-Luciferase vector (Clontech). During the second round, the clones were screened by 48 h of doxycycline treatment, and immunofluorescence analysis was performed for Gsx2 and Gsx2–Ebf1.

Immunofluorescence. Cells were fixed in 4% (vol/vol) paraformaldehyde (PFA) for 15 min at room temperature (RT) and washed 3× with PBS. Cells were then permeabilized with 0.5% Triton (Sigma) and blocked with 10% normal goat serum (Vector) for 1 h at RT. Next, cells were incubated overnight at 4 °C with the following primary antibodies and dilutions: anti-OCT4, 1:100 (Santa Cruz); anti-OTX2, 1:500 (Chemicon); anti-PAX6, 1:2,000 (Hybridoma Bank); anti-NESTIN, 1:200 (R&D); anti–βIII-Tubulin, 1:1,000 (Promega); anti-MAP2, 1:500 (BD Bioscience); anti-CALBINDIN, 1:200 (Swant); anti-GABA, 1:500 (Sigma); anti-CTIP2, 1:500 (Abcam); anti-DARPP32, 1:200 (Epitomics); anti-GSX2 (Millipore); hNuclei (Chemicon); and Calbindin, Calretinin, and Parvalbumin (Swant). After three washes in PBS 0.1% Triton, appropriate secondary antibodies conjugated to Alexa fluorophores 488 or 568 (Molecular Probes, Invitrogen) were diluted 1:500 in blocking solution and mixed with Hoechst 33258 (5 $\mu g{\cdot}mL^{-1}$; Molecular Probes, Invitrogen) to counterstain the nuclei. Images were acquired with a Leica DMI 6000B microscope (5×, 10×, and 20× objectives) and analyzed with LAS-AF imaging software and then processed using Adobe Photoshop, only to adjust contrast for optimal RGB rendering with the same procedure in doxycycline-treated and untreated cells.

Histological specimens from transplantations were examined using a Leica TCS SP5 confocal microscope. Confocal images were taken at a resolution of 1024 × 1024 dpi and 150 Hz speed, and each focal plane was 1 μm thick. Laser intensity, gain, and offset were maintained constant in each analysis. Three animals for each transplant type were analyzed. hNCAM fiber quantification was performed using Spaceballs (MBFbiosciences).

Cell-Cycle Analysis with IdU and BrdU. IddU (Sigma) was first added in the culture medium for 1.5 h followed by BrdU (Sigma) for 30 min. Cells were then fixed at the end of the BrdU treatment. For IdU/BrdU double labeling, primary

antibodies used were mouse anti-BrdU/IdU (which recognizes both BrdU and IdU, clone B44, 1:100; BD), and rat anti-BrdU (clone BU1/75, 1:100; Abcam). After 4% PFA fixation, cells are first treated with 0.2N HCl for 5 min at RT and then with 2N HCl for 20 min at 37° for BrdU/IdU immunofluorescence. Cell-cycle lengths (estimation) were calculated as previously described (18): Cells labeled initially with IdU and leaving S-phase during the interval between IdU and BrdU were labeled with IdU but not BrdU (leaving fraction).

Cumulative BrdU Labeling. BrdU is added to the cell culture medium for different time windows in different wells. BrdU immunofluorescence is performed as described above for the cell-cycle analysis.

Cell-Cycle Exit Study. iGOF cell lines were treated with doxycycline from day 20 to day 30 of neuronal differentiation. At day 25 cells were exposed to BrdU for 2 h to label cells in the S-phase of the cell cycle. Neuronal differentiation was carried on until day30, when cells were fixed and processed as described above for BrdU immunofluorescence. Cells were also stained for Ki67 to label all proliferating cells at day 30. Cell-cycle exit index was calculated by dividing the total number of $BrdU^+$ $Ki67^-$ cells by the total number of $BrdU^+$ cells.

mmRNA Transfections. The transfection mix was prepared according to the manual of the StemMACS mRNA Reprogramming Kit (Miltenyi Biotec) using the StemMACS mRNA Transfection Reagent and StemMACS mRNA Transfection Buffer. We used 200 ng mmRNA of GSX2 and EBF1 (gently provided by Miltenyi Biotec) daily for 5 consecutive days. As a transfection control, 100 ng of nuclear GFP (Miltenyi Biotec) was used the first day of transfection to monitor the transfection efficiency.

Transplantations. Athymic NIH-FOXN1 Nude rats (Charles River) of 200–250 g were lesioned 8 d before transplantation with quinolinic acid (QA). The lesion was generated by monolateral injection of 210 nmol of freshly made QA in the right striatum using the following stereotaxic coordinates: AP, +0.6; L, ±2.8; V, 5.0. We injected 1 M PBS in the left striatum. Gsx2–Ebf1 iGOF cells were differentiated as described above. Cells were treated with doxycycline from day 20 to day 30 of differentiation to induce Gsx2 and Ebf1 expression. At day 30, cells were detached with Accutase supplemented with N2 1:100 for 20–30 min at 37 °C. Cells were then resuspended to obtain a single cell suspension at a concentration of 50×10^3 cells per μL and then transplanted in complete medium by bilateral stereotaxic transplantation in lesioned adult athymic rats using the following coordinates: AP, +0.9; L, +3.1/–3.1; DV, 5.0. A total of 2×10^5 cells (4 μL) per injection site were delivered by a single injection. Two months after transplantation, the animals were killed, transcardially perfused, and the brains cryosectioned for immunohistochemical analyses. Animal experiments were carried out according to the National regulatory requirements and the Institutional Animal Care and Use Committee (IACUC). The experimental protocol has been approved by the Ethics Committee of the San Raffaele Scientific Institute and by the Italian Ministry of Health (Protocol no. 722 approved on January 12th, 2016).

Patch-Clamp Recordings and Data Analysis. Whole-cell patch-clamp recordings were performed at RT in voltage and current-clamp configuration. During recordings cells were visualized using an inverted microscope (Nikon Eclipse TE200) and maintained in a solution containing (in mM) NaCl (140), KCl (3), glucose (10), Hepes (10), MgCl2 (1), and CaCl2 (2) at pH 7.4 with NaOH. Pipettes were produced from borosilicate glass capillary tubes (Hilgenberg GmbH) by means of a horizontal puller (P-97, Sutter instruments), and their resistance was 2–4 MΩ, when filled with (in mM) CsCl (135), NaCl (3), Hepes (10), EGTA (10), CaCl2 (0.5), and MgCl2 (1) at pH 7.3 with CsOH. To isolate the sodium current, cells were recorded using an extracellular solution containing (in mM) NaCl (140), KCl (3), TEA-Cl (10), Hepes (10), 4-AP (5), MgCl2 (1), and CaCl2 (1) at pH 7.4 with NaOH, and pipettes were filled with a solution containing (in mM) CsCl (120), NaCl (10), TEA-Cl (20), Hepes (10), EGTA (10), and MgCl2 (2) at pH 7.3 with CsOH. Recordings were performed with an AXOPATCH 200B amplifier (Molecular Devices) and digitized with a DigiData1322A (Molecular Devices). Data were acquired using the software Clampex (Molecular Devices), sampled at 50 kHz and filtered at 10 kHz. The series resistance was minimized and monitored throughout the experiment.

Analysis was performed with Clampfit (Molecular Devices) and Origin 6.0 (Microcal Software Inc.). Statistics reported are mean ± SEM, unless otherwise specified. Statistical tests were performed using Instat (GraphPad Software). Two-tailed *P* values were used throughout.

Statistical Analysis. Statistical tests were performed with PRISM software (GraphPad, version 6). Statistical significance was tested with the unpaired (nonparametric) *t* test as reported in each figure and legend. All results were expressed as means ± SD. The sample size was chosen based on our preliminary studies and on the variability across differentiations. Given that the long-term differentiation experiments (80 d) are susceptible to variability, we decided to perform five different biological experiments (Fig. 3) to address this issue. No data points were excluded from the reported analyses. Differentiation experiments were excluded when a poor neural induction was obtained (low Otx2, *N*-cadherin, and Pax6 expression).

The majority of the cell counting experiments (Figs. 1–4) were performed using specific softwares (CellProfiler, fully automatic, or ITCN in ImageJ, partially automatic); therefore, they were performed blindly. The remaining cell counts were performed manually; no blinding was performed.

ACKNOWLEDGMENTS. We thank Alice Abbondanza for help with cell cultures; Oliver Brustle and Philippe Koch for their help in the generation of LT-NES cells; Paola Conforti and other members of our group for fruitful comments and technical assistance; WiCell for providing the H9 cell line; Roslin Cells for the RC17 cell line; and the families of HD patients for their continuous support. This work was supported by Marie Curie Reintegration Grant 268248 (to A.F.), CHDI Foundation Grant A7333 (to E. Cattaneo), Programmi di Ricerca Scientifica di rilevanza Nazionale Grant 2008JKSHKN_001 (to E. Cattaneo), and NeurostemcellRepair Grant NSCR 602278 (to E. Cattaneo).

1. Calabresi P, Picconi B, Tozzi A, Ghiglieri V, Di Filippo M (2014) Direct and indirect pathways of basal ganglia: A critical reappraisal. *Nat Neurosci* 17(8):1022–1030.
2. Finger S, Heavens RP, Sirinathsinghji DJ, Kuehn MR, Dunnett SB (1988) Behavioral and neurochemical evaluation of a transgenic mouse model of Lesch-Nyhan syndrome. *J Neurol Sci* 86(2-3):203–213.
3. Zhang X, et al. (2010) Pax6 is a human neuroectoderm cell fate determinant. *Cell Stem Cell* 7(1):90–100.
4. Corbin JG, Gaiano N, Machold RP, Langston A, Fishell G (2000) The Gsh2 homeodomain gene controls multiple aspects of telencephalic development. *Development* 127(23):5007–5020.
5. Pei Z, et al. (2011) Homeobox genes Gsx1 and Gsx2 differentially regulate telencephalic progenitor maturation. *Proc Natl Acad Sci USA* 108(4):1675–1680.
6. Toresson H, Potter SS, Campbell K (2000) Genetic control of dorsal-ventral identity in the telencephalon: Opposing roles for Pax6 and Gsh2. *Development* 127(20):4361–4371.
7. Waclaw RR, Wang B, Pei Z, Ehrman LA, Campbell K (2009) Distinct temporal requirements for the homeobox gene Gsx2 in specifying striatal and olfactory bulb neuronal fates. *Neuron* 63(4):451–465.
8. Yun K, Potter S, Rubenstein JL (2001) Gsh2 and Pax6 play complementary roles in dorsoventral patterning of the mammalian telencephalon. *Development* 128(2):193–205.
9. López-Juárez A, et al. (2013) Gsx2 controls region-specific activation of neural stem cells and injury-induced neurogenesis in the adult subventricular zone. *Genes Dev* 27(11):1272–1287.
10. Méndez-Gómez HR, Vicario-Abejón C (2012) The homeobox gene Gsx2 regulates the self-renewal and differentiation of neural stem cells and the cell fate of postnatal progenitors. *PLoS One* 7(1):e29799.
11. Garel S, Marín F, Grosschedl R, Charnay P (1999) Ebf1 controls early cell differentiation in the embryonic striatum. *Development* 126(23):5285–5294.
12. Lobo MK, Karsten SL, Gray M, Geschwind DH, Yang XW (2006) FACS-array profiling of striatal projection neuron subtypes in juvenile and adult mouse brains. *Nat Neurosci* 9(3):443–452.
13. Lobo MK, Yeh C, Yang XW (2008) Pivotal role of early B-cell factor 1 in development of striatonigral medium spiny neurons in the matrix compartment. *J Neurosci Res* 86(10):2134–2146.
14. Delli Carri A, et al. (2013) Human pluripotent stem cell differentiation into authentic striatal projection neurons. *Stem Cell Rev* 9(4):461–474.
15. Delli Carri A, et al. (2013) Developmentally coordinated extrinsic signals drive human pluripotent stem cell differentiation toward authentic DARPP-32+ medium-sized spiny neurons. *Development* 140(2):301–312.
16. Liew CG, Draper JS, Walsh J, Moore H, Andrews PW (2007) Transient and stable transgene expression in human embryonic stem cells. *Stem Cells* 25(6):1521–1528.
17. Waclaw RR, Wang B, Campbell K (2004) The homeobox gene Gsh2 is required for retinoid production in the embryonic mouse telencephalon. *Development* 131(16):4013–4020.
18. Martynoga B, Morrison H, Price DJ, Mason JO (2005) Foxg1 is required for specification of ventral telencephalon and region-specific regulation of dorsal telencephalic precursor proliferation and apoptosis. *Dev Biol* 283(1):113–127.
19. Shibui S, Hoshino T, Vanderlaan M, Gray JW (1989) Double labeling with iodo- and bromodeoxyuridine for cell kinetics studies. *J Histochem Cytochem* 37(7):1007–1011.
20. Becker KA, et al. (2006) Self-renewal of human embryonic stem cells is supported by a shortened G1 cell cycle phase. *J Cell Physiol* 209(3):883–893.
21. Koch P, Opitz T, Steinbeck JA, Ladewig J, Brüstle O (2009) A rosette-type, self-renewing human ES cell-derived neural stem cell with potential for in vitro instruction and synaptic integration. *Proc Natl Acad Sci* 106(9):3225–3230.
22. Ho SY, et al. (2011) NeurphologyJ: An automatic neuronal morphology quantification method and its application in pharmacological discovery. *BMC Bioinformatics* 12:230.
23. Salomoni P, Calegari F (2010) Cell cycle control of mammalian neural stem cells: Putting a speed limit on G1. *Trends Cell Biol* 20(5):233–243.
24. Tabar V, Studer L (2014) Pluripotent stem cells in regenerative medicine: Challenges and recent progress. *Nat Rev Genet* 15(2):82–92.